Diss. ETH No. 15777

SOLID CONTACTS FOR AND CURRENT RESPONSES OF ION-SELECTIVE ELECTRODES

A dissertation submitted to the

SWISS FEDERAL INSTITUTE OF TECHNOLOGY ZURICH

for the degree of

DOCTOR OF NATURAL SCIENCES

presented by

Jolanda Sutter

Dipl. Chem. ETH

born on February 24, 1976

from Rapperswil (BE)

accepted on the recommendation of

Prof. Dr. Ernö Pretsch, examiner

Prof. Dr. Bernhard Wehrli, co-examiner

Zürich 2005

Acknowledgements

I would like to thank:

Prof. Dr. Ernö Pretsch for the opportunity to work in his group, for his scientific and personal guidance, for his enthusiastic interest in this research, for his patience, and for the freedom he gave me in carrying out this work;

Dr. Xue-Qun Zhang for her help with the polysiloxane project;

Dr. Robert Gyurcsányi and Prof. Dr. Ernö Lindner for their collaboration on the polypyrrole solid-contact ISE project and for helpful discussions;

Shane Peper, Alexandar Radu, and Prof. Dr. Eric Bakker for their collaboration on the "sticky stuff" membrane project;

Dr. Werner E. Morf and Dr. Martin Badertscher for their collaboration on the project of the current response of ion-selective electrodes at controlled potential;

Prof. Dr. Bernhard Wehrli for accepting the co-examination of this doctoral thesis;

Liya Muslinkina, Dr. Dorothée Wegmann and Alan Ceresa for proofreading this manuscript;

Monia Fibbioli, Alan Ceresa, and Liya Muslinkina for their help and encouragement during my thesis and Tamás Vigassy for his "magic hands";

finally, everyone from the Pretsch group for their help, friendship, and the good atmosphere in the laboratory.

Part of this work is described in the following publications:

Sutter, J.; Lindner, E.; Gyurcsányi, R. E.; Pretsch, E. *Anal. Bioanal. Chem.* **2004**, *380*, 7-14, A polypyrrole-based solid-contact Pb^{2+}-selective PVC-membrane electrode with a nanomolar detection limit.

Sutter, J.; Radu, A.; Peper, S.; Bakker, E.; Pretsch, E. *Anal. Chim. Acta* **2004**, *523*, 53-59, Solid-contact polymeric membrane electrodes with detection limits in the subnanomolar range.

Sutter, J.; Morf, W. E.; de Rooij, N. F.; Pretsch, E. *J. Electroanal. Chem.* **2004**, *571*, 27-35, Current response of ion-selective solvent polymeric membranes at controlled potential.

Table of contents

1 Summary

In conventional liquid-contact ion-selective electrodes (LC ISEs), the internal reference electrode is separated from the sensing membrane by an internal solution. Although these sensors are widely used in clinical analysis, their fields of application would certainly increase if the sensor size could be drastically reduced. To accomplish this, there must be no internal solution and the membrane must be placed directly on the internal electrode. To construct these so-called solid-contact ion-selective electrodes (SC ISEs) so that they show stable and reproducible responses, a SC layer must be placed between membrane and internal metal electrode having two properties of crucial importance: redox activity in order to transduce the ionic response of the membrane into an electronic signal, and high surface lipophilicity to avoid the formation of a water layer between membrane and internal electrode. In this thesis, several lipophilic, redox-active materials (polysiloxanes and conducting polymers (CPs)) are investigated in view of their application in miniaturized SC ISEs.

Various approaches for preparing redox-active, lipophilic polysiloxane (poly(methylhydrosiloxane) (PMHS) and poly(dimethylsiloxane) (PDMS)) layers on gold substrates were investigated. Ca^{2+}-SC ISEs based on these layers were characterized by potentiometric measurements. Although the SC materials tested were highly lipophilic, the formation of an inner water layer was observed for the PMHS-based SC ISEs. The water layer impaired the stability of the response as well as the lower detection limit of these sensors. Its presence was explained by the hydrolysis of Si–H groups of PMHS during the conditioning of the ISEs, which resulted in a decrease in the lipophilicity of the solid contact. It was also shown that the polysiloxane layers contain pinholes, which cause the ISEs to be sensitive to oxygen. Overall, it was found that PMHS and PDMS

layers are not adequate for preparing SC ISEs with stable and reproducible electrode potentials.

Very good results were achieved by using CPs (mainly poly(3-octylthiophene) (POT) and polypyrrole (PPy)) as SC material for Ca^{2+}- and Pb^{2+}-ISEs. For many of these SC ISEs, compared to the corresponding ISEs without CP layer, the sensitivity to oxygen was reduced or even completely eliminated and the reproducibility of the day-to-day response was improved considerably. By using POT, also the formation of an inner water layer was suppressed with all the membranes examined. The selectivities of CP-based sensors were generally similar to those of optimized LC ISEs, and with optimized SC ISEs, detection limits in the nanomolar range could be achieved. However, the experiments clearly showed that the conducting polymer and membrane matrix must be chosen carefully to obtain reproducible and stable ISE responses.

The last part of this thesis presents a new theory describing the electrochemical behavior of conventional ISEs and related systems, such as ITIES (interface between two immiscible electrolyte solutions). The former are based on highly viscous polymeric membranes, whereas the latter consist of two immiscible electrolyte solutions of similar viscosity with the organic phase containing an ionophore. The apparently contradictory amperometric and voltammetric response of PVC-based ISE membranes (logarithmic vs. the ion activity or concentration) compared with that of ITIES (linear vs. the ion concentration) was shown to originate from different kinetic limitations in the two systems.

The amperometric response of plasticized PVC membranes and membranes without PVC but based on inert microporous matrices were investigated and compared with the theory. With the PVC membranes, the expected logarithmic dependency from the sample activity was obtained, whereas the behavior of the PVC-free membranes was intermediate between that of PVC membranes and ITIES systems. The measured responses were in good agreement with the theoretical model.

2 Zusammenfassung

Konventionelle ionenselektive Flüssigkontaktelektroden enthalten eine Innenlösung, die die innere Referenzelektrode von der Sensormembran trennt. Diese Sensoren werden bis jetzt vor allem in der klinischen Chemie eingesetzt, eine wesentliche Verkleinerung ihrer Dimension würde sie jedoch sicherlich einem breiteren Anwendungsfeld zugänglich machen. Dafür müsste auf die Innenlösung verzichtet werden, und die Membran müsste sich direkt auf der Innenelektrode befinden. Um so genannte ionenselektive Festkontaktelektroden zu bauen, die ein stabiles und reproduzierbares Elektrodenpotential ergeben, muss zwischen innerer Metallelektrode und Membran ein Festkontakt existieren, der über die folgenden Eigenschaften verfügt: Er muss redoxaktiv sein, um als Kopplungsstelle zwischen der ionischen Leitung der Membran und der elektrischen Leitung der Metallelektrode zu dienen, und er muss sehr lipophil sein, um die Ausbildung einer Wasserschicht zwischen Innenelektrode und Membran zu verhindern. In der vorliegenden Arbeit wurden verschiedene redoxaktive, lipophile Materialien (Polysiloxane und leitende Polymere) auf ihre Eignung zum Einsatz in miniaturisierten Festkontaktelektroden geprüft.

Es wurden verschiedene Wege zur Herstellung von redoxaktiven, lipophilen Polysiloxanschichten (Poly(methylhydrosiloxan) (PMHS) und Poly(dimethylsiloxan) (PDMS)) auf Gold untersucht. Mittels potentiometrischen Messungen charakterisierte man auf solchen Schichten basierende Ca^{2+}-selektive Elektroden. Obwohl diese PMHS-Festkontakte sehr lipophil waren, konnte die Ausbildung einer inneren Wasserschicht in den entsprechenden Elektroden nicht verhindert werden. Die Wasserschicht beeinträchtigte sowohl die Potentialstabilität als auch die untere Nachweisgrenze dieser Elektroden. Ihre Ausbildung erklärte man mit der Hydrolyse von Si–H-Gruppen während der Konditionierung des Sensors, wodurch die Lipophilie der Festkontaktschicht abnahm. Es wurde auch gezeigt, dass PMHS- und PDMS-Schichten Löcher

enthalten, die zu einer Sauerstoffempfindlichkeit der Sensoren führen. Insgesamt stellte man fest, dass diese Polysiloxane für die Verwendung in ionenselektiven Festkontaktelektroden ungeeignet sind.

Sehr gute Resultate wurden jedoch mit leitenden Polymeren (v.a. Poly(3-octylthiophen) (POT) und Polypyrrol (PPy)) als Festkontakt für Ca^{2+}- und Pb^{2+}-Sensoren erzielt. Verglichen mit analogen Elektroden ohne Polymerschicht konnte für diese Festkontaktelektroden die Sauerstoffempfindlichkeit reduziert oder ganz eliminiert und die Reproduzierbarkeit der Elektrodenfunktion wesentlich verbessert werden. Bei Elektroden mit POT bildete sich zudem bei keiner der untersuchten Membrantypen eine innere Wasserschicht. Das Selektivitätsverhalten der Festkontaktelektroden mit leitenden Polymeren war generell vergleichbar mit dem optimierter Flüssigkontaktelektroden. Auch konnte mit optimierten Festkontaktelekroden Nachweisgrenzen im nanomolaren Bereich erreicht werden. Die Experimente zeigten jedoch klar, dass die Wahl des leitenden Polymers und der Membranmatrix massgebend sind, um stabile und reproduzierbare Elektrodenfunktionen zu erhalten.

Der letzte Teil dieser Arbeit zeigt ein neues theoretisches Modell, das das elektrochemische Verhalten von konventionellen ionenselektiven Elektroden (ISE) und verwandten Systemen, wie z.B. ITIES (d.h. von Grenzflächen zwischen zwei nicht mischbaren Elektrolytlösungen), beschreibt. Erstere basieren auf hochviskosen Polymermembranen, Letztere auf zwei nicht mischbaren Elektrolytlösungen gleicher Viskosität, wobei die organische Phase einen Ionophor enthält. Es konnte gezeigt werden, dass die offensichtlich gegensätzlichen amperometrischen und voltammetrischen Antwortfunktionen von ISE mit PVC-Membranen (logarithmisch bzgl. der Ionenaktivität oder -konzentration) und ITIES-Systemen (linear bzgl. der Ionenkonzentration) von verschiedenen kinetischen Limitierungen in den zwei Systemen herrühren.

Die amperometrischen Antwortfunktionen von weichgemachten PVC-Membranen und solchen ohne PVC, die auf inerten, mikroporösen Matrizen

basieren, wurden untersucht und mit der Theorie verglichen. Für die PVC-Membranen fand man dabei die erwartete logarithmische Abhängigkeit ihrer Elektrodenfunktion von der Probenaktivität, die PVC-freien Membranen zeigten jedoch ein intermediäres Verhalten zwischen jenem von PVC-Membranen und ITIES-Systemen. Die gemessenen Antwortfunktionen stimmten gut mit dem theoretischen Modell überein.

Seite Leer /
Blank leaf

3   Basic principles of ion-selective electrodes

3.1   Introduction

Chemical sensors are small analytical devices that transform chemical properties of the examined sample (liquid or gas) into an electrical or optical signal [1,2]. Ideally, sensors do not require any sample preparation, they consume no analyte during the measurement, and they work reversibly. They are typically used in clinical and environmental analyses and for process control in industry and biotechnology.

The chemical sensors with the longest history are ion-selective electrodes (ISEs) [3]. They allow the potentiometric determination of a selected analyte ion in aqueous solution in the presence of other ionic species [4]. The most important part of an ISE is the ion-selective membrane, which provides the required selectivity. Different materials such as glass, polymers, and various crystalline materials are used for membrane preparation. The most versatile ISEs are based on plasticized polymeric membranes containing ion-selective components. They have been described for a large number of inorganic and organic analytes [5]. Their main applications are clinical routine and pH analyses. Owing to recent progresses concerning a deeper understanding of the response mechanisms and the improvement of their lower detection limits, they have become of interest in other fields of application as, e.g., environmental trace analysis [6,7]. Future work in the field of ISEs will focus on the development of robust ion-selective sensors with optimized lower detection limits. This will include the design and synthesis of highly selective ionophores as well as new polymeric membrane materials.

3.2 Components of liquid polymeric membranes

Polymeric membranes used for ion-selective electrodes are highly viscose, water-immiscible liquids consisting of the following components [3]:

Matrix

The matrix provides mechanical stability to the ISE membrane. Ideally, it is inert and does not interact with the sensed ions. Commonly, poly(vinyl chloride) (PVC) is used as a matrix for liquid ISE membranes.

Plasticizer or membrane solvent

The plasticizer acts as a solvent for the membrane components. In addition, it reduces the electrical resistance of the membrane and guarantees its flexibility. To a minor extent, it may also influence its selectivity behavior. The most commonly used plasticizers are bis(2-ethylhexyl) sebacate (DOS) and 2-nitrophenyl octyl ether (*o*-NPOE).

Lipophilic ion-exchangers or ionic sites

Ion-exchangers for ISE membranes consist of a lipophilic ion that does not partition into the aqueous phase, and a water-soluble inorganic counter ion. They are added to guarantee the permselectivity of the membrane, i.e. the coextraction of the analyte (primary) ion together with a counterion is kept negligibly small as compared with the total amount of analyte ion in the membrane. As a consequence, the total concentration of analyte ion in the membrane is sample-independent over the whole measuring range and determined only by the amount of added ion-exchanger. A constant total amount of primary ion in the membrane is the principal requirement for a Nernstian response of ISEs (compare Equations 3.6 and 3.7). Membranes that do not

contain non-partitioning ionic sites exhibit no response to changes in the analyte ion activity of the sample [4,8].

Ionophore or carrier

Ionophores are lipophilic complexing agents that provide selectivity to the membrane by binding the primary ion stronger than all other ions (interfering, secondary, or discriminated ions) in the sample. The selectivity pattern of membranes containing only an ion-exchanger but no ionophore is determined by the partitioning properties of the sample ions in the membrane plasticizer. After adding an ionophore, the selectivity of the membrane depends on the value of the complex formation constant between the different ions and the ionophore.

For optimal working conditions, membranes based on electrically neutral carriers require the addition of a lipophilic ion whose charge sign is opposite to that of the measuring ion. Membranes without a lipophilic ion-exchanger show a potentiometric response only if the polymer matrix or the plasticizer contains ionic impurities [3].

Lipophilic salts

To increase the conductivity of an ion-selective membrane, a lipophilic salt without ion-exchanger properties can be added [9]. Its addition also increases the ionic strength of the membrane and makes it more selective for divalent over monovalent ions [10].

3.3 Response mechanism of ion-selective electrodes

Figure 3.1 shows the schematic setup of a potentiometric measuring cell. It consists of two galvanic half-cells [4], i.e., an ISE and a reference electrode.
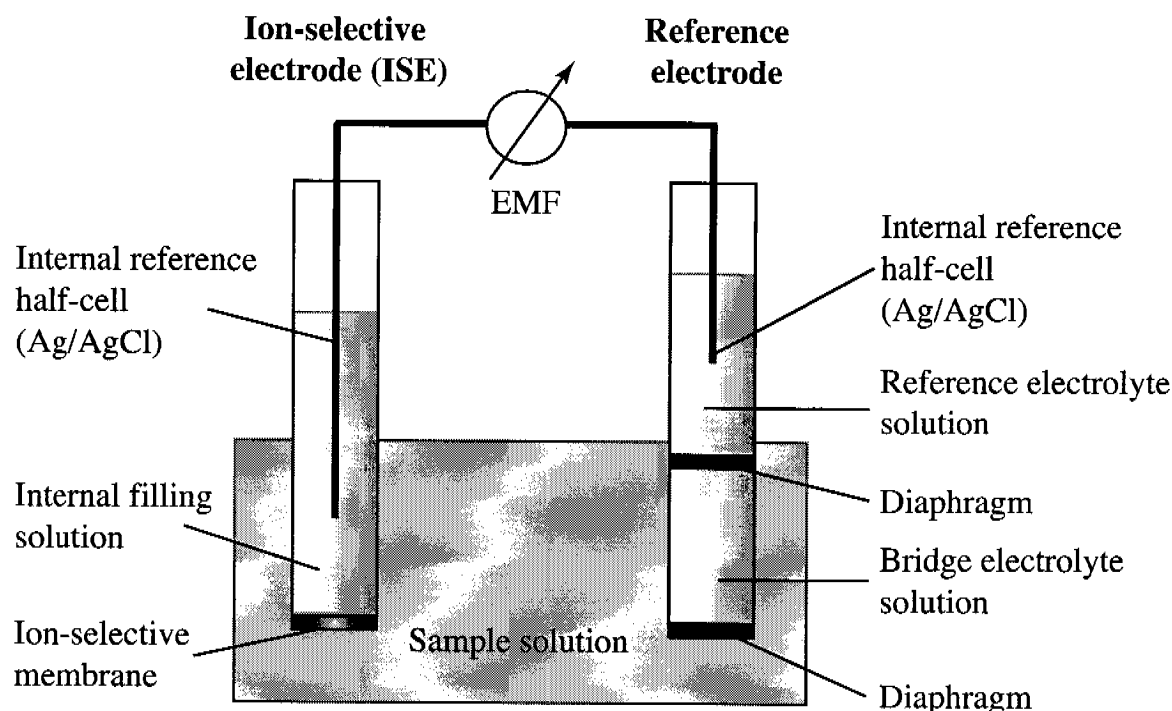
Ag/AgCl|KCl (3 M)|bridge electrolyte|sample|membrane|internal filling solution|Ag/AgCl

Figure 3.1. Schematic representation of a potentiometric measuring cell (vertical lines represent phase boundaries).

The EMF (electromotive force) of the potentiometric cell is the sum of all potential differences arising at each phase boundary under zero-current conditions. It is measured as the potential difference between the two electrodes. For a given electrode assembly and fixed temperature, only two contributions to the EMF are sample-dependent: the liquid-junction potential ($E_{D,ref}$) of the reference electrode and the membrane potential (E_M) of the ISE. All other contributions are sample-independent and are combined in E_{const}. Thus, the EMF can be expressed as follows [3,4]:

$$EMF = E_{const} + E_{D,ref} + E_M \qquad (3.1)$$

The internal half-cell of the reference electrode (usually Ag/AgCl or Hg/Hg_2Cl_2 in a highly concentrated aqueous solution of a chloride salt) is often separated from the sample solution by an additional bridge electrolyte solution. The liquid-junction potential $E_{D,ref}$ originates from the different ion mobilities at the phase boundary between sample solution and bridge electrolyte. It can be kept small by using a highly concentrated, equitransferent bridge electrolyte, e.g., 1 M NH_4NO_3, KCl, or LiOAc. If the exact composition of the sample solution is known, $E_{D,ref}$ can be estimated by the Henderson formalism [11]:

$$E_{D,ref} = -\frac{RT}{F}\frac{\sum_J z_J u_J (a_{J,s} - a_{J,ref})}{\sum_J z_J^2 u_J (a_{J,s} - a_{J,ref})} \ln \frac{\sum_J z_J^2 u_J a_{J,ref}}{\sum_J z_J^2 u_J a_{J,s}} \tag{3.2}$$

where

R   universal gas constant (8.314 J K^{-1} mol^{-1})

T   absolute temperature [K]

F   Faraday constant (96 485 C mol^{-1})

z_J charge number of ion J

u_J absolute mobility of ion J [cm^2 mol s^{-1} J^{-1}]

a_J activity of ion J in the sample solution (s) and in the bridge electrolyte solution of the reference electrode (ref) [mol L^{-1}]

Ion activities can be calculated from ion concentrations by the Debye-Hückel method [12].

The membrane potential (E_M) is the sum of three potential contributions, namely the phase boundary potential at the sample/membrane interface, the phase boundary potential at the internal filling solution/membrane interface, and the

diffusion potential inside the ion-selective membrane. The phase boundary potential between the internal filling solution and the membrane is considered as sample-independent and, as a consequence, to be constant. The diffusion potential in the membrane, in most practical cases, it is negligibly small [13-15]. With these assumptions, E_M can be expressed as follows [3]:

$$E_M = E_{M,const} + E'$$

(3.3)

where

E' phase boundary potential at the sample solution/membrane interface

$E_{M,const}$ sum of the phase boundary potential at the internal filling solution/ membrane interface and of the diffusion potential in the membrane

The value of E' can be calculated on the basis of thermodynamic considerations. If chemical and electrical potential contributions are taken into account, the electrochemical potential ($\bar{\mu}$) of the aqueous (aq) and the organic (org, i.e., membrane) phase can be formulated as:

$$\bar{\mu}(aq) = \mu(aq) + z_I F\Phi(aq) = \mu^\circ(aq) + RT\ln a_I(aq) + z_I F\Phi(aq)$$

(3.4)

$$\bar{\mu}(org) = \mu(org) + z_I F\Phi(org) = \mu^\circ(org) + RT\ln a_I(org) + z_I F\Phi(org)$$

(3.5)

where

μ chemical potential (μ° under standard conditions) [J mol^{-1}]

Φ electric potential [V]

a_I activity of the uncomplexed ion I [mol L^{-1}]

If equilibrium conditions at the phase boundary between $a_I(aq)$ and $a_I(org)$ are given, the electrochemical potential is equal for both phases. Therefore, the phase boundary potential can be expressed as:

$$E' = \Delta\Phi' = -\frac{\mu^\circ(org) - \mu^\circ(aq)}{z_I F} + \frac{RT}{z_I F} \ln \frac{a_I(aq)}{a_I(org)} \tag{3.6}$$

If $a_I(org)$ is sample-independent and constant, Equations 3.3 and 3.6 can be reduced to the well-known Nernstian equation, where E° includes all constant terms of the membrane potential:

$$E_M = E^\circ + \frac{RT}{z_I F} \ln a_I(aq) \tag{3.7}$$

For the ISE measuring cell (see Figure 3.1) the Nernstian equation can be converted into the following expression:

$$E = EMK - E_{D,ref} = E_I^\circ + s_I \log a_I(aq) \tag{3.8}$$

where

$$s_I = \frac{RT}{z_I F} \ln 10 \tag{3.9}$$

and

E_I° standard potential of the ISE measuring cell (corresponds to the intercept

        of the linear electrode response function for ion I)

s_I slope of the linear electrode response function for ion I (at 25°C,

$s_I = 59.16 \, mV/z_I$)

3.4 Selectivity

An important criterion for judging the performance of an ISE is its selectivity. Under ideal conditions, without interferences from interfering ions, the response of an ISE depends only on the primary ion activity in the sample and is described by the Nernstian equation (3.8). In practice, an ISE works ideally only in a limited concentration range. Outside this range, the measured potential is influenced by other contributions caused by the presence of interfering ions. The potentiometric selectivity coefficient, $K_{I,J}^{pot}$, allows to predict at which concentration of the primary ion the interference occurs.

The difference between the standard potentials, E_I^o and E_J^o, of the separately measured electrode functions for the primary ion (I) and an interfering ion (J) is directly related to the potentiometric selectivity coefficient, which is defined as follows:

$$\log K_{I,J}^{pot} = \frac{E_J^o - E_I^o}{s_I}$$

(3.10)

According to this equation, it is possible to calculate unbiased selectivity coefficients only if the standard potentials have been determined with an ISE exhibiting a Nernstian response to the primary and the interfering ions [16,17]. Usually, an ISE membrane gives a Nernstian response for highly discriminated interfering ions only if calibration curves are recorded before contact with

primary ions. Several other methods have been proposed to determine selectivities but many of them suffer from biases [18].

The response of an ion-selective membrane in a sample that simultaneously contains primary and interfering ions of the same charge, is exactly described by the semi-empiric Nicolskii-Eisenman formalism. In this equation, the activity term of the Nernstian equation (3.8) is replaced by the sum of activities weighted according to the selectivity of the corresponding ions:

$$E = E_I^o + \frac{RT}{z_I F} \ln(a_I + \sum_{J \neq I} K_{I,J}^{pot} a_J^{z_I/z_J})$$

(3.11)

where

a_I activity of the primary ion in the sample solution [mol L^{-1}]

a_J activity of interfering ions in the sample solution [mol L^{-1}]

The nonlinear range of the electrode function obtained for samples containing ions of different charges is not correctly described by the Nicolskii-Eisenman equation. An exact description of the potentiometric response in a solution of any number of monovalent and divalent ions is given by the following equation [19]:

$$E = E_I^o + \frac{RT}{F} \ln \left[\frac{1}{2} \sum_{J(1)} K_{I,J(1)}^{pot}{}^{1/z_I} a_{J(1)} + \right.$$

$$\left. \sqrt{\left(\frac{1}{2} \sum_{J(1)} K_{I,J(1)}^{pot}{}^{1/z_I} a_{J(1)} \right)^2 + \sum_{J(2)} K_{I,J(2)}^{pot}{}^{2/z_I} a_{J(2)}} \right]$$

(3.12)

where J(1) and J(2) indicate monovalent and divalent primary ion or interfering ion, respectively ($K_{I,I}^{pot} = 1$).

3.5 Detection limits

At high and low primary ion activities the electrode function deviates from the Nernstian behavior and becomes flat. According to IUPAC, the corresponding upper and lower detection limits are defined by the cross-section of the two extrapolated linear segments of the calibration curve (see Figure 3.2) [20].
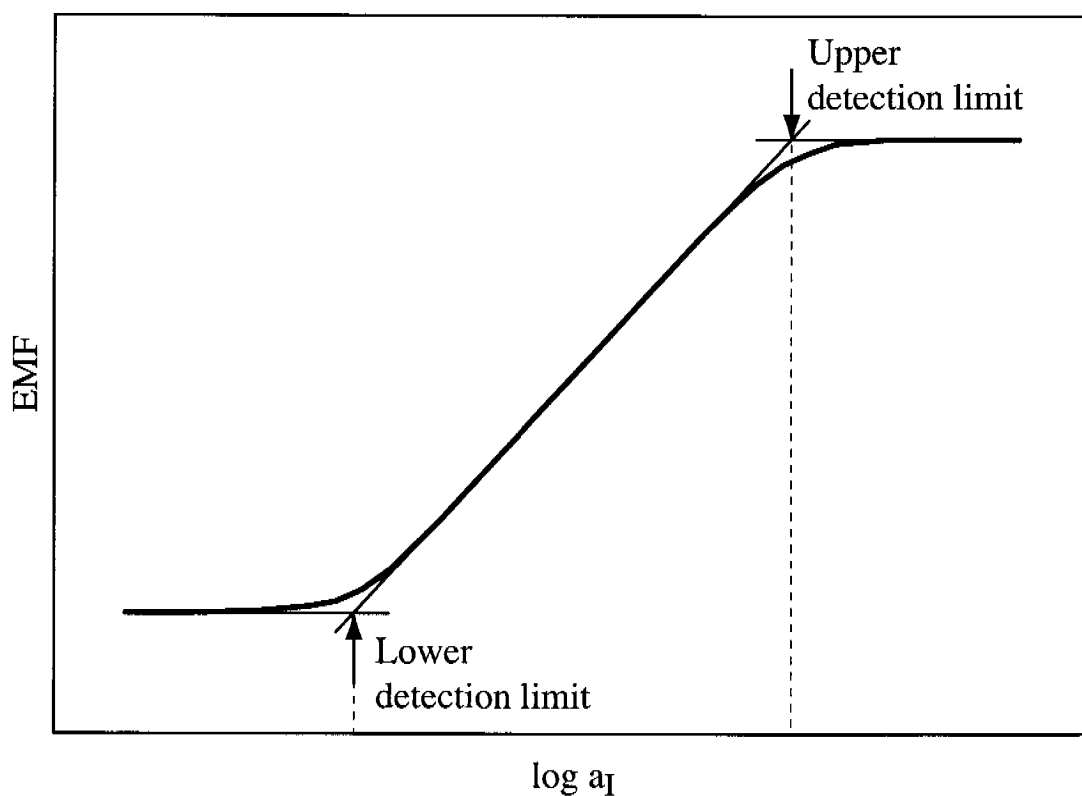
Figure 3.2. Definition of the upper and the lower detection limits according to IUPAC [20].

26

A few years ago, another definition of the lower detection limit has been proposed for ISEs showing super-Nernstian response [21]. This new formalism sets the detection limit at the primary ion activity where the electrode potential deviates by $(RT/z_I F) \ln 2$ from the linear Nernstian response. For ISEs behaving in a Nernstian way, the two descriptions are almost identical.

If the concentration of the measuring ion in the membrane depends on the sample composition, the ISE function deviates from the Nernstian behavior. At the upper detection limit, the coextraction of primary ions together with counterions causes an increase in the concentration of primary ions inside the ISE membrane. This process is also known as loss of membrane permselectivity or Donnan failure. It usually occurs in samples with high concentrations of primary ions or containing very lipophilic counterions [22,23].

Two different processes can influence the lower detection limit. In the absence of ion fluxes from the membrane into the sample, the lower detection limit is only determined by interferences from other ions present in the sample solution. This so called "static" lower detection limit can be calculated according to Equation 3.13 if the selectivity coefficients for the ISE membrane and the concentration of the interfering ions in the sample solution are known:

$$a_I(DL) = K_{I,J}^{pot} a_J^{z_I/z_J} \qquad (3.13)$$

In practice, the lower detection limit predicted by Equation 3.13 is reached only if it is above ca. 10^{-6}–10^{-7} M. Otherwise, it is biased by primary ions leaching from the membrane into the aqueous diffusion layer (Nerstian diffusion layer, see paragraph 3.6).

Various treatments of the lower detection limit induced by ion fluxes are described in the literature [21,24-26].

3.6 Zerro-current ion fluxes

Traditionally, the internal filling solution of ISEs used to contain a highly concentrated chloride salt of the primary ion, typically in the range of 10^{-3}–10^{-1} M. The lower detection limits of this kind of ISEs were usually in the micromolar range and the reported selectivities were relatively poor ($K_{I,J}^{pot} = 10^{-3}$–10^{-4}) [6]. In contrast, with optical sensors based on the same ionophores and membrane material as the ISEs, it was possible to achieve detection limits in the picomolar range [27]. Only when the primary ion in the sample solution was buffered by chelating agents or insoluble salts, did the selectivities of ISEs apparently improve [28,29]. These discrepancies can be understood by considering a leaching (or flux) of primary ions from the ISE membrane into the sample solution. Although ISEs work under zero-current conditions, it has been demonstrated that concentration gradients of ions can exist inside the ion-selective membrane [30]. They are caused by two distinct processes occurring at the membrane surfaces: coextraction and ion exchange. Both of them imply exchanges of ions between the aqueous and the membrane phases without a net charge transfer. Coextraction is the simultaneous extraction of the primary ion together with an ion of opposite charge (counterion) from the aqueous phase into the membrane. If it occurs at the inner membrane phase boundary, it leads to an increased concentration of primary ions on the inner membrane side. Therefore, a concentration gradient arises leading to a flux of primary ions and counterions toward the outer membrane surface, where the ions then leach into the sample solution [31]. Ion exchange is the process during which primary ions are transferred from the membrane to the aqueous phase and, simultaneously, interfering ions of the same charge from the aqueous phase to the membrane, or vice versa. This process produces concentration asymmetries leading to ion fluxes across the membrane. In contrast to fluxes induced by coextraction, the diffusion of primary ions across the membrane is counterbalanced by a flux of

interfering ions in the opposite direction. Depending on the experimental conditions, the primary ion can be transported either toward the sample or the internal solution, with the consequent enrichment or depletion of the water layer in contact with the membrane at the sample side.

In order to obtain the best possible performance, ion fluxes in ISE membranes must be avoided. Theoretically, this is only possible if the internal solution matches the sample composition at any moment. In practice, this is impossible because the internal solution cannot be varied during measurements. As soon as the concentration of the primary ion in the sample is lower than in the internal filling solution, outward fluxes occur biasing the lower detection limit. Similarly, if the primary ion concentration in the internal filling solution is chosen too low, inward fluxes will lead to a depletion of primary ions in the diffusion layer on the sample side of the membrane. In this case, very good lower detection limits can be achieved, but, at the same time, a so-called super-Nernstian response is observed, i.e., the slope is higher than predicted by the Nernstian equation [32].

The correct tuning of ion gradients inside the membrane is not an easy task. Although for some applications, strong inward fluxes were created intentionally [33,34], most of the efforts done to improve the ISE performance were focused on the reduction of ion fluxes through the membrane. The first attempts to reduce outward ion fluxes and improve the lower detection limits of ISEs was to keep the primary ion activity in the internal solution low and constant using buffering agents or ion-exchange resins [35]. For example, by the use of Na_2EDTA, the lower detection limit of Pb^{2+}-selective electrodes could be extended to the picomolar range [36]. Similar results were obtained by decreasing the ion-exchanger concentration, increasing the thickness of the membrane, decreasing the content of plasticizer [37], or incorporating lipophilic particles into the surface layer of the ISE membrane [38]. However, all these

procedures often had adverse effects such as loss of selectivity and increase in the conditioning or response time.

Another very promising approach to reduce ion fluxes through the membrane and to improve the lower detection limit of ISEs is the use of solid-contact ion-selective electrodes, which are the main topic of this thesis and are introduced in the next chapter.

4 Solid-contact ion-selective electrodes

4.1 Introduction

Conventional liquid-contact ion-selective electrodes (LC ISEs) containing an internal filling solution (see Figure 4.1) exhibit very stable and reproducible potentials (typical standard deviation of noise, 60–80 μV). These are provided by coupling the ionic conductivity of the membrane and internal filling solution (aqueous chloride salt solution) with the electronic conductivity of the internal reference half-cell ($Ag/AgCl$ or Hg/Hg_2Cl_2) via a reversible redox reaction (Ag/Ag^+ or Hg/Hg^+). For microfabrication technologies, which are required e.g., for real time in-vivo monitoring, classical LC ISEs with a large volume of internal filling solution are not adequate. To reduce this volume, the use of thin hydrogel layers in combination with conventional internal reference electrodes or with ion-selective field effect transistors (ISFETs) (e.g. [39]) was proposed. Later, it was demonstrated that such ISEs can be, e.g., successfully applied for in-vivo H^+ monitoring [40,41]. Unfortunately, the decrease in sensor size (hydrogel volume) was accompanied by a loss of potential stability and reproducibility. For true miniaturization, it was, therefore, necessary to replace the internal filling solution in ISEs with a solid contact (see Figure 4.1). The first type of a solid-contact ISE (SC ISE) was the so-called coated-wire ISE where the membrane cocktail was directly cast on a metal electrode [42-45]. The coated-wire setup suffers from large drawbacks: The electrodes show long-term potential instabilities (potential drifts) and irreproducibilities, which are usually attributed to the lack of a thermodynamically well defined interface between the ionically conductive ISE membrane and the electronically conductive internal metal electrode [44,46]. Additionally, osmotic transport of water into the ill-

defined region between membrane and internal electrode due to poor membrane adhesion causes further potential drifts [47].

LC ISE   **SC ISE**

Internal reference
half-cell
(Ag/AgCl)

Internal metal
electrode

Internal filling
solution

Solid contact

Ion-selective
membrane
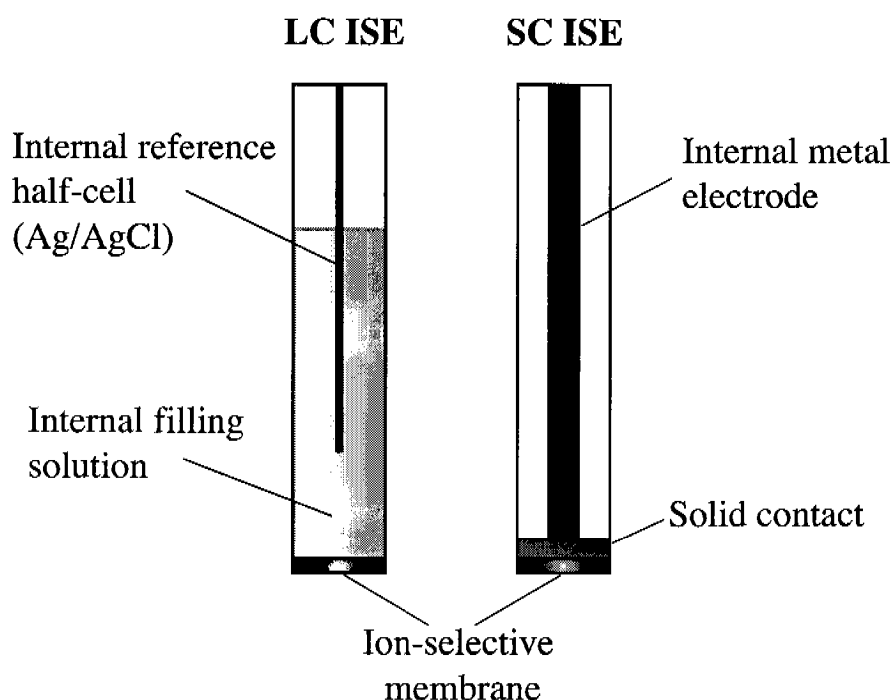
Figure 4.1. Comparison of a liquid-contact (LC ISE) and a solid-contact ion-selective electrode (SC ISE).

In order to obtain a thermodynamically well-defined electrochemical interface between membrane and internal electrode, it was suggested to employ a redox-active intermediate layer (solid contact) or add an appropriate redox-active compound to the ISE membrane. To validate this approach, various solid-contact materials have been examined in different working groups. Hauser et al. used poly(vinyl ferrocene) [46]. The resulting electrodes were not sensitive to oxygen and showed improved potential stabilities as compared with coated-wire ISEs, but still not as good as those of LC ISEs. Another attempt to improve the potential stability was made by Liu et al. who incorporated a lipophilic Ag^+ complex into the ion-selective membrane that was in contact with a Ag surface. Although the redox couple improved the potential stability of the electrode, its

working range was reduced as compared with the coated-wire analogue [48]. The most widely established solid-contact materials are conducting polymers. They are used in a variety of sensors (e.g., polypyrrole [49-52], polythiophenes [53-57], and polyaniline [53,58]) and will be discussed in Chapter 6.

The next paragraph deals with the working mechanisms of the SC ISE response and elucidates consequential requirements for solid-contact materials.

4.2 Basic principles of SC ISEs

The basic working mechanisms of SC ISEs are shown in Figure 4.2 for K^+-selective SC electrodes a) without and b) with an internal redox-active layer on gold as the internal electrode. As mentioned above, the transition between ionic (membrane) and electronic (internal electrode) charge transport in coated-wire electrodes (Figure 4.2 a) is electrochemically not well defined. Nevertheless, they give Nernstian response, although they show drifting potentials. Therefore, a redox-active intermediate is required at the membrane/metal interface. Since PVC membranes are permeable to both, oxygen and water, it was suggested that in coated-wire electrodes an oxygen half-cell is built-up at the membrane/metal interface acting as a redox couple [42,43]. Most likely, futher redox-active species (e.g., impurities) present in the membrane or on the metal surface are involved in this process [45]. On introducing a redox-active material as a solid contact between membrane and metal providing a well-defined potential at this interface, the potential stability of the SC ISE is improved (Figure 4.2 b). In the case of the coated-wire setup or of insufficient lipophilicity of the solid-contact material, a water layer is formed between membrane and metal electrode. The composition of this water film changes upon changes in the sample composition, thus, causing additional potential drifts [59].
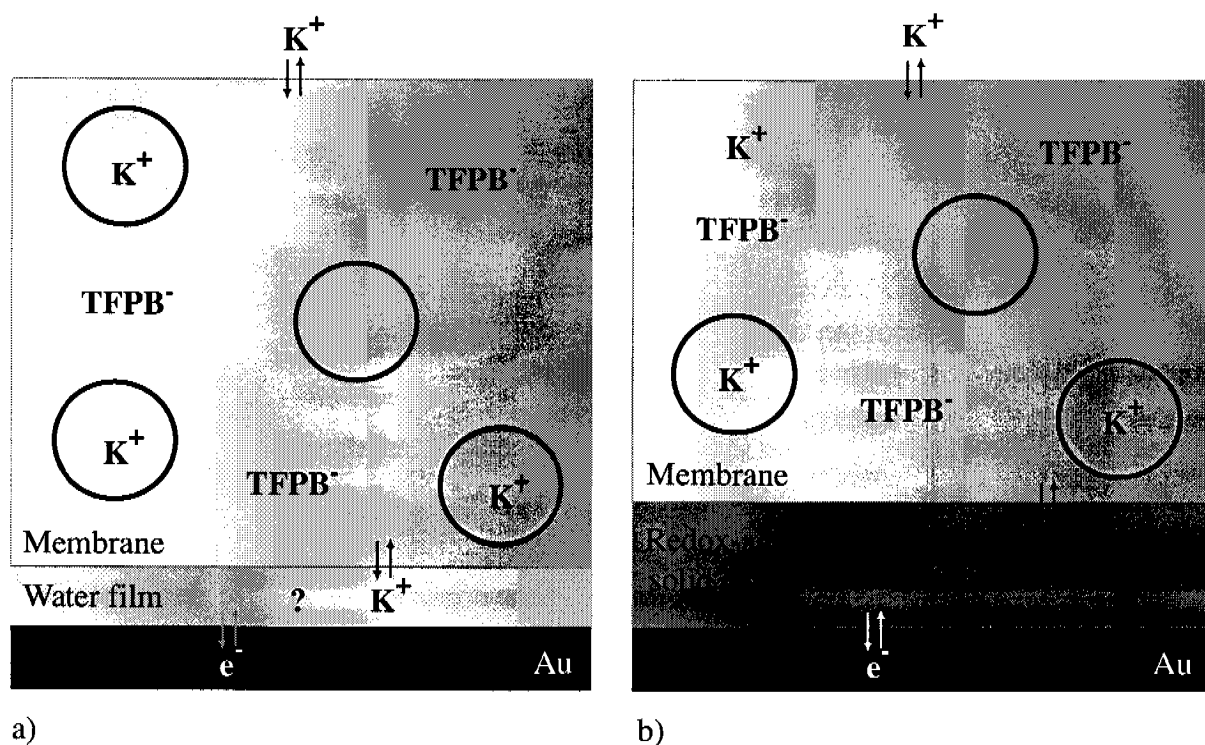
Figure 4.2. Working mechanisms of SC ISEs: a) coated-wire ISE, b) ISE with a redox-active solid contact. **O**: Valinomycin; TFPB⁻: tetrakis[3,5-bis-(trifluoromethyl)phenyl]borate; R/R⁺: redox couple; A⁻: counter ion of R⁺ (e.g.,TFPB⁻).

For the above, it was concluded that in order to get SC ISEs with stable potentials, the solid-contact material must meet the following requirements:

- It has to be redox-active to provide an interface for ionic and electric charge transport between membrane and metal electrode.

- It has to be highly lipophilic (contact angles >80° [60], see also paragraph 4.3.1) to prevent the formation of a water layer between membrane and internal electrode.

The second requirement should also assure improved lower detection limits since leaching of primary ions from the internal filling solution as observed in LC ISEs is avoided. So far, this was shown only by Fibbioli et al. [60,61] on the

example of a K^+-selective polyurethane membrane electrode with a self-assembled monolayer (SAM) as a solid contact.

Not only the solid-contact material but also the composition and the resulting adhesion of the membrane to the internal electrode are crucial to inhibit the formation of an internal water layer in SC ISEs [60]. Additionally, for planar sensors like SC ISEs, ISFETs, and hydrogel-based ISEs, poor membrane adhesion determines to a great extent the sensor's lifetime because it leads to electrolyte shunts around the membrane rendering the sensor inoperative [40,41,47,62]. It is known that the matrix/plasticizer ratio influences the adhesion properties of the membrane [47,63]. Aside from the commonly used PVC, such matrices as hydroxylated PVC, polyurethane, and silicon rubber were examined. Especially membranes based on polyurethane and silicon rubber showed better adhesion properties than plasticized PVC membranes [47,57,63-66].

Sensors for in-vivo measurements, additionally, have to be biocompatible [47,62,63,67] and, therefore, any dissolution of membrane components into living tissue has to be avoided or at least reduced because it may cause serious inflammatory reactions and even thrombosis, apart from giving unstable measurements. It was shown that the reduction of plasticizer content improves the biocompatibility of ISE membranes. For example, polyurethane (Tecoflex®)-based membranes (for structure, see Figure 4.3) were used with low amounts of, or even without, plasticizer leading to improved biocompatibility and membrane adhesion, with no significant deterioration of the general analytical characteristics of the sensors [63].

$$\left[O-(CH_2)_4-O\left[\overset{O}{\underset{}{C}}-\overset{}{\underset{H}{N}}-\bigcirc-CH_2-\bigcirc-\overset{H}{\underset{}{N}}-\overset{}{\underset{O}{C}}-O\right]_n(CH_2)_4\right]_m$$
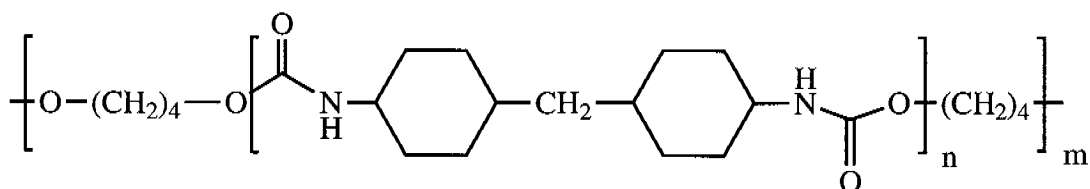
Figure 4.3. Structure of Tecoflex® polyurethane.

The class of polyacrylate and poly(n-alkyl)acrylate copolymers applied in optical ion sensors [68,69] as well as in ISFETs [70] became also attractive as a matrix for ion-selective membranes. Due to their low glass transition temperature, these polymers allow the preparation of plasticizer-free membranes as described, e.g., in [71-80]. Diffusion in such membranes is approximately a thousand times lower than in plasticized PVC membranes [81]. Only recently, ISEs with a polypyrrole solid contact and a methacrylic-acrylic polymer membrane were introduced showing an example of successful application of plasticizer-free membranes in solid-contact electrodes [82].

In order to examine solid-contact materials and the potential stability of the corresponding SC ISEs, a variety of investigations were done. The techniques used in this thesis are reviewed in the next paragraph.

4.3 Study on solid-contact layers and the corresponding SC ISEs

4.3.1 Analytical tools for the investigation of solid-contact layers

Contact angle measurements

Contact angle measurements are used to determine the wetting properties of surfaces [83]. In this work, only the so-called advancing contact angles (Θ_a) were measured. The contact angle corresponds to the angle between a surface

and the boundary of a liquid droplet placed on it and can be measured with a goniometer.

a)   b)
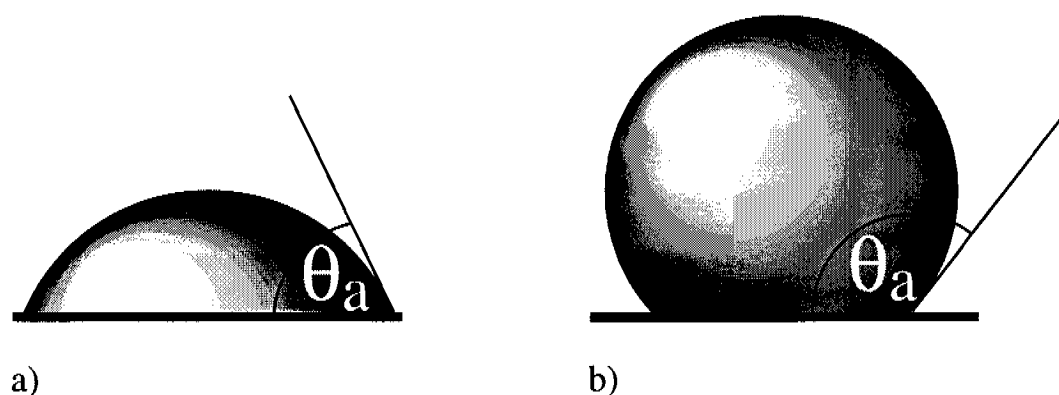
Figure 4.4. Contact angle of a) a hydrophilic and b) a hydrophobic surface.

For solid-contact materials, the contact angle of water is of interest. If the surface is hydrophilic, the measured angles are close to 0°, whereas for hydrophobic surfaces, angles over 90° are observed (see Figure 4.4).

Cyclic voltammetry

The electrochemical behavior of redox-active layers (monolayers and thicker films) can be examined by cyclic voltammetry. Figure 4.5 shows a cyclic voltammogram (CV) of a metal electrode modified with a monolayer of a redox-active species. Characteristic features of the CV are marked in the Figure. The peak current (i_p) is given by the following Equation [84,85]:

$$i_p = \frac{n_e{}^2 F^2 A v \Gamma}{4RT} \tag{4.1}$$

where

R universal gas constant (8.314 J K^{-1} mol^{-1})

T absolute temperature [K]

F Faraday constant (96 485 C mol^{-1})

i_p peak current [A]

n_e stoichiometric number of electrons involved in the redox reaction

A surface area of the metal electrode [cm^2]

v scan rate [V s^{-1}]

Γ molar surface coverage of the metal electrode with redox-active species

  [mol cm^{-2}]

Here, i_p is proportional to the scan rate. This is in contrast to the peak current of ideal Nernstian voltammetric waves for freely diffusing species in solution, which is proportional to $v^{\frac{1}{2}}$, see also Equation 4.6).
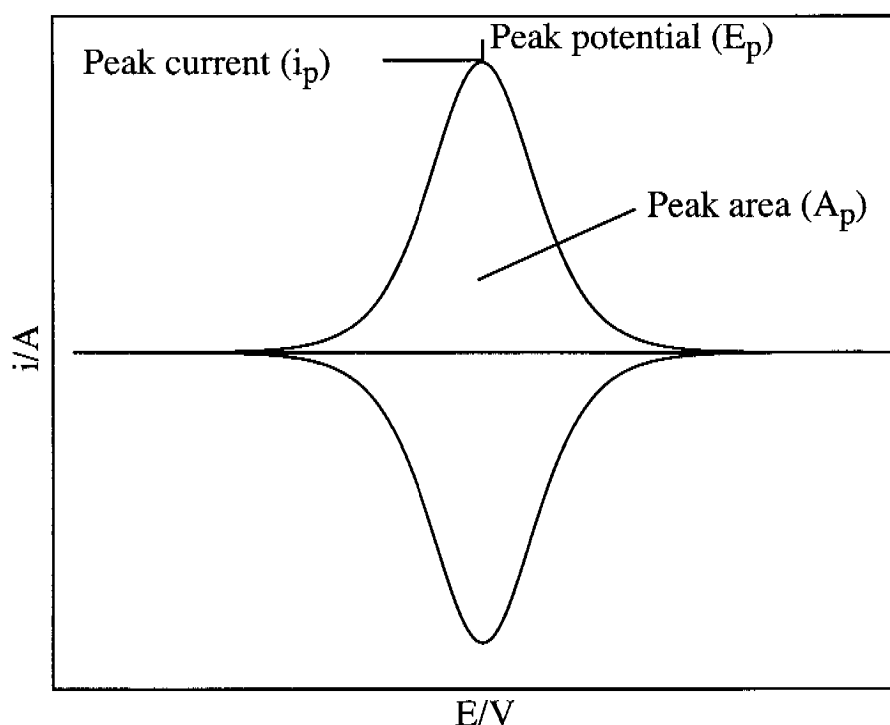
Figure 4.5. Theoretical, reversible cyclic voltammogram of a metal electrode modified with a redox-active monolayer.

For ideal, surface-determined redox reactions with the redox-active substance immobilized on the metal electrode, the anodic (E_{pa}) and cathodic (E_{pc}) peak potentials are identical, whereas for redox-active species in solution, the peak separation (ΔE_p) is given by Equation 4.2:

$$\Delta E_p = \frac{59.16}{n_e} \qquad [mV] \qquad\qquad (4.2)$$

The standard potential ($E°$) of the redox reaction is calculated as follows:

$$E° = \frac{E_{pa} + E_{pc}}{2} \qquad\qquad (4.3)$$

Under certain conditions, the treatment discussed in this section for thin redox-active monolayers can also be applied to thicker films, but voltammetric waves of such systems often deviate from the above discussed ideal behavior [85]. For thicker films, e.g., the presence of inhomogeneities as well as charge transport through the film play a role.

The surface coverage of a metal electrode with redox-active species can be estimated by cyclic voltammetry. First, the peak area (A_p, see Figure 4.5) of either the reduction or the oxidation peak, which are equal for ideal reactions, is integrated. This allows to calculate the electric charge (Q, Equation 4.4) used in this redox process and from it, the overall amount of redox-active species on the electrode surface (n):

$$Q = \frac{A_p}{v} \qquad\qquad (4.4)$$

and

$$n = \frac{Q}{F} \tag{4.5}$$

with

A_p peak area of the reduction or the oxidation peak [W]

Q electric charge used in the redox process [C]

n overall amount of redox-active species on the metal electrode surface [mol]

After this, the redox-active layer is removed from the metal electrode. By recording CVs at different scan rates in a redox marker solution, for which the diffusion coefficient in the solvent is known, the slope of the plot of i_p vs. $v^{\frac{1}{2}}$ is determined (Equation 4.6) and from there, the electrode surface (A) [84]:

$$i_p = 0.4463 \left(\frac{F^3}{RT} \right)^{1/2} n_e^{3/2} A D_o^{1/2} c_o^* v^{1/2} \tag{4.6}$$

where

D_o diffusion coefficient of redox marker in the solvent used [cm^2 s^{-1}]

c_o^* concentration of redox marker in the solution [mol cm^{-3}]

With n and A being known, the molar surface coverage (Γ) is obtained from the Equation 4.7:

$$\Gamma = \frac{n}{A} \qquad\qquad (4.7)$$

4.3.2 Study on the potential stability of SC ISEs

It is not easy to quantify potential drifts and erratic changes in the response of SC ISEs. Therefore, several potentiometric tests were developed in order to have a measure for these potential instabilities.

Water layer test

The presence of a water layer in SC ISEs between the internal electrode and the membrane was proved, for the first time, by Fibbioli et al. [59] by means of a so-called potentiometrical water layer test where the behavior of a coated-wire type electrode was compared to that of a SC ISE having a lipophilic, redox-active SAM as solid contact.
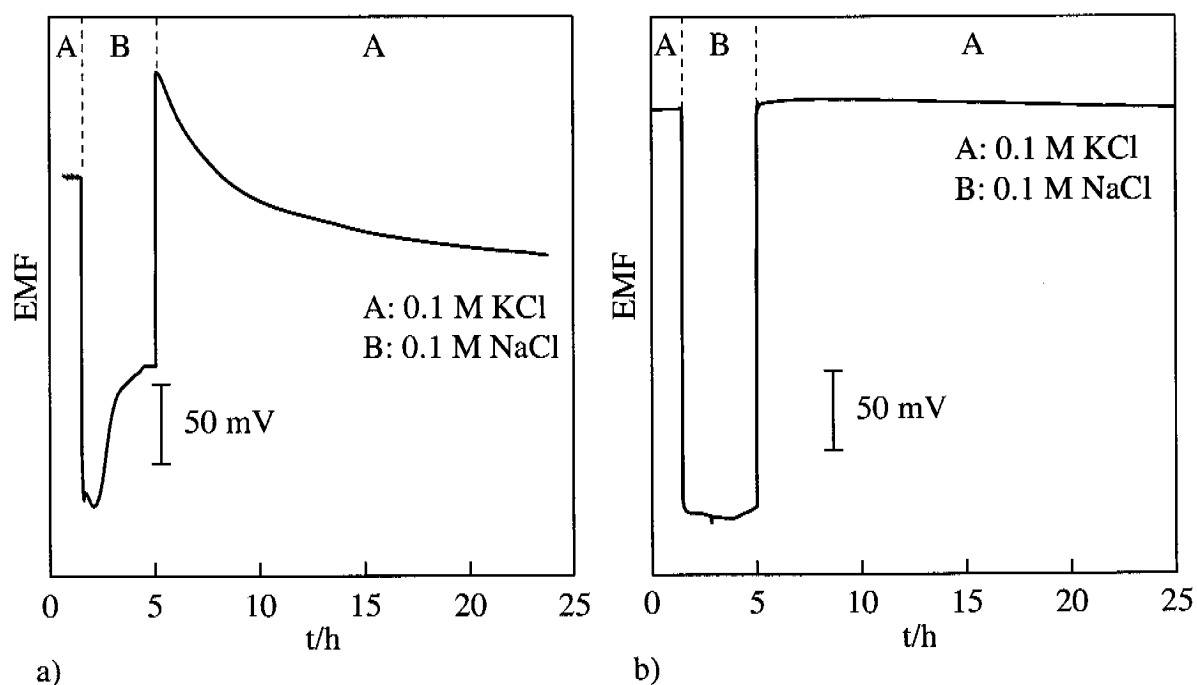

Figure 4.6. Water layer tests of K^+-selective SC ISEs: a) coated-wire type ISE, b) SC ISE with a lipophilic, redox-active SAM on gold as solid contact [59].

41

The SC ISEs under study were conditioned in a concentrated solution of the primary ion. Then, the sample was exchanged for a solution of an interfering ion and after that, for the conditioning solution again (see Figure 4.6). For coated-wire electrodes, an EMF drift to higher potentials was observed when the primary ion solution was exchanged for one of an interfering ion. The drift was attributed to a fast exchange of K^+ ions in the internal water layer for Na^+. Exposed to the primary ion solution again, the SC ISEs showed a drift to lower potentials, indicating that Na^+ ions in the internal water layer were slowly exchanged for K^+. The observed electrode response was also predicted by a theoretical model based on an ISE with a very thin water film as an internal reference solution [59]. By using a lipophilic, redox-active SAM as solid contact, the drift of electrode potentials upon changes in the sample composition was eliminated. Hence, it was concluded that the lipophilic SAM on the gold electrode prevents the formation of an internal water layer.

Oxygen test

By the oxygen test, the SC ISE is tested for its response toward a redox-active species in solution capable of diffusing into and through the sensor membrane. The O_2 concentration of the sample solution is altered by bubbling alternately argon (or nitrogen) and oxygen through it, while the EMF of the SC ISEs is monitored. An example of such an oxygen test is shown in Figure 4.7, where the response of a coated-wire type electrode is compared with that of a SC ISE having a SAM of ethyl (8-sulfanyloctyl)-1,2-methano[60]fullerene-61,61-dicarboxylate as solid contact [61]. While the electrode without SAM showed a large potential step (about 20 mV) under the influence of oxygen, the use of the redox-active SAM as solid contact prevented the sensitivity to oxygen of these SC ISEs.
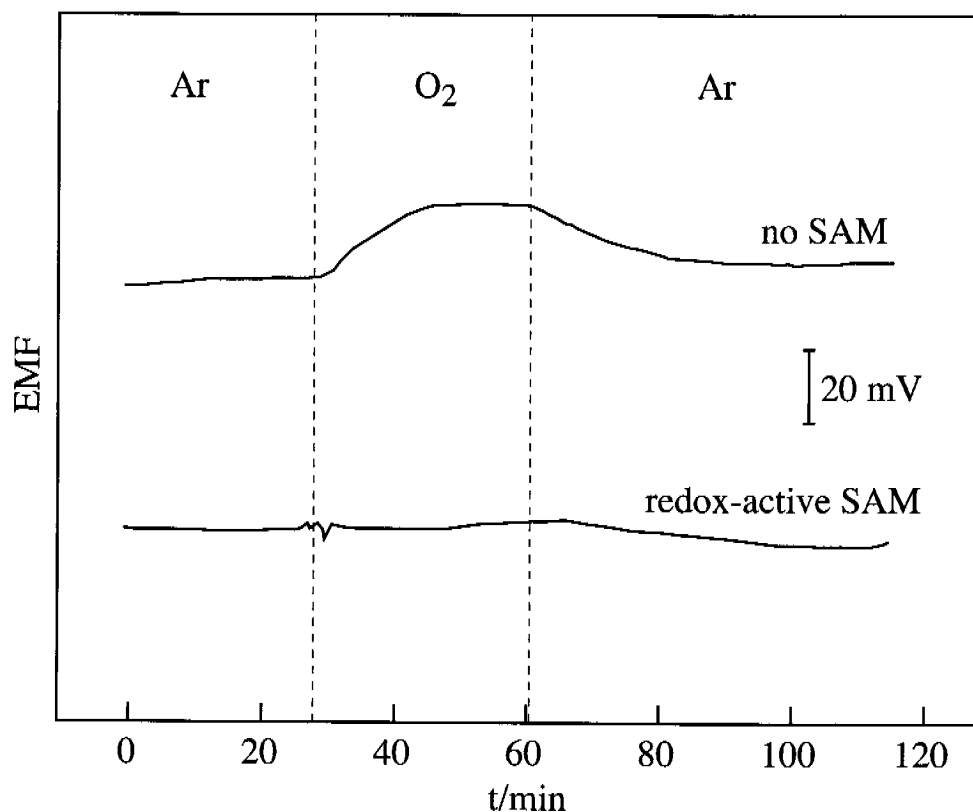
Figure 4.7. Example of an oxygen test on SC ISEs without and with a redox-active SAM [61].

CO_2 test

In analogy to the oxygen test, the CO_2 concentration of the sample solution is altered by bubbling alternately argon (or nitrogen) and carbon dioxide through it, while the EMF of the SC ISEs is recorded. It is mainly applied in order to check if SC ISEs respond to pH changes in the sample (see e.g., [86]). It was not applied in this work.

Seite Leer /
Blank leaf

5 Redox-active polysiloxane layers on gold surfaces for solid-contact ion-selective electrodes

5.1 Introduction

Recently, in a number of works by Fibbioli et al. [60,61,87], it was shown that redox-active lipophilic self-assembled monolayers (SAMs) can be used as transducers for the process of switching between ionic and electronic conductivity required for the preparation of solid-contact ISEs. Examined SC ISEs based on SAMs exhibited a significantly improved potential stability and lower detection limits as compared with the analogous coated-wire type ISEs. However, in view of miniaturization, which is one of the main goals in the development of SC ISEs, the application of SAMs has a disadvantage. The number of defects in a SAM strongly depends on the surface properties of the substrate. The preparation of sufficiently dense layers requires microscopically smooth substrate surfaces [88], which are extremely difficult to obtain with the dimensions of microelectrodes. To overcome this problem, it was proposed to apply a novel surface modification with polysiloxanes introduced by the group of Prof. U. Suter at the ETH Zürich in 1998. These highly lipophilic polysiloxane layers can be further modified with redox-active compounds and, thus, they meet the requirements necessary for developing SC ISEs. According to ref. [89], polysiloxanes containing Si–H bonds can be covalently bound to metal surfaces (Al, Ti, Cr, Fe, and Cu) by activation of the Si–H bond with the Pt catalyst, cis-[PtCl$_2$(PhCH=CH$_2$)$_2$]) (Ph: C$_6$H$_5$–). The surface lipophilicity of substrates modified with Si–H-terminated H-poly(dimethylsiloxane) (H-PDMS, see Figure 5.1, a) is very high. The advancing contact angles of water measured on these substrates are in the range of 108–115°, which is comparable to those of bulk H-PDMS. As the contact angle is very susceptible to the surface

composition, it was concluded that the surface was covered to a large extent with the polymer and that the polymer layer determined the surface properties. Upon washing the sample in organic solvents (chloroform, toluene, hexane, and tetrahydrofuran), the thickness of the polysiloxane layer initially decreased slightly and then remained constant for several days, proving that the polymer was strongly bound to the surface.

a)   b)
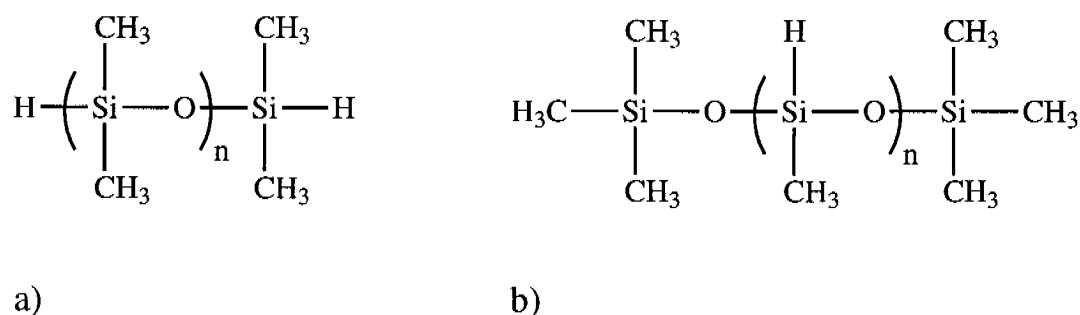
Figure 5.1. Structures of a) H-poly(dimethylsiloxane) (H-PDMS) and b) poly(methylhydrosiloxane) (PMHS).

Poly(methylhydrosiloxane) (PMHS, see Figure 5.1, b) containing Si–H bonds in the polymer backbone was successfully attached to Al, Fe, and Cu surfaces resulting in layers of 5–8 nm thickness, giving advancing contact angles of 94–110°.

Gold, which is often used for preparing SC ISEs, was also examined as a substrate for the polysiloxane modifications. The mechanism of the reaction is not yet fully understood. However, it is known that in the presence of *cis*-[PtCl$_2$(PhCH=CH$_2$)$_2$], hydrosilane compounds can be linked to alkenes, acetylenes, ketones, and alcohols upon cleavage of the Si–H bond [90-92]. Therefore, Hirayama et al. proposed two alternative mechanisms for attaching polysiloxanes to metallic substrates: either via formation of Au–Si bonds or by binding the polymer as a Pt–Si complex to the surface [93]. The layer

thicknesses for H-PDMS and PMHS were in the range of 5 nm and the advancing contact angles 115° and 91°, respectively [93]. The formation of such thick layers of polysiloxane corresponds to the folded conformation of the immobilized polymer forming loops and tails on the surface (for schematic illustration, see Figure 5.2).
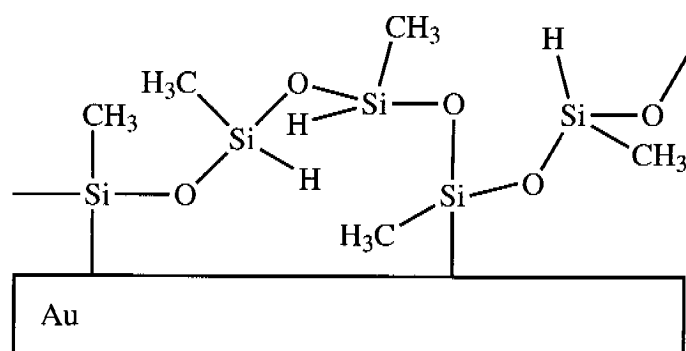
Figure 5.2. Schematic illustration of a PMHS-modified gold surface, adapted from [93].

5.2 Modifications of PMHS and PDMS layers on gold surfaces with redox-active compounds

The high lipophilicity achieved for polysiloxane-modified substrates makes these polymers very attractive for the preparation of new solid-contact materials. Further development of polysiloxanes in this direction requires their modification with redox-active compounds providing redox activity to the lipophilic material. Hirayama et al. demonstrated that PMHS layers on metal surfaces act as an adhesion promoter for two-component silicone resins in the presence of a Pt catalyst [94]. The reaction is based on the catalytic hydrosilylation of alkene bonds in the resin by Si–H bonds still present in the PMHS layer after attaching it to the metal. Recently, it was also shown that a

biotin derivative containing a double bond can be attached to PMHS layers on Au in the presence of cis-[PtCl$_2$(PhCH=CH$_2$)$_2$] [95].

On the basis of the results mentioned above, it was concluded that redox-active species bearing an adequate functional group, such as a double bond or a hydroxyl group, can be bound to PMHS layers immobilized on metal surfaces. Vinylferrocene and hydroxymethylferrocene were chosen as reasonable candidates for this purpose since ferrocene compounds are well studied and broadly used for electrochemical applications.

5.2.1 PMHS layers modified with vinylferrocene or hydroxymethylferrocene on gold surfaces

A direct route to modify polysiloxane layers with redox-active centers is the binding of a ferrocene compound to the freshly prepared PMHS layer in the presence of the same Pt catalyst used for the attachment of that layer to the metal substrate (Fig. 5.3). Advancing contact angle measurements are used to verify the formation of the PMHS layer and to have a measure of its surface lipophilicity, while cyclic voltammetry is applied to confirm the attachment of ferrocene.

The modification of polysiloxane-coated gold surfaces was performed with vinylferrocene from two batches of different age. The reaction with a five years old portion resulted in a layer characterized by a clear ferrocene peak observed in the cyclic voltammogram (CV), while modification with a newer one (less than one year old) yielded a layer without any redox activity. Comparison of these two portions of vinylferrocene in thin layer chromatography revealed the presence of at least four impurities in the older batch. Although the amount of impurities was too small to be identified, each of them or even their combination could act as a cocatalyst, allowing the desired attachment of vinylferrocene to the PMHS layer. Unfortunately, neither the variation of reaction conditions nor

the addition of known cocatalysts for cis-[PtCl$_2$(PhCH=CH$_2$)$_2$] resulted in the attachment of the vinylferrocene of the newer batch to the PMHS layer.
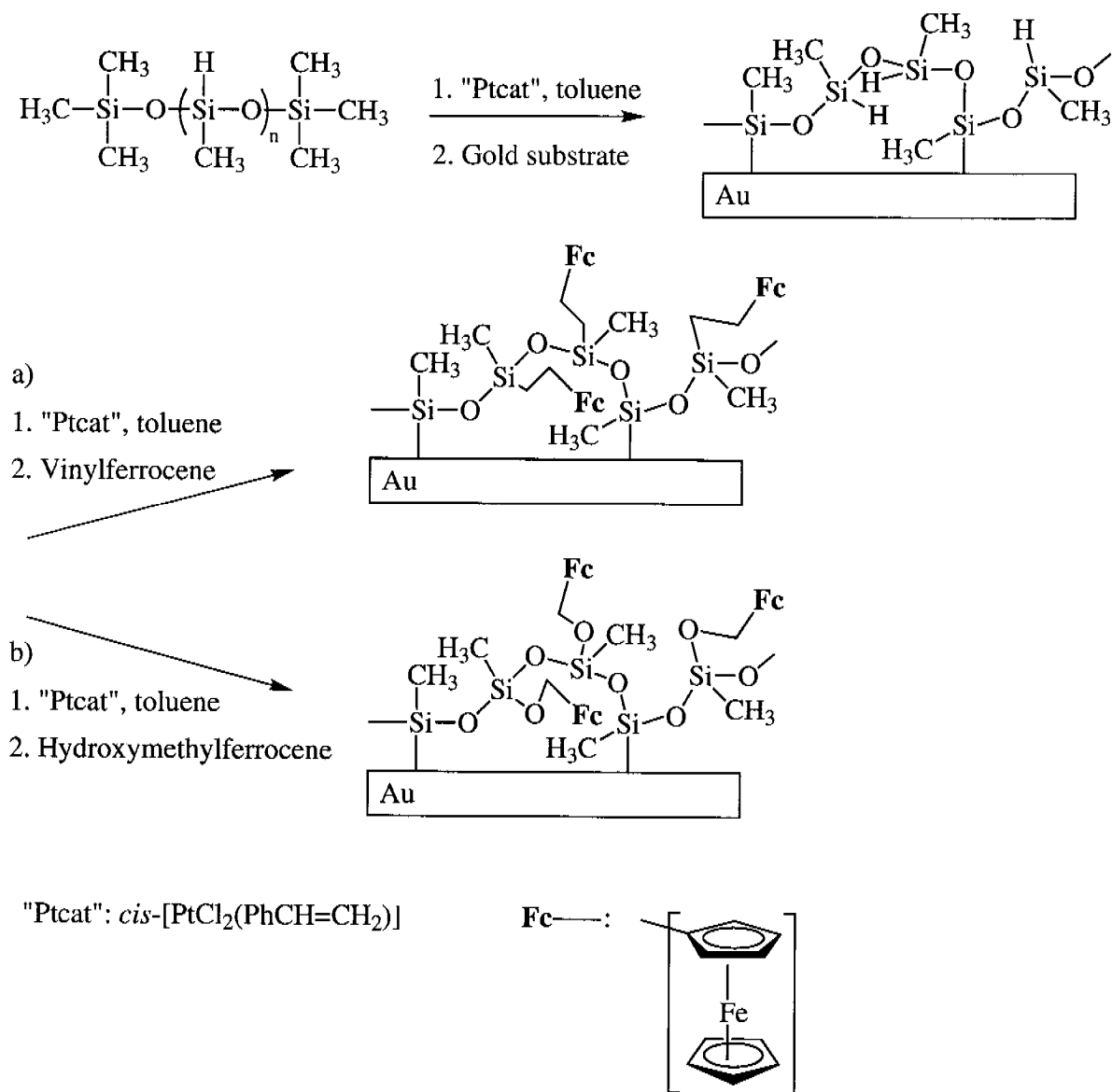
Figure 5.3. Reaction sequence for modifying a gold surface with PMHS followed by the modification with a) vinylferrocene or

b) hydroxymethylferrocene, respectively.

The desired immobilization of ferrocene on the PMHS layer was achieved after replacing vinylferrocene by hydroxymethylferrocene. However, the redox peaks

of ferrocene observed in the CVs corresponded to a very small amount of redox-active compound present on the surface. Increases in the reaction time of up to 24 h or in the reaction temperature of up to 60–80°C did not significantly affect the yield (see Figure 5.4). To improve the yield, the modification of PMHS with ferrocene compounds before its attachment to gold surfaces was examined as an alternative route for preparing redox-active polysiloxane layers.
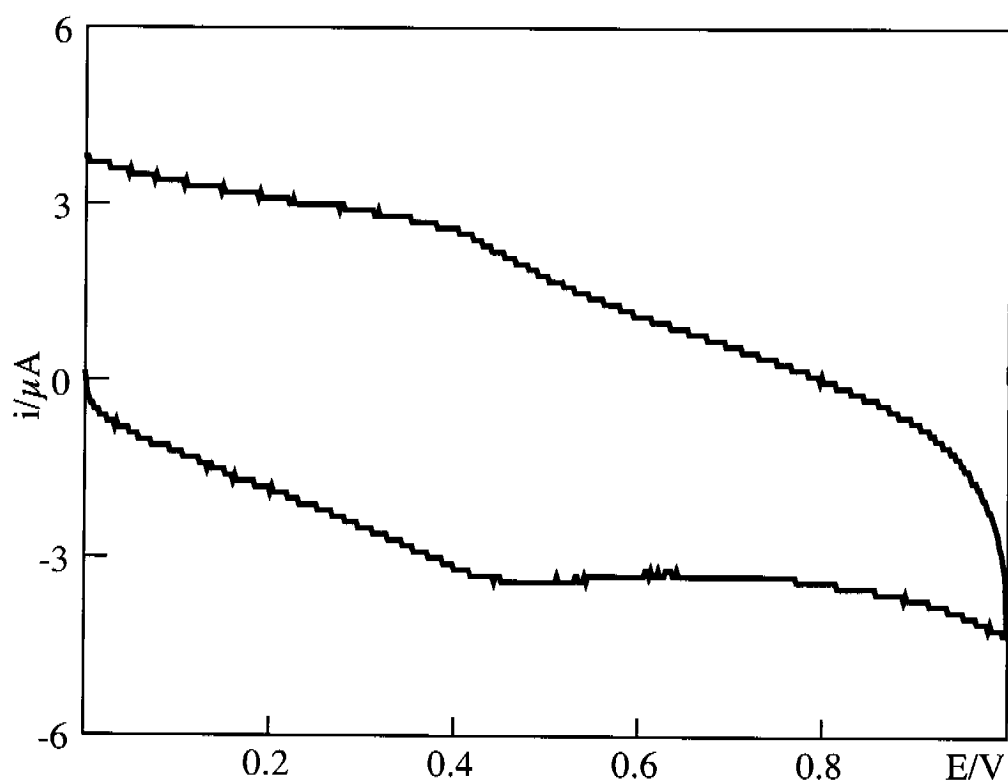
Figure 5.4. CV of a gold wire consecutively modified with PMHS and hydroxymethylferrocene (reaction time: 24 h), recorded in 0.1 M Bu$_4$NPF$_6$ in methylene chloride at a scan rate of 1 V s^{-1}.

5.2.2 Gold surface modifications with PMHS-vinylferrocene and PMHS-hydroxymethylferrocene polymers

The reaction of PMHS with vinylferrocene and the subsequent coverage of a gold surface with the resulting polymer were performed in the same reaction

solution. Since Si–H bonds participate in both reactions, the amount of vinylferrocene added in the first step was calculated to substitute only about 8 % of these bonds in PMHS so that the remaining reaction centers could be used for the reaction of the polymer with the gold surface.

After adding the Pt catalyst to a solution of PMHS and vinylferrocene in toluene-d_8, ^{1}H-NMR spectroscopy data clearly showed that the peaks corresponding to the double bond of vinylferrocene (6.4, 5.3, and 5.0 ppm) had disappeared. On the other hand, the reaction was accompanied by the appearance of multiplets at 2.6, 1.5, and 1.1 ppm ascribed to the newly formed CH_2–CH_2 bond between Si and the ferrocene group. Unfortunately, the complexity of the ^{1}H-NMR spectrum did not allow any conclusion concerning the exact structure of the newly formed polymer. Two possible structures corresponding to the main (a) and side (b) reactions according to [92] are shown in Figure 5.5.

a)   b)
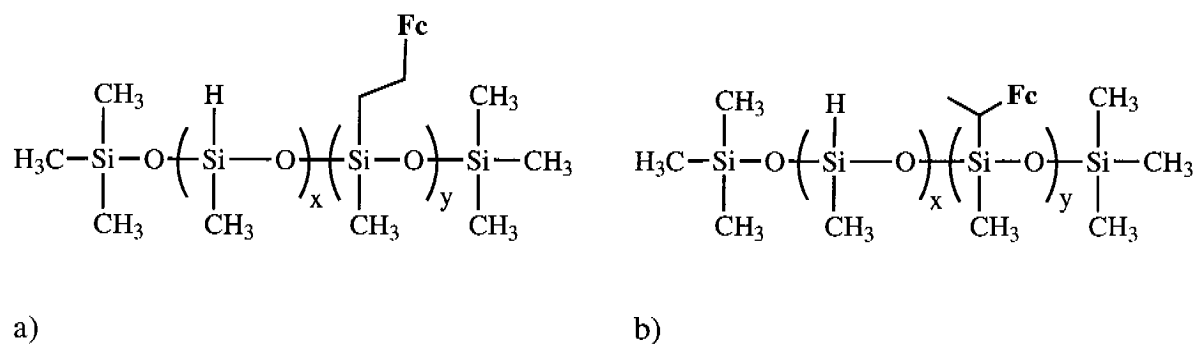
Figure 5.5. Possible structures of the PMHS-vinylferrocene polymer (**Fc**: ferrocenyl):

a) poly[methyl-(2-ferrocenylethyl)siloxane-co-methylhydrosiloxane],

b) poly[methyl-(1-ferrocenylethyl)siloxane-co-methylhydrosiloxane].

The CVs, measured immediately after removing the gold beads from the reaction solution, clearly showed the redox peaks of the ferrocene group. To

51

monitor the stability of the ferrocene attachment, the modified beads were immersed in toluene for 14 days and CVs were recorded almost every second day. After 12 days in toluene, the ferrocene peaks had completely disappeared (see Figure 5.6; for simplicity reasons, only 3 CVs are shown). It was concluded that ferrocene was entrapped but not covalently bound to the polysiloxane layer. As a result, ferrocene was washed out during the immersion in toluene.
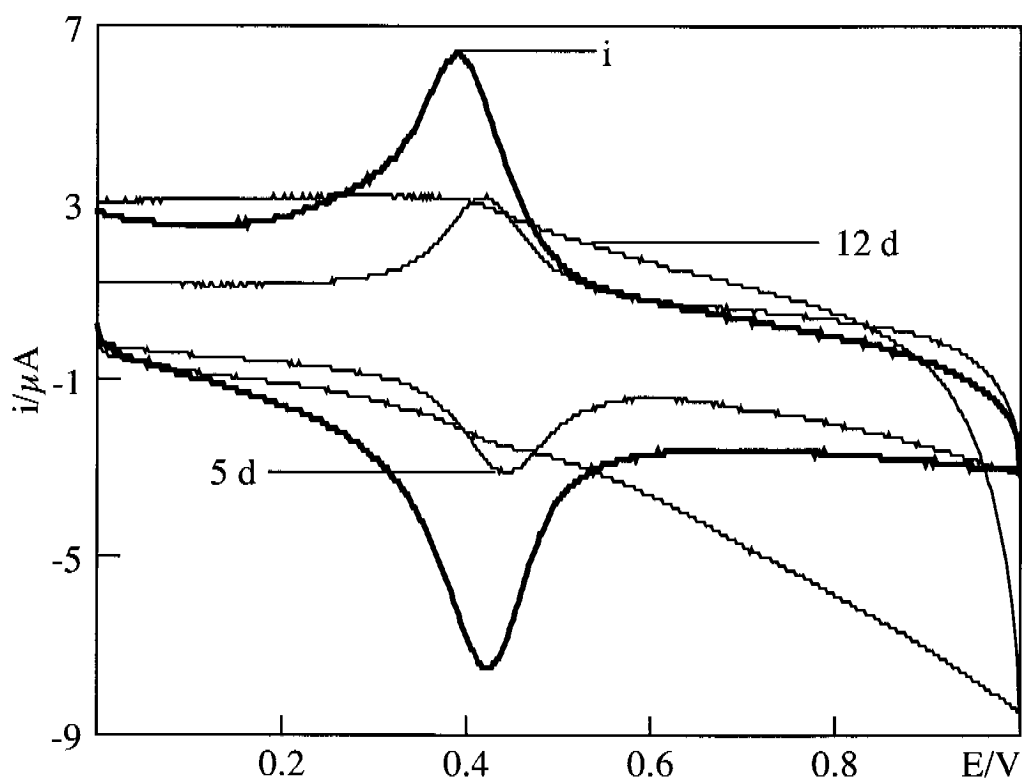
Figure 5.6. CVs of a gold bead modified with PMHS-vinylferrocene polymer acquired immediately after the surface modification (i) and after 5 days (5 d) and 12 days (12 d) of immersion in toluene. The CVs were recorded in 0.1 M Bu_4NPF_6 in methylene chloride at a scan rate of 1 V s^{-1}.

The lipophilicity of the polymer-covered surface was monitored by measuring the advancing contact angles on glass slides, whose surface was covered first with gold and then with the PMHS-vinylferrocene polymer. Immediately after

completing the reaction, the contact angles were about 80°. Washing of the modified substrates in toluene for 14 days did not affect this value, indicating that the PMHS layer was still present on the gold substrate, even though vinylferrocene had been washed out. This conclusion, evidentely, contradicts the ^{1}H-NMR data, which showed that the double bond in vinylferrocene had disappeared, indicating that it had reacted with the polysiloxane. The sole explanation for both observations is that only a relatively low number of PMHS chains, which had reacted with vinylferrocene, were bound to the gold surface.

In complete analogy to the above reaction with vinylferrocene, the modification of PMHS with hydroxymethylferrocene was explored as a potential route for the preparation of redox-active polysiloxane layers. Overnight immersion of gold samples (slides and beads) in the reaction solution was accompanied by the formation of a light brown precipitate, most likely due to polysiloxane cross-linking in the presence of the OH groups of hydroxymethylferrocene.

The advancing contact angles of water measured on gold slides covered with this precipitate were in the range of 95–110°, i.e. 15–30° higher than those observed for the PMHS-vinylferrocene polymer, which confirms the suggested cross-linking. However, these values decreased by about 10° after immersing the slides in water, presumably because of hydrolysis of the Si–O bond. As to the modified gold beads, on part of them were soaked in toluene and the other in water. The corresponding CVs displayed ferrocene peaks that were more or less stable after 3 weeks of immersion in toluene but after the same treatment in water, the CVs showed a drastic decrease in the amount of ferrocene on the modified surface, which was also explained by hydrolysis of the Si–O bonds of the attached ferrocene groups.

5.2.3 PMHS layers modified with 1-ferrocenylundec-10-en-1-one on gold surfaces

Compared with hydroxymethylferrocene, vinylferrocene looks much more promising as a reagent for introducing redox-active centers in PMHS since the Si–C bond formation is not affected by hydrolysis. Most probably, steric hindrance caused by the close proximity of the double bond to the ferrocene unit prevented successful attachment of vinylferrocene to the PMHS layers. A new ferrocene derivative, 1-ferrocenylundec-10-en-1-one (Figure 5.7) with a long alkyl chain between ferrocene and the double bond was synthesized and its reaction with PMHS was examined.
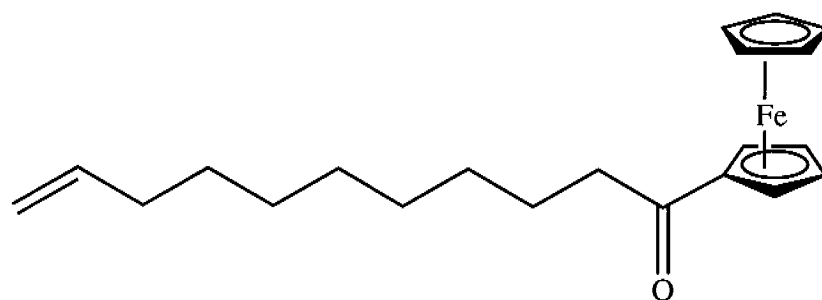
Figure 5.7. Structure of 1-ferrocenylundec-10-en-1-one.

The CVs of gold beads consecutively modified with PMHS and 1-ferrocenylundec-10-en-1-one clearly showed the redox peaks of the ferrocene group (see Figure 5.8). The peak current and, therefore, the amount of ferrocene on the different Au beads cannot be compared with each other because the size of the electrode area varies from bead to bead.

After the first CV measurement, one part of the beads were immersed in water and the other in toluene. The ferrocene peaks measured directly after the reaction decreased drastically by immersing the beads in toluene (see Figure 5.8) indicating a noncovalent attachment of the ferrocene to the PMHS layer.

For the beads immersed in water, a decrease in the ferrocene peaks was observed too, even though less distinctly (see Figure 5.8). Most probably, it was caused by cross-linking of the polysiloxane layer since the poor solubility of 1-ferrocenylundec-10-en-1-one in water would exclude the elution processes.

a)   b)
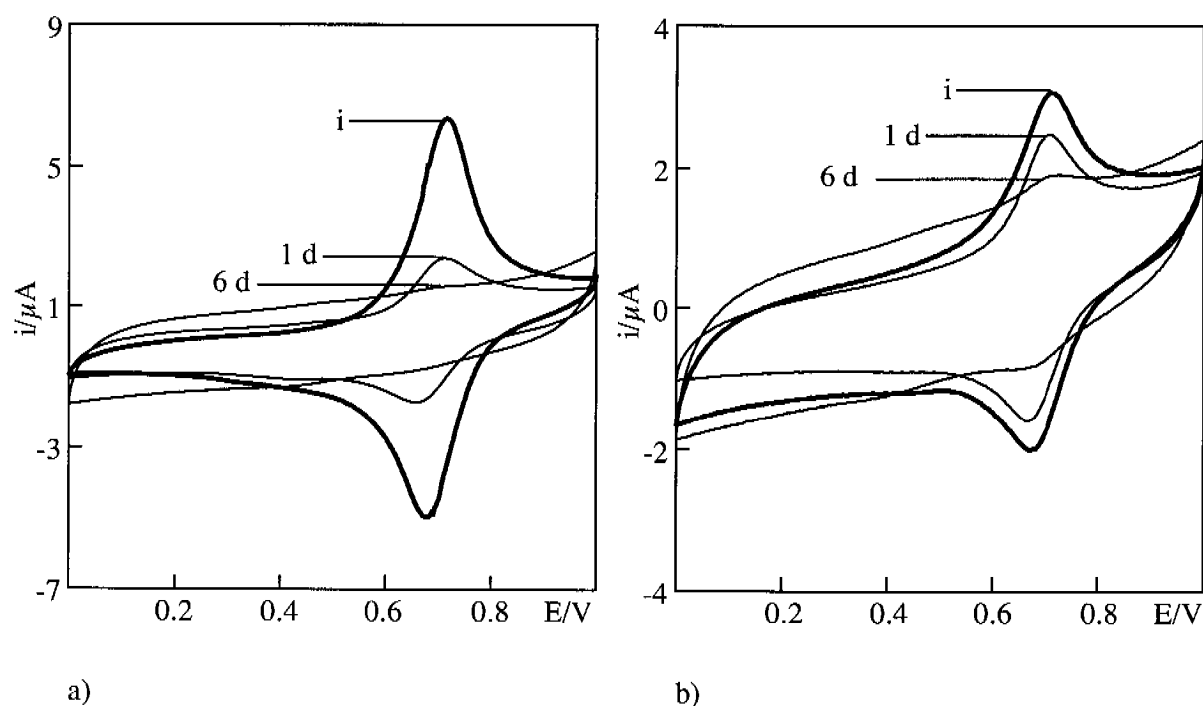
Figure 5.8. CVs of gold beads whose surface was first modified with PMHS and then with 1-ferrocenylundec-10-en-1-one, recorded immediately after surface modification (i) and after one day (1 d) and 6 days (6 d) of immersion in a) toluene and b) water. The CVs were recorded in 0.1 M Bu$_4$NPF$_6$ in methylene chloride, scan rate 1 V s^{-1}.

5.2.4 Gold surface modification with PMHS-1-ferrocenylundec-10-en-1-one polymer

The reaction of PMHS and 1-ferrocenylundec-10-en-1-one in solution was examined in the same manner as described in paragraph 5.2.2. The amount of ferrocene compound used for the reaction was calculated to substitute

approximately 3% of the Si–H bonds in PMHS. The CVs of gold beads modified in this way, measured directly after completing the reaction showed two redox couples present on the electrode surface, with E° at ca. 0.4 V and ca. 0.7 V (see Figure 5.9).
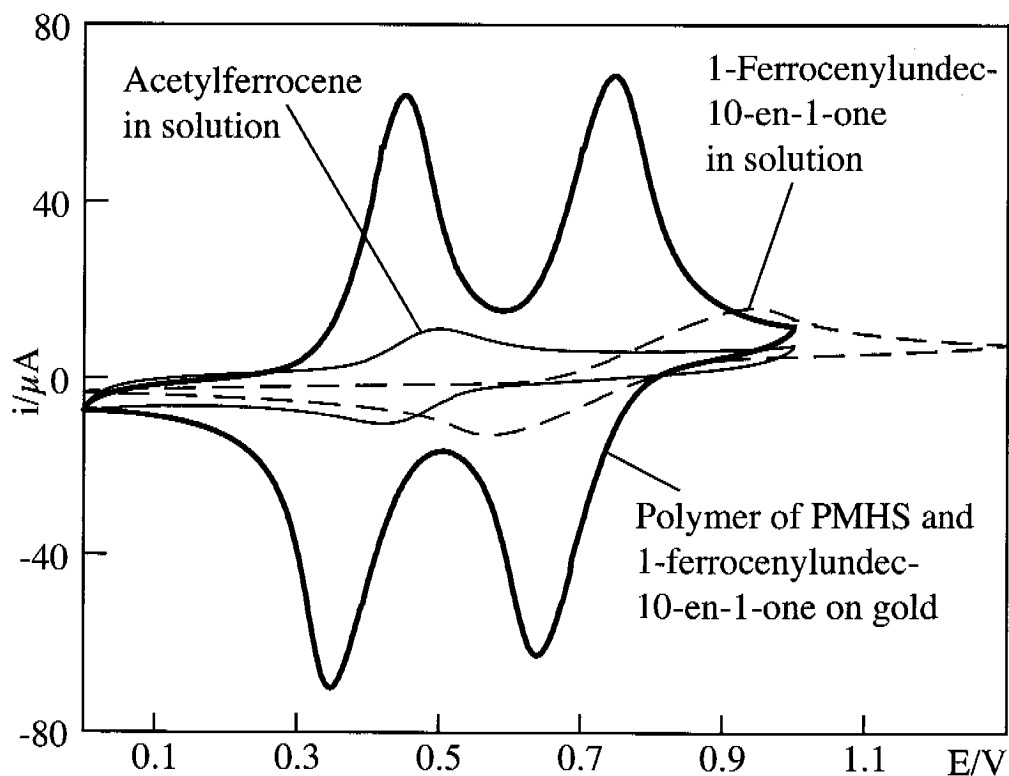
Figure 5.9. The CV of a gold bead treated with a polymer of PMHS and 1-ferrocenylundec-10-en-1-one measured directly after completing the reaction in comparison with CVs of dissolved acetylferrocene and 1-ferrocenylundec-10-en-1-one (each 1 mM; working electrode: gold disk of 7 mm^2 area). The CVs were all recorded in a solution of 0.1 M Bu$_4$NPF$_6$ in methylene chloride, scan rate 1 V s^{-1}.

The formation of these two redox species correlates with the presence of two centers, i.e. a carbonyl group and a double bond, in 1-ferrocenylundec-10-en-1-one capable of reacting with PMHS in the presence of the Pt catalyst. The redox

potential of the couple at 0.7 V is close to that obtained for 1-ferrocenylundec-10-en-1-one dissolved in the same electrolyte solution and was ascribed to the ferrocene attached to PMHS via a CH_2–Si bond (see Figure 5.10 a). In this case, the polymer backbone is separated from the redox center by the large C_{10} alkyl chain and, therefore, has no influence on the redox potential of the ferrocene group.

To confirm the hypothesis of two reaction centers present in 1-ferrocenylundec-10-en-1-one, the reaction of PMHS was repeated with acetylferrocene. The CVs of gold beads modified with this new polymer showed peaks of a redox couple with $E°$ at 0.45 V. Thus, the couple at 0.4 V in the CV of the gold beads modified with the PMHS-1-ferrocenylundec-10-en-1-one polymer was ascribed to the ferrocene compound bound to PMHS via an O–Si bond (see Figure 5.10 b).

a)   b)
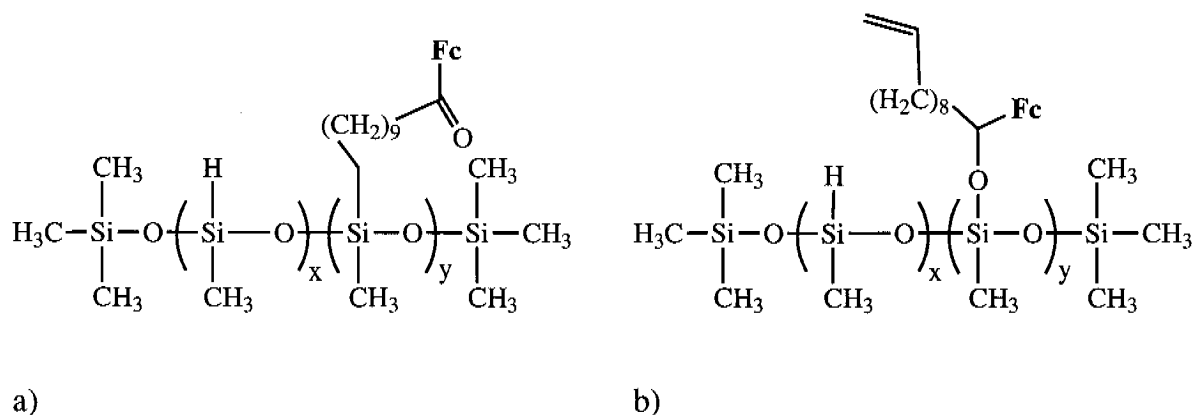
Figure 5.10. Possible structures of the PMHS-1-ferrocenylundec-10-en-1-one polymer (**Fc**: ferrocenyl): a) poly[methyl-(11-ferrocenyl-11-oxoundecyl)-siloxane-*co*-methylhydrosiloxane], b) poly[methyl-(1-ferrocenylundec-10-enyloxy)siloxane-*co*-methylhydrosiloxane].

Beads modified with the PMHS-1-ferrocenylundec-10-en-1-one polymer were immersed in toluene or water. For both solvents, the amount of ferrocene centers

present on the surface decreased with time. After 3 weeks in toluene, according to the CVs, the amount of the redox couple at 0.4 V was still decreasing, whereas it remained approximately the same for the couple at 0.7 V. In water, the amount of both redox couples monotonously decreased (see Figure 5.11). Immersion in water for more than 5 weeks resulted in a shift of both oxidation peaks to higher potentials. This potential shift, however, was not observed in the case of CV measurements at a lower scan rate (0.1 V s^{-1}). For the samples immersed in toluene, neither peak shifts nor the influence of different scan rates on the redox potentials could be detected (see Figure 5.12).

a)   b)
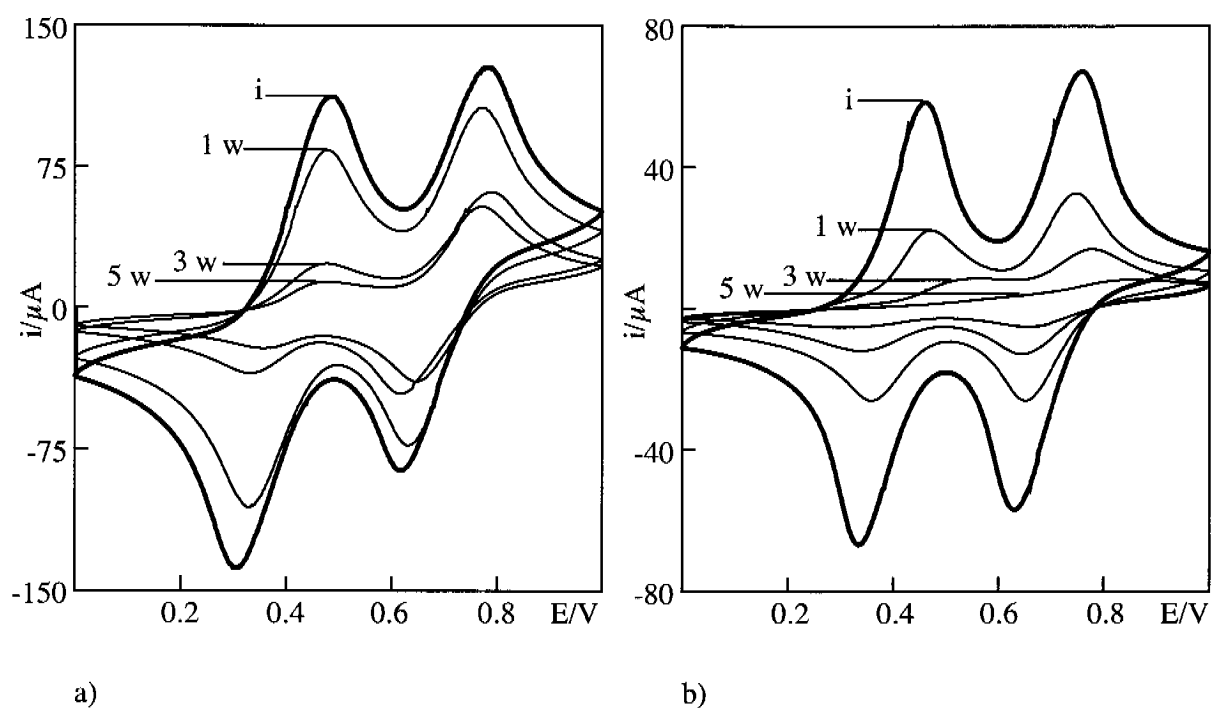
Figure 5.11. CVs of gold beads treated with PMHS-1-ferrocenylundec-10-en-1-one polymer acquired immediately after surface modification (i) and after 1, 3, and 5 weeks (1 w, 3 w, and 5 w, respectively) of immersion in a) toluene and b) water. The CVs were recorded in 0.1 M Bu$_4$NPF$_6$ in methylene chloride, scan rate 1 V s^{-1}.

During the oxidation of the immobilized ferrocene, the electrolyte anion must be transported into the polysiloxane layer to preserve electroneutrality. Hence, the character of the CVs recorded depends on the size of the anion, the structure of the examined layer, and the scan rate, as has been shown previously for ferrocenes immobilized in sol-gels [96].

These repeated CV measurements strongly indicated that Si–H and Si–OR bonds were slowly hydrolyzed in the presence of water, whereupon cross-linking of PMHS took place. Within a cross-linked polysiloxane layer, redox centers become less accessible for the electrolyte anion and therefore, their oxidation requires higher potentials.

a)   b)
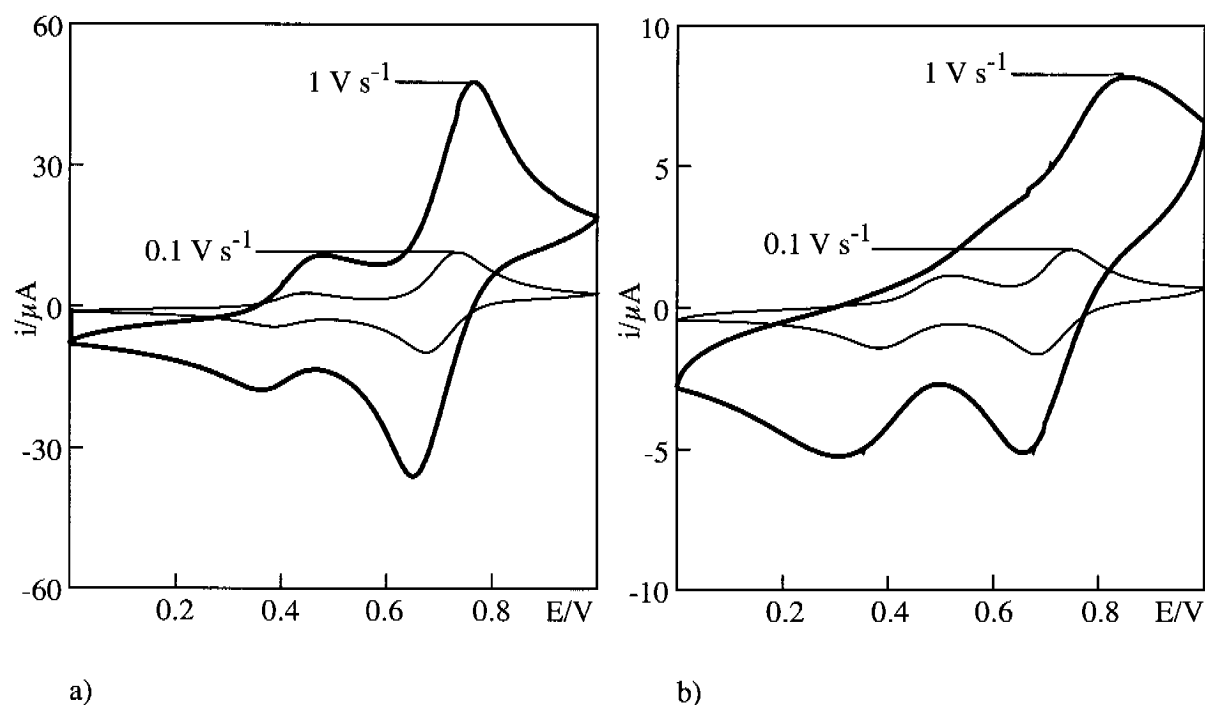
Figure 5.12. CVs of gold beads treated with PMHS-1-ferrocenylundec-10-en-1-one polymer measured at two different scan rates (1 and 0.1 V s^{-1}) after 5 weeks of immersion in a) toluene and b) water. The CVs were recorded in 0.1 M Bu$_4$NPF$_6$ in methylene chloride.

Saturation of non-reacted Si–H bonds with an alkene of low molecular mass, e.g., 1-pentene, was proposed in order to minimize cross-linking in PMHS polymer layers. After the treatment of gold beads with a toluene solution containing pentene and the Pt catalyst, the peaks of the redox couple at 0.4 V almost (in some cases, even completely) disappeared (see Figure 5.13) indicating a partial substitution of Si–O bonds by Si–CH$_2$ bonds.
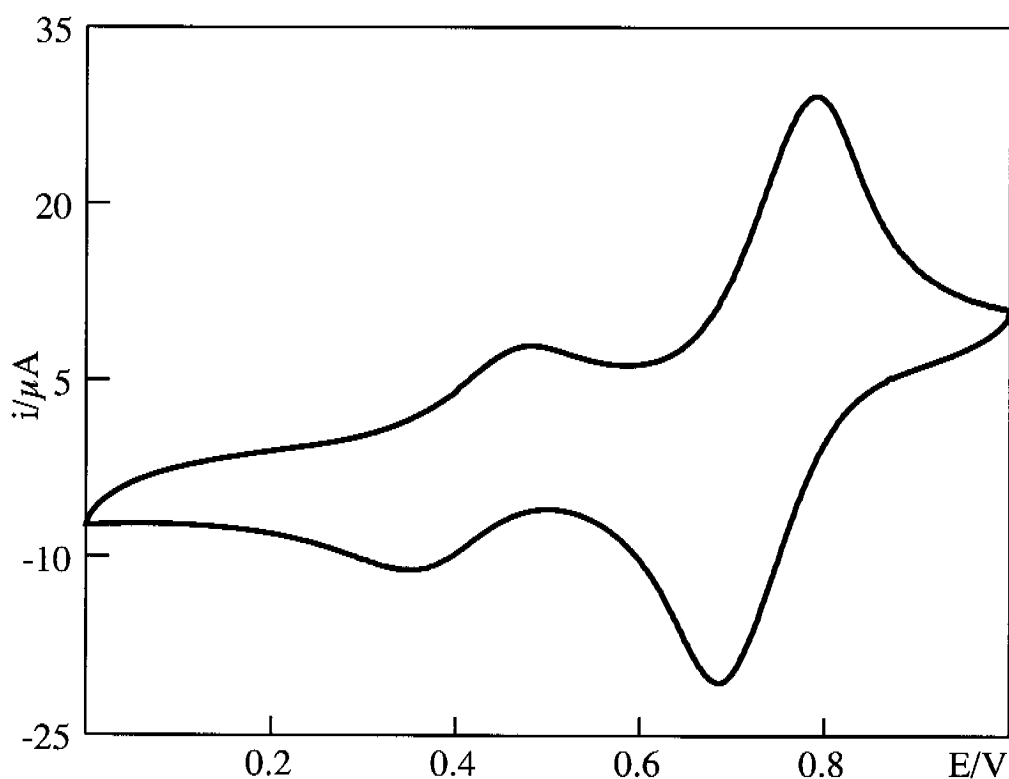
Figure 5.13. The CV of a gold bead whose surface was first modified with PMHS-1-ferrocenylundec-10-en-1-one polymer and afterwards with 1-pentene, recorded in 0.1 M Bu$_4$NPF$_6$ in methylene chloride, scan rate 1 V s^{-1}.

Advancing contact angles measured on gold-coated silicon wafers modified in this way with 1-pentene were even higher than for the samples modified with the PMHS-1-ferrocenylundec-10-en-1-one polymer only (see Table 5.1),

demonstrating that the lipophilicity of the polymer surface could be increased by treatment with 1-pentene.

Table 5.1. Advancing contact angles of water measured on nonmodified and modified gold-coated silicon wafers (SD, n = 6).

Surface	Contact angle [°]
Gold	55.1 ± 3.7
PMHS-1-ferrocenylundec-10-en-1-one polymer on gold	83.0 ± 2.3
PMHS-1-ferrocenylundec-10-en-1-one polymer and 1-pentene on gold	97.6 ± 1.6

5.2.5 Poly(vinylferrocene) entrapped in PMHS and H-PDMS

Physical entrapment of poly(vinylferrocene) (PVF) in polysiloxane layers on Au surfaces was the third approach examined for modifying polysiloxane layers with redox-active species. This type of modification can be carried out at higher concentrations of polysiloxane since a high amount of the redox-active species is already present in the reaction solution. As a result, physical entrapment allows the preparation of thicker polymer films, which provide better electrode surface coverage and higher density of redox-active compound.

Entrapment of PVF in PMHS layers

Poly(vinylferrocene) was entrapped in PMHS by simply adding it to the reaction solution during the surface modification of gold with the polysiloxane.

Comparison of the CVs of PVF in solution and that of a gold bead modified with PMHS in the presence of PVF demonstrated that PVF was indeed immobilized in this newly formed PMHS layer (see Figure 5.14). Owing to the

inhomogeneous surroundings within the polysiloxane matrix, the redox peaks of PVF in the PMHS layer were broader than those of PVF in solution.
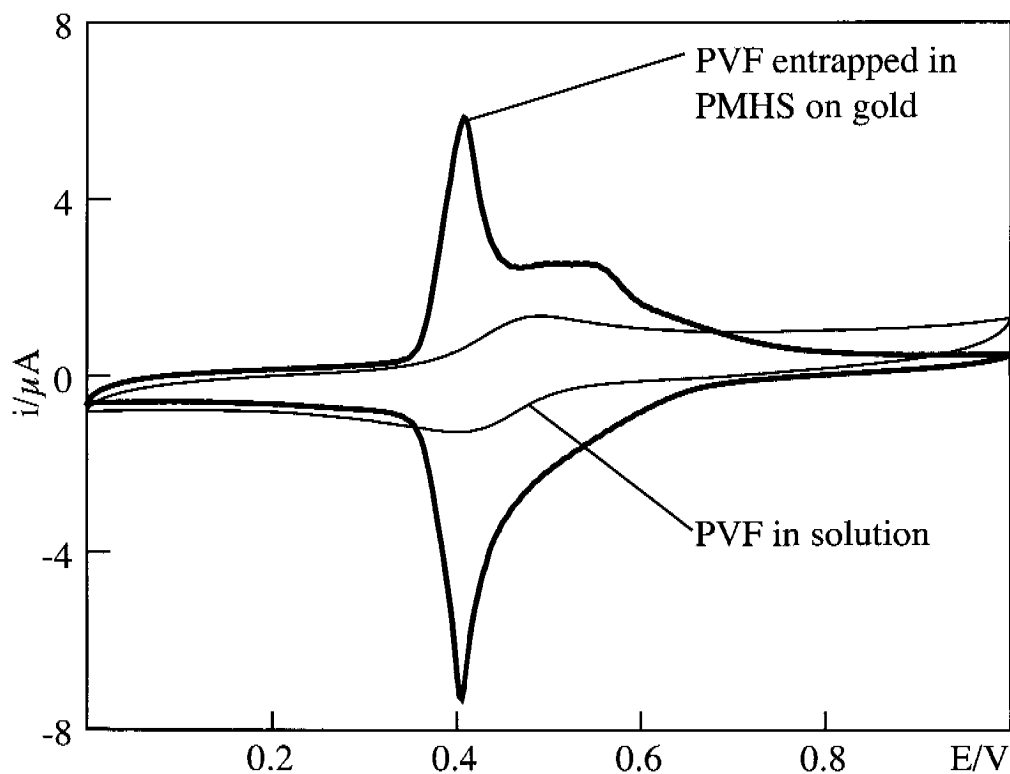
Figure 5.14. CV of a 0.2 mM solution of PVF in methylene chloride containing 0.1 M NBu$_4$PF$_6$ and of a gold bead covered with a PMHS-PVF layer monitored in 0.1 M Bu$_4$NPF$_6$ in methylene chloride; scan rate 0.1 V s^{-1}.

The difference between cathodic and anodic peaks increased with increasing scan rate (see Figure 5.15). Similarly to cross-linked PMHS-ferrocenylundec-10-en-1-one polymer layers (cf. paragraph 5.2.4), CVs of the PMHS-PVF layer showed poor accessibility of the redox centers for the electrolyte anion.
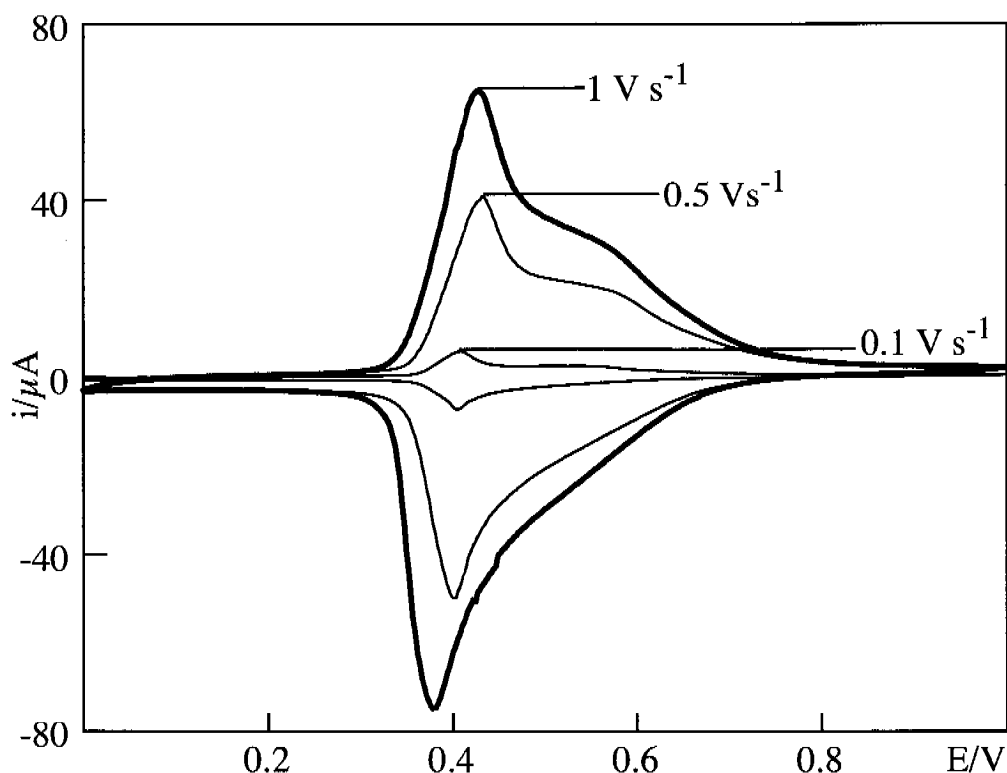
Figure 5.15. CVs of a gold bead covered with a PMHS-PVF layer recorded in 0.1 M Bu$_4$NPF$_6$ in methylene chloride and measured at different scan rates (1, 0.5, and 0.1 V s^{-1}).

The stability of the PMHS-PVF layer on modified gold beads immersed in methylene chloride or water were examined by repeated CV measurements. In this case, methylene chloride was used as a solvent for surface modification because PVF is better soluble in it than in toluene. After 5 d, the CVs of Au beads immersed in methylene chloride became stable (Figure 5.16 a) indicating that a large part of PVF was not washed out of the polysiloxane matrix. On the other hand, the CVs of beads immersed in water were still changing shape and peak height even after 30 d (Figure 5.16 b). Most probably, cross-linking in the PMHS layer induced by water led to changes in the surroundings of the redox centers and therefore to changes in the observed CVs.

The surface coverage of PVF on gold beads was determined by cyclic voltammetry immediately after the surface modification and was $1.1 \pm 0.3 \times 10^{-9}$ mol cm^{-2} (relative to the monomer). This is about one order of magnitude higher than what was found with redox-active SAMs successfully used for SC ISEs [61].
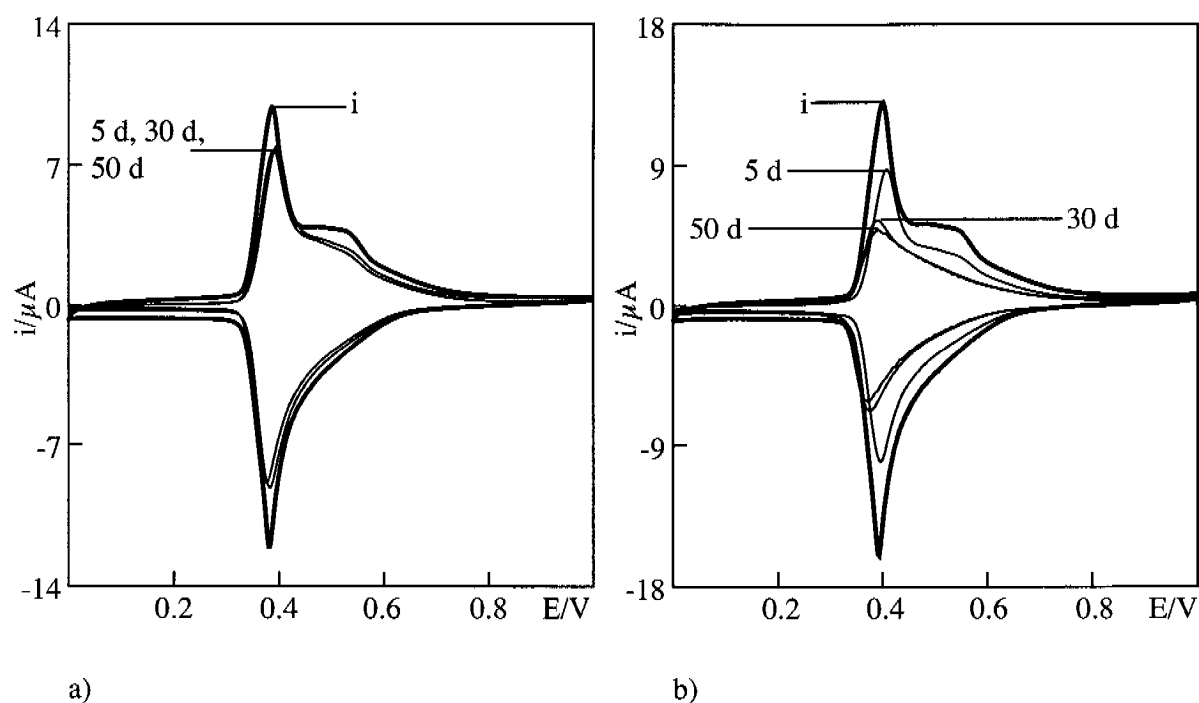
Figure 5.16. CVs of gold beads modified with a PMHS-PVF layer acquired immediately after surface modification (i) and after 5, 30, and 50 days (5 d, 30 d, and 50 d, respetively) of immersion in a) methylene chloride and b) water. The CVs were recorded in 0.1 M Bu_4NPF_6 in methylene chloride, scan rate: 0.1 V s^{-1}.

Gold-coated silicon wafers were modified with a PMHS-PVF layer in the same way as the gold beads to measure advancing contact angles and characterize the lipophilicity of the coating layer (see Table 5.2).

Table 5.2. Advancing contact angles of water measured on nonmodified and modified gold-coated silicon wafers (SD, n = 6).

Surface	Contact angle [°]
Gold	55.1 ± 3.7
PMHS-PVF layer on gold	89.8 ± 1.4

The data in Table 5.2 shows that PMHS-PVF-modified surfaces have higher lipophilicity than bare gold electrodes and that the PMHS was attached to the gold in the presence of PVF in the reaction solution. Thus, the contact angle measurements confirmed the results obtained by CV measurements.

The entrapment of PVF in PMHS layers was successful, although most probably, cross-linking took place upon contact of the layer with water. This led to the idea to apply H-PDMS instead of PMHS for the modification of gold substrates, since it contains Si–H bonds merely as end groups ($-Si(CH_3)_2H$) and, therefore, cannot react with water after the formation of Si–Au bonds.

Entrapment of PVF in H-PDMS

As in the case of PMHS, CVs of gold beads modified with H-PDMS in the presence of PVF and cis-[PtCl$_2$(PhCH=CH$_2$)$_2$] demonstrated that the entrapment of PVF in the polysiloxane has been successful (Figure 5.17).

The polysiloxane H-PDMS has less Si–H groups available for the reaction with gold and, thus, forms bigger loops on the substrate surface. Therefore, it was expected that PVF is washed out faster from the PDMS than from the PMHS layers. This expectation was confirmed by repeated CV measurements of PDMS-PVF-modified gold beads after different immersion times in methylene chloride or water (Figure 5.17). The CVs of beads whose surface was modified with a PDMS-PVF layer, washed in methylene chloride still showed decreasing peak currents after 50 d of washing, while corresponding beads with a PMHS-

PVF layer exhibited stable CVs already after 5 d. This demonstrated that in methylene chloride, PVF was slowly washed out of the PDMS matrix.

The CVs of the samples immersed in water also showed a continuous peak decrease. Since hydrolysis of the polysiloxane layer can be excluded and PVF is not soluble in water, another explanation had to be found for this observation. It is possible that, in a polar medium (water), a rearrangement of the lipophilic layer occurred, which led to a change in the surroundings of the redox centers. This, of course, could also occur in PMHS layers exposed to water.
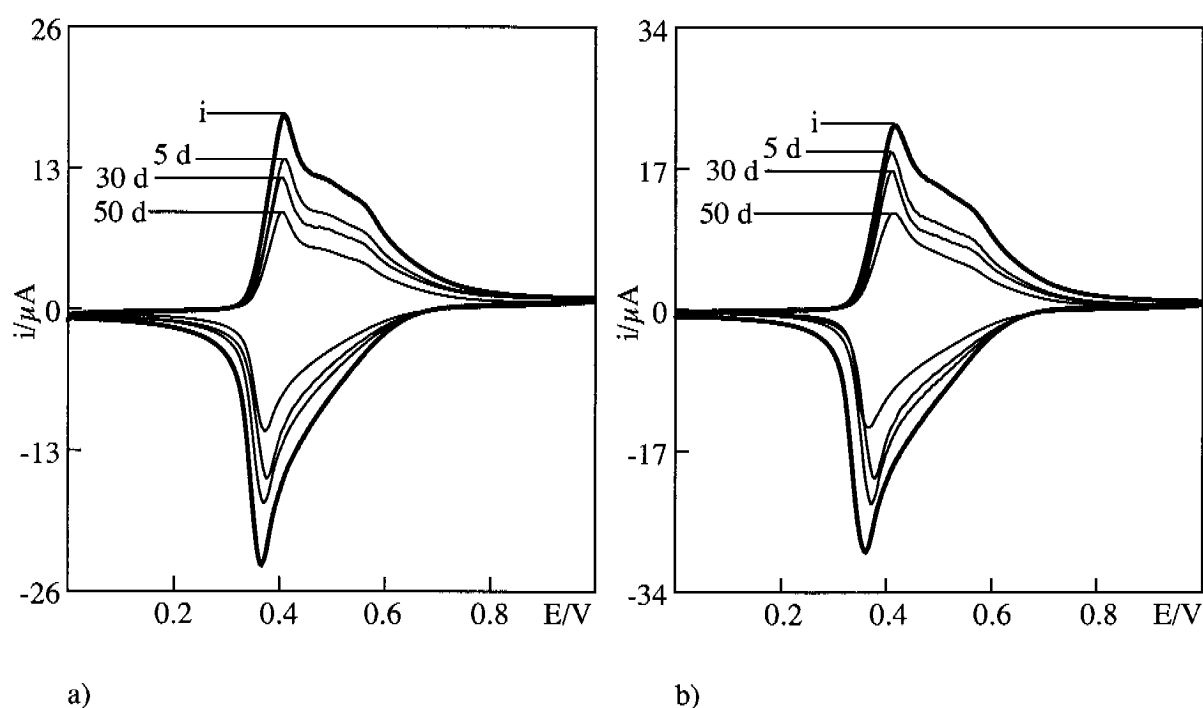
Figure 5.17. CVs of PDMS-PVF-modified gold beads recorded immediately after surface modification (i) and after 5, 30, and 50 days (5 d, 30 d, and 50 d, respectively) of immersion in a) methylene chloride and b) water. The CVs were recorded in 0.1 M Bu$_4$NPF$_6$ in methylene chloride, scan rate 0.1 V s^{-1}.

Gold-coated silicon wafers were modified in the same way as the beads in order to measure contact angles (see Table 5.3).

Table 5.3. Advancing contact angles of water measured on nonmodified and modified gold-coated silicon wafers (SD, n = 6).

Surface	Contact angle [°]
Gold	55.1 ± 3.7
PDMS-PVF layer on gold	97.5 ± 1.5

Advancing contact angles measured on the PDMS-PVF-modified surfaces were about 10° higher than those for PMHS-PVF samples, making the PDMS modification a promising possibility with regard to its application for SC ISEs.

5.3 Electrode design

The experiments described in the previous parts of this chapter showed that any clean gold surface can be modified with layers of PMHS and PDMS if appropriate reaction conditions are chosen. Therefore, various constructions based on internal gold electrodes were taken into account and examined for developping SC ISEs with polysiloxane layers as solid contact material.

The two electrode assemblies considered first are presented in Figure 5.18. Assembly a) is based on 1 mm thick gold wires and is interesting in view of minimizing electrode dimensions. Assembly b) employs commercially available gold disk electrodes, which are widely utilized for SC ISEs, especially when SC material is prepared by electropolymerization. Good insulation of gold wire electrodes was hard to achieve and imperfect construction often caused electrical short-circuits, whereas gold disk electrodes were purchased with a Teflon® insulation and did not show this problem. However, the Teflon® insulation cannot be removed during the polysiloxane modification reaction and, therefore, PMHS coverage of the gold disk was often incomplete.

a)   b)
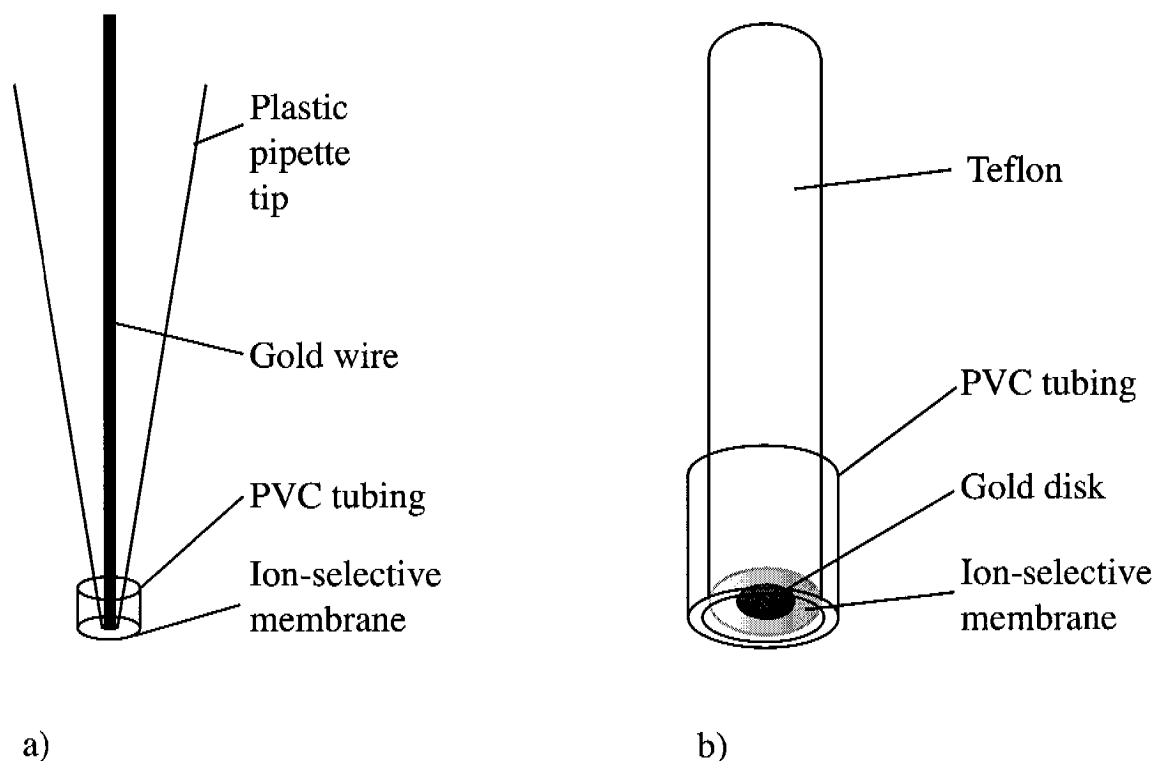
Figure 5.18. Two different electrode assemblies for polysiloxane-modified SC ISEs: a) gold wire and b) gold disk electrode.

In another, completely different ISE geometry, the internal electrodes used as substrates for the polysiloxane modification reaction consisted of gold-coated glass slides or silicon wafers. The ion-selective membrane was simply drop-cast onto the modified gold surface and the electrodes were fixed in two measuring cells developed for the purpose. The first one, described in [97] (p. 153), used three SC ISEs mounted in parallel (three-electrodes cell) and a batch-mode measuring system. The second one was a flow-through cell with two arrays of electrodes (one of 4 and the other of 5 electrodes) pressed onto the flow channel holes in the cell body (Figure 5.19).
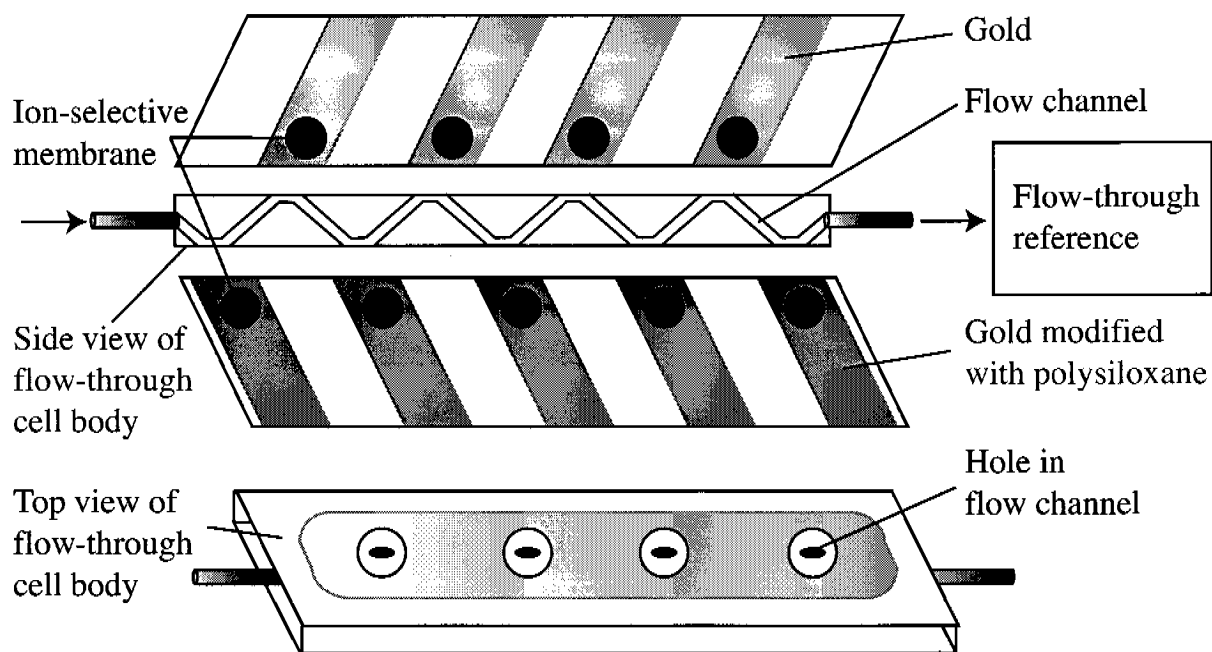
Figure 5.19. Schematic illustration of flow-through cell with Au electrodes (the cell body is also described in [86]).

The three-electrodes cell was used in order to compare the results obtained with those of similar Ca^{2+}-selective SC ISEs using a SAM as a solid contact and measured in the same cell [97]. Compared with the three-electrodes cell in which the sample was stirred mechanically, the flow-through cell had the advantage of smaller Nernstian diffusion layers on the electrode surface. This, together with a strongly reduced electrode area (2 mm^2 compared with 13 mm^2 in the three-electrodes cell), could be an important advantage in view of measurements at very low sample concentrations.

5.4 SC ISEs modified with PMHS-PVF layers

In the following, potentiometric experiments are described for characterizing SC ISEs based on Au/PMHS-ferrocene as solid contact. For simplicity reasons, results are presented only for PMHS-PVF layers since the other solid contact

materials examined (PMHS-1-ferrocenylundec-10-en-1-one polymer without or with additional pentene modification) gave very similar results.

The composition of the Ca^{2+}-selective polyurethane-based ISE membrane (CaPuM, cf. paragraph 5.8.6) was the same as that used for the SC ISEs with redox-active SAMs described in ref. [97]. It was chosen in order to directly compare the results found here with those of the above-mentioned reference. The selectivity coefficients of LC ISEs with this membrane obtained for the most important interfering ions are given in Table 5.4.

Table 5.4. Potentiometric selectivity coefficients, log K_{CaJ}^{pot}, and response slopes (in parantheses, mV decade^{-1}; concentration range 10^{-1}–10^{-3} M) obtained by the separate solution method [16] with LC ISEs based on membrane CaPuM (SD, n = 5).

Ion J	CaPuM (LC ISEs)
Na^+	-5.9 ± 0.3 (54.6 ± 1.1)
K^+	-6.6 ± 0.3 (49.8 ± 0.3)
H^+	-2.0 ± 0.2 (54.2 ± 0.9)
Mg^{2+}	-8.5 ± 0.1 (26.9 ± 0.9)

The corresponding SC ISEs were prepared from gold-coated glass slides subsequently covered with a PMHS-PVF layer and the ISE membrane. After drop casting the membrane solution and allowing it to dry, the electrodes were mounted in the three-electrodes cell. For comparison purposes, the membrane of one of the three electrodes was directly cast onto the gold without PMHS-PVF surface modification (coated-wire type electrode). Figure 5.20 shows the SC ISE calibration curves measured after 12 h of conditioning in 10^{-3} M $CaCl_2$.

Figure 5.20. Calibration curves obtained by successively decreasing the Ca^{2+} activity of the sample (background: 10^{-4} M NaCl) in the three-electrodes cell for Ca^{2+}-selective SC ISEs with (A) and without (B) PMHS-PVF layer on Au.

Neither the slope nor the linear response range of the coated-wire type electrode differed from those of the SC ISE with a PMHS-PVF layer on Au. The relatively high detection limit of 10^{-6} M Ca^{2+} - the lower detection limit of Ca^{2+}-selective SC ISEs with a redox-active SAM was around $10^{-7.5}$ M [97] - may have been caused either by insufficient stirring of the sample solution in the measuring cell and/or by the formation of an inner water layer between membrane and gold electrode. As expected, the water layer test (cf. Chapter 4, paragraph 4.3.2) conducted on these electrodes revealed the presence of a water layer between ISE membrane and solid-contact material or gold in both kinds of SC ISEs (Figure 5.21).
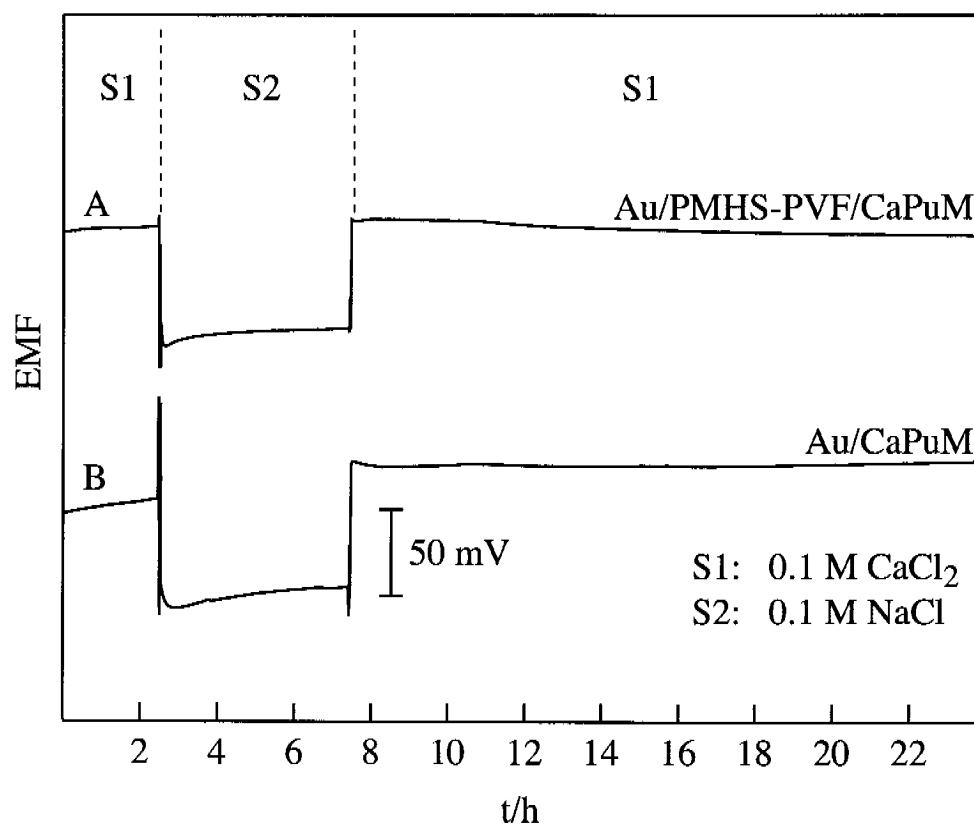
Figure 5.21. Water layer test in the three-electrodes cell on Ca^{2+}-selective SC ISEs with (A) and without (B) PMHS-PVF layer on Au.

The SC ISEs were also tested for oxygen sensitivity (Figure 5.22). For this test, oxygen was first removed from the solution by bubbling argon through it. In a second step, the solution was saturated with oxygen, which was removed again after a certain time. The potential steps observed upon saturation of the sample with oxygen were similar for both kinds of SC ISEs. Thus, by using a PMHS-PVF solid contact, neither the formation of an inner water layer nor oxygen sensitivity could be prevented and the electrode performance was not improved compared with the SC ISEs having an unmodified gold surface.

Figure 5.22. Influence of O_2 on the EMF of Ca^{2+}-selective SC ISEs with (A) and without (B) PMHS-PVF layer on Au in the three-electrodes cell. Sample solution: 0.1 M $CaCl_2$.

Shortly after these experiments, a new flow-through cell (cf. Figure 5.19) became available in which flat electrodes based on gold-covered silicon wafers can be used. Compared with the three-electrodes cell, better lower detection limits were expected with this measuring setup because the sample flow would reduce the thickness of the Nernstian diffusion layer at the electrode surface. Calibration curves as well as water layer and oxygen sensitivity tests were repeated in the flow-through cell with an array of five electrodes modified with a PMHS-PVF layer on one side and an array of four electrodes with unmodified Au surface on the other.
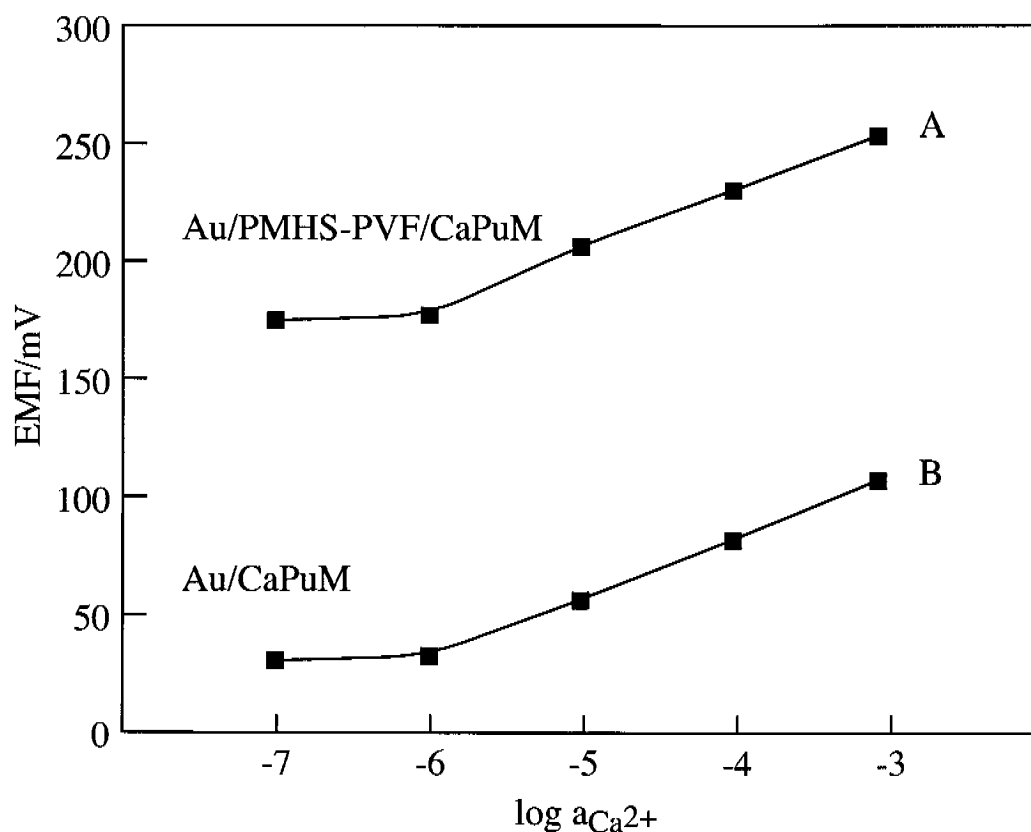
Figure 5.23. Calibration curves obtained by successively decreasing the Ca^{2+} activity of the sample (background: 10^{-4} M NaCl) in the flow-through cell for Ca^{2+}-selective SC ISEs with (A) and without (B) PMHS-PVF layer on Au.

Here too, no difference was observed in the slopes and lower detection limits of the calibration curves between PMHS-PVF-modified and coated-wire type SC ISEs (Figure 5.23). However, their lower detection limits were better by about two orders of magnitude as compared with the analogous SC ISEs in the three-electrodes cell. This improvement was first ascribed to a reduction in the thickness of the Nernstian diffusion layer owing to the new flow-through setup. Surprisingly, in the water layer test, none of the SC ISEs showed potential drifts when changing from a sample solution of the primary ion to one of an interfering ion, which indicates the absence of an inner water layer (Figure 5.24).

Figure 5.24. Water layer test in the flow-through cell on Ca^{2+}-selective SC ISEs with (A) and without (B) PMHS-PVF layer on Au.

It was proposed that the pressure applied on the membrane surface owing to the construction of the cell, prevented the formation of an inner water layer. This hypothesis was supported by results obtained by Gyurcsányi et al. for K^+-selective polypyrrole SC ISEs examined in the same flow-through cell as used here [86]. The absence of an inner water layer can also explain the better lower detection limit observed in the flow-through cell.

The sensitivity of the electrodes toward oxygen was examined next (Figure 5.25). Based on the results of the water layer test, no sensitivity to oxygen was expected. Additionally, in the case of PMHS-PVF electrodes, a redox-active layer was present between internal electrode and membrane, which should prevent or, at least, reduce the oxygen sensitivity of the SC ISEs. Coated-wire

type electrodes showed only a slight response (1–2 mV) toward increasing oxygen concentration in the sample solution, whereas PMHS-PVF electrodes, unexpectedly, responded slightly stronger. However, with a potential step of about 3 mV, they were less sensitive than the corresponding SC ISEs in the three-electrodes cell (potential step of about 15 mV). It was assumed that also with PMHS-PVF ISEs applied in the flow-through cell, some water was present between membrane and internal electrode that led to the observed oxygen sensitivity. However, because of the pressure applied on the membrane, this layer was not sufficiently thick to be revealed by the water layer test.
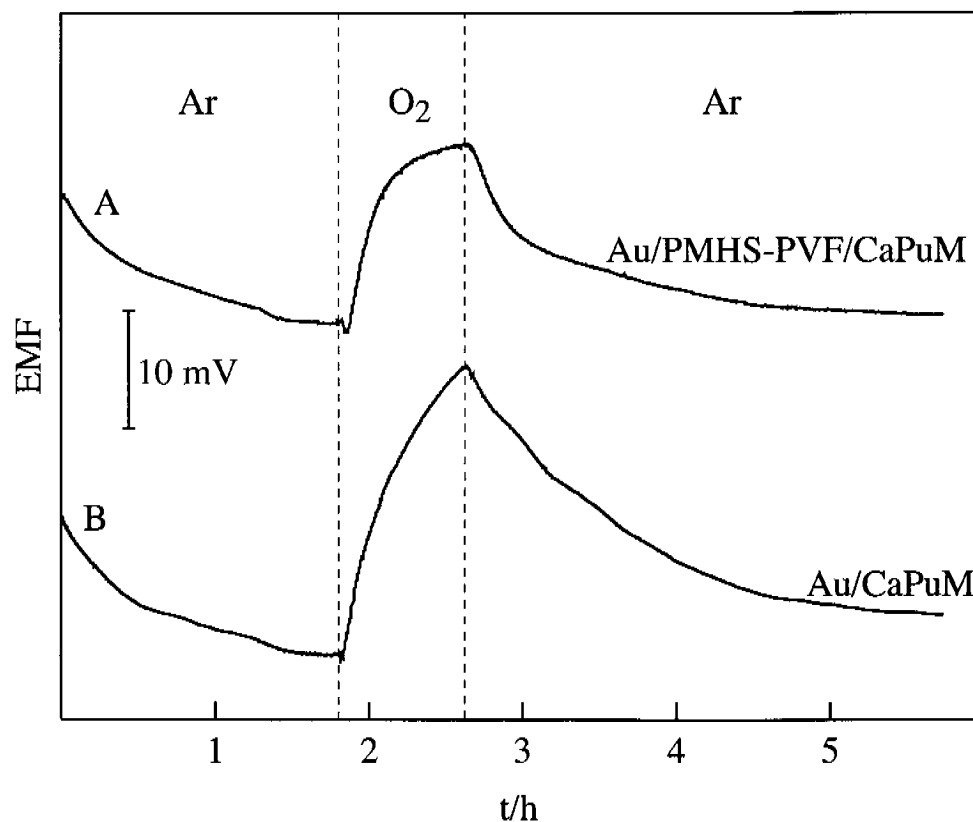
Figure 5.25. Influence of O_2 on the EMF of Ca^{2+}-selective SC ISEs with (A) and without (B) PMHS-PVF layer on Au in the flow-through cell. Sample solution: 0.1 M $CaCl_2$.

5.5 SC ISEs modified with PDMS-PVF layers

From the potentiometric experiments described in the previous paragraph, it was concluded that a water layer is formed in SC ISEs based on redox-active PMHS solid-contact material, and, in spite of the fact that advancing contact angles measured on PMHS-PVF layers suggested a high surface lipophilicity (cf. paragraph 5.2.5, Table 5.2). Possibly, a decrease in lipophilicity took place during the conditioning of the ISEs in aqueous samples. It was assumed that during this process, water diffused through the membrane hydrolyzing the non-reacted Si–H bonds in the PMHS layer so that polar Si–OH groups were formed.
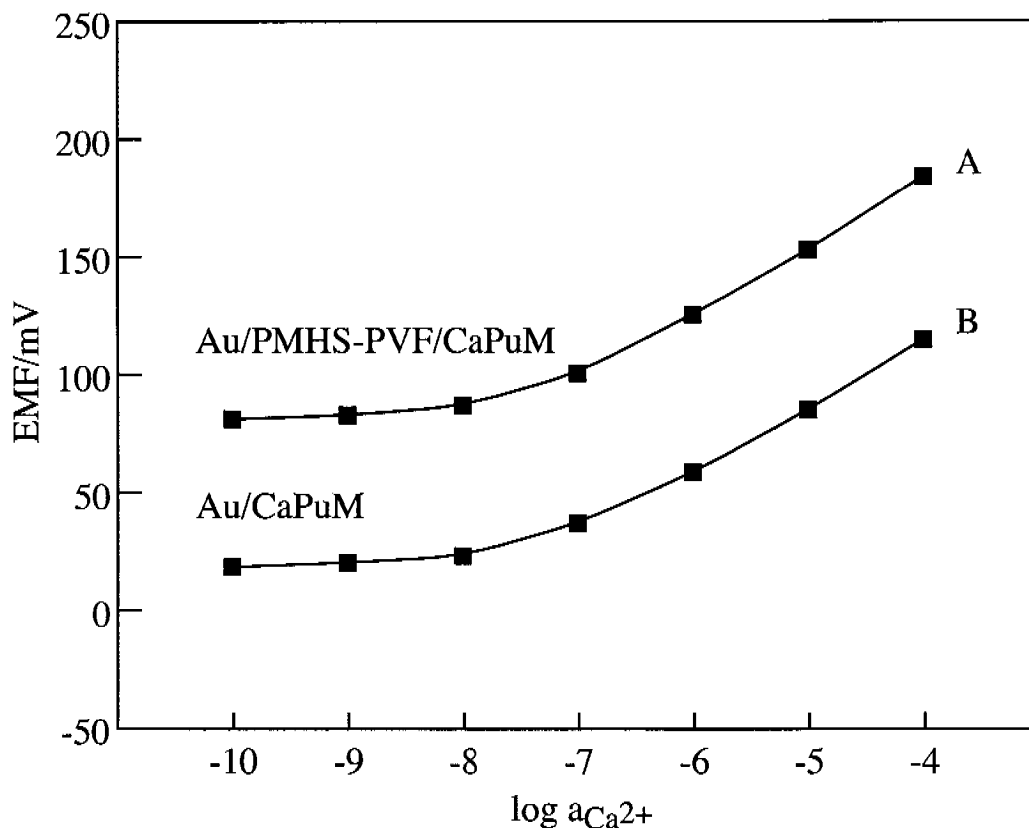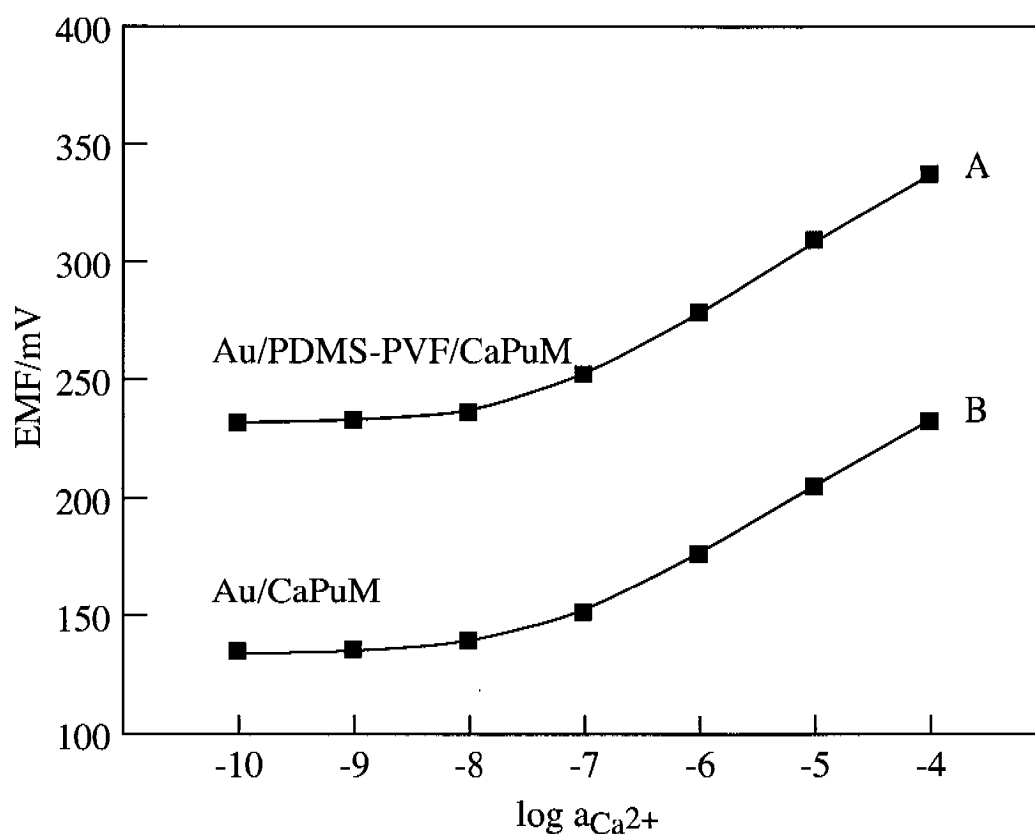

Figure 5.26. Calibration curves obtained by successively decreasing the Ca^{2+} activity of the sample (background: 10^{-4} M NaCl) in the flow-through cell for Ca^{2+}-selective SC ISEs with (A) and without (B) PDMS-PVF on Au.

In contrast to PMHS, PDMS layers cannot react with water and were therefore examined next as potential solid-contact material. Potentiometric measurements with PDMS-PVF-modified gold electrodes were carried out in the flow-through cell. The calibration curves (Figure 5.26) and results of the water layer test (Figure 5.27) did not differ from those of PMHS-PVF SC ISEs measured in the same cell. Also in this case, an inner water layer could not be detected.
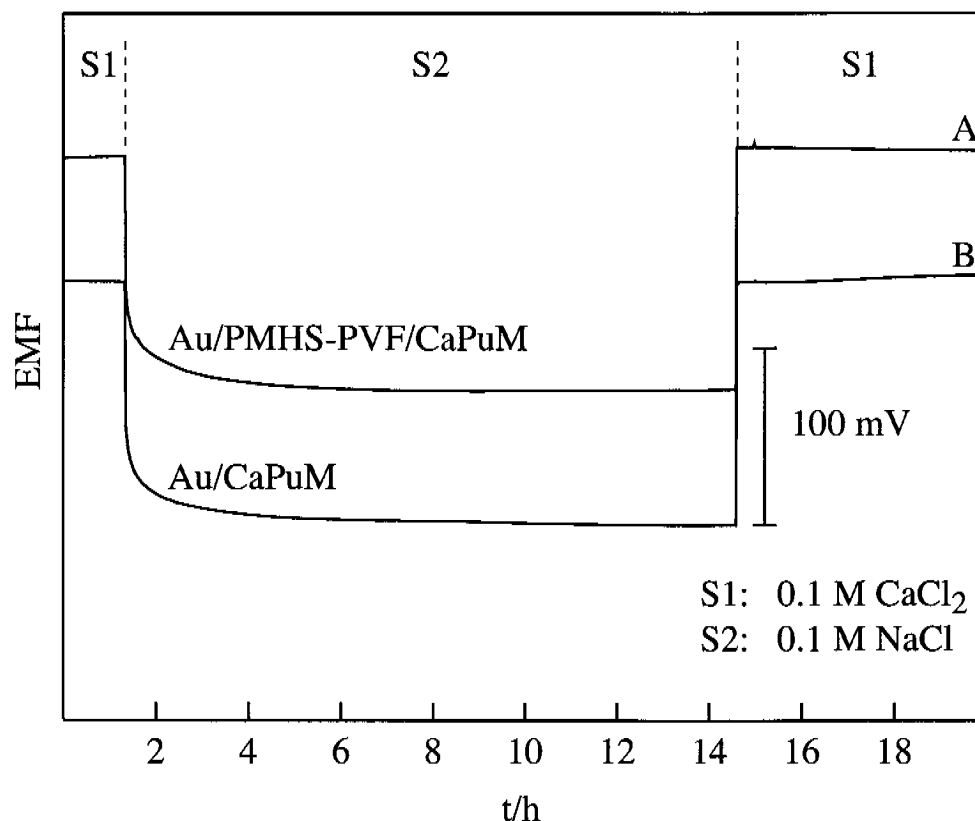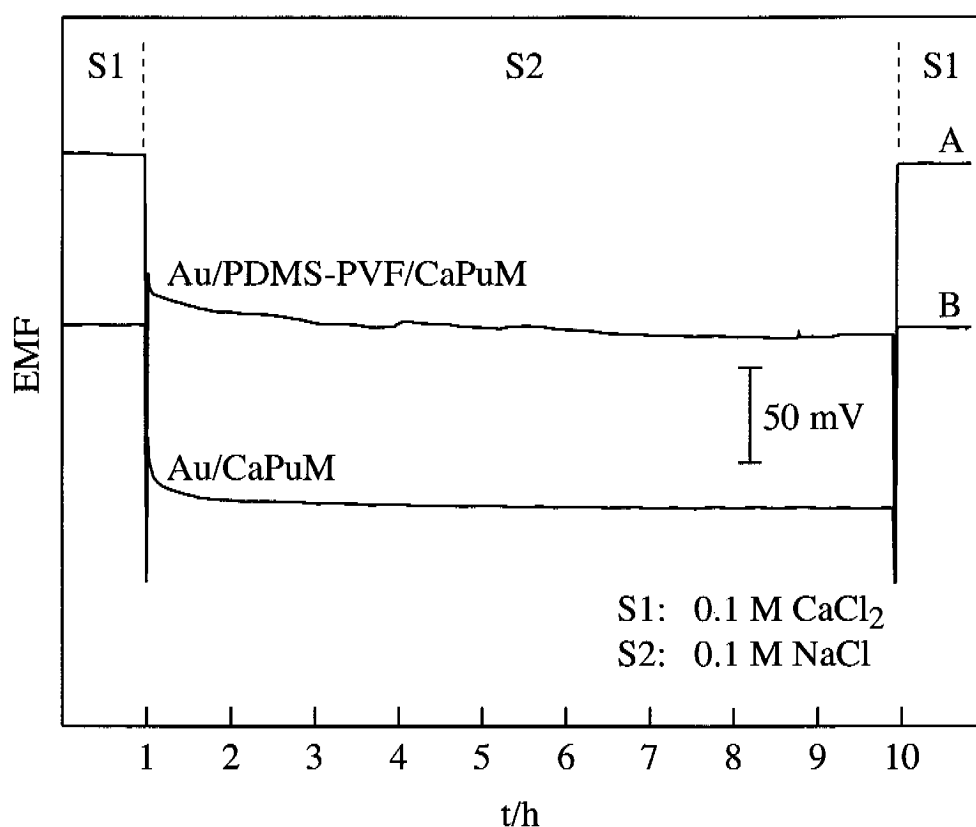

Figure 5.27. Water layer test in the flow-through cell on Ca^{2+}-selective SC ISEs with (A) and without (B) PDMS-PVF layer on Au.

When tested for sensitivity to oxygen, PDMS-PVF SC ISEs showed a much higher EMF response (step of about 18 mV) than the corresponding PMHS-PVF electrodes (Figure 5.28). Since PDMS-PVF layers do not contain Si–H groups, hydrolysis could not be considered as the reason for this oxygen sensitivity.

Thus, it was assumed that pinholes in the polysiloxane layer are responsible for this phenomenon. H-PDMS forms big loops on the gold surface and hence, its layers may contain larger holes than similarly prepared PMHS layers. Although these holes have no influence on the measured contact angle of water on such layers, they render the lipophilicity of the SC layer inhomogeneous and, therefore, can be responsible for the penetration of water into it and, subsequently, for the sensitivity of the SC ISE to oxygen.
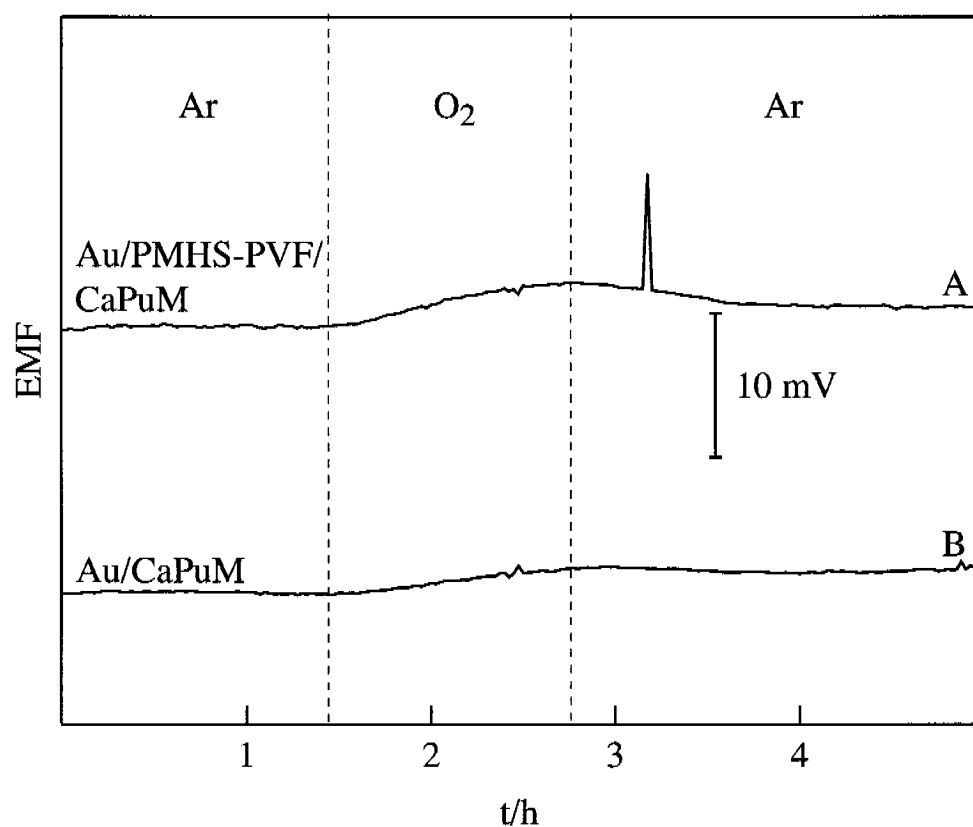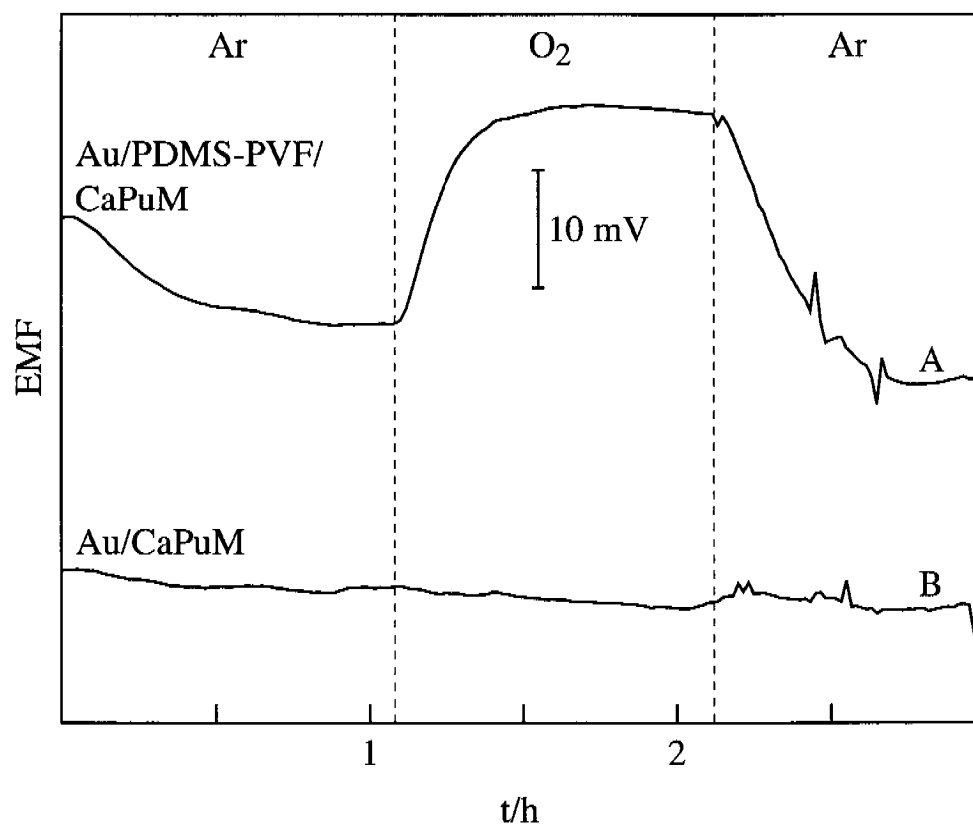

Figure 5.28. Influence of O_2 on the EMF of Ca^{2+}-selective SC ISEs with (A) and without (B) PDMS-PVF layer on Au in the flow-through cell. Sample solution: 0.1 M $CaCl_2$.

5.6 Study on pinholes in polysiloxane layers on gold surfaces

5.6.1 Study on pinholes in PMHS layers

It is well known that the presence of pinholes and defective sites in isolating layers on conducting surfaces can be examined with the help of voltammetric experiments, e.g., cyclic voltammetry performed in a solution containing a redox marker. Electron transport at an electrode covered with a surface layer acting as an electron and ion barrier can occur in three ways [85,98]:

- tunneling of electrons through the layer;

- permeation of redox species from the solution into the layer followed by diffusion to the electrode surface where electron transfer takes place;

- diffusion of redox species through pinholes and/or defective sites to the electrode surface where electron transfer takes place.

In order to examine whether PMHS layers attached to gold substrates contained pinholes or not, gold bead electrodes were modified with PMHS analogously to the procedure used for the preparation of Au/PMHS-PVF layers (cf. paragraph 5.2.5) but in a reaction solution without PVF added. As a redox marker for cyclic voltammetry, $K_4[Fe(CN)_6]$ in aqueous solution was used. The CV of a bare gold electrode with the same area served as a reference.

The PMHS layers studied are fairly thick (4–5 nm, [93]) and have a relatively high hydrophobicity according to contact angle measurements. For this reason, neither electron tunneling through the polysiloxane layer nor permeation of the highly hydrophilic ions of $K_4[Fe(CN)_6]$ into it seems to be a probable mechanism of charge transport. Therefore, if the polysiloxane layer is free of pinholes and defective sites, no redox peaks of the redox marker in solution should be observed.

Cyclic voltammograms (Figure 5.29) showed that Fe^{2+}/Fe^{3+} redox peaks of gold electrodes modified with PMHS were clearly reduced in comparison to those of

a bare Au electrode. The polarogram-shaped voltammogram (sigmoidal curve) observed for the PMHS-covered electrodes indicates that the surface coverage is close to unity [99]. Only a very small part of the gold surface was not blocked by PMHS.

An increase in the reaction time from 1 h up to 24 h, during which gold electrodes were exposed to PMHS solution, did not improve the insulation of the gold surfaces.
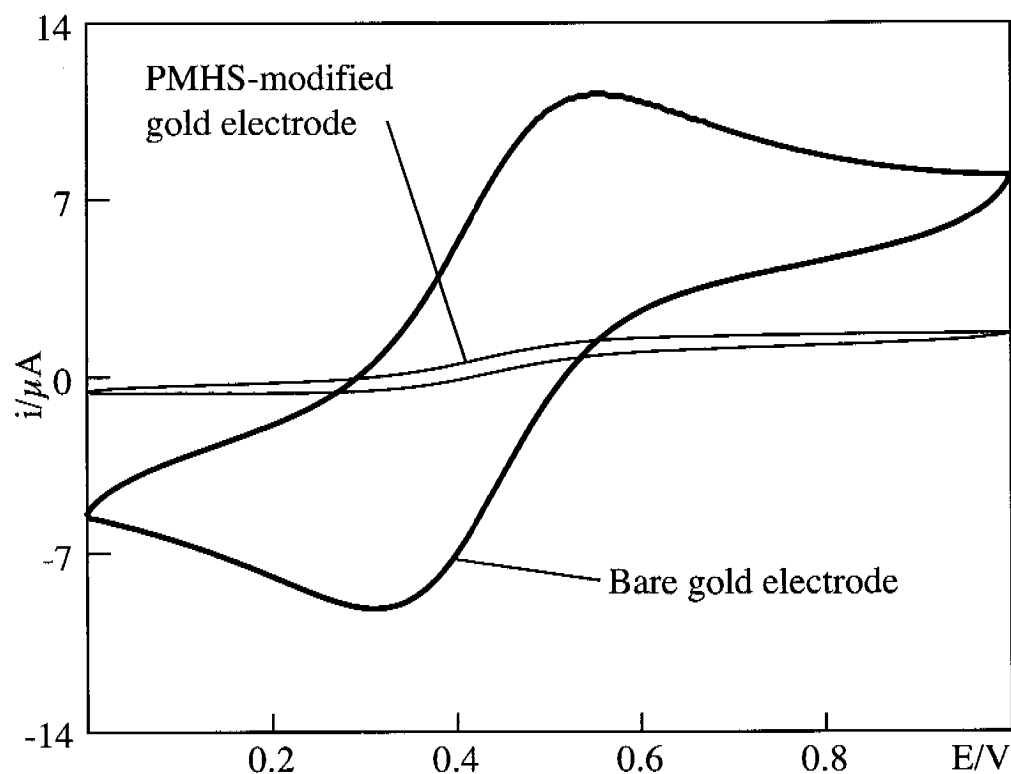
Figure 5.29. CVs of a bare gold bead electrode and of one modified with PMHS measured in 1 mM K$_4$[Fe(CN)$_6$] in a 1 M KCl solution, scan rate 0.1 V s^{-1}.

5.6.2 Study on pinholes in PDMS layers

The pinhole test was repeated for electrodes modified with H-PDMS. The peak currents of modified electrodes were only slightly lower than those of the bare gold electrode of the same area (see Figure 5.30). The modification did not

affect the shape of the CV clearly showing that the surface coverage obtained with H-PDMS was much lower than in the case of PMHS. Thus, the assumption was confirmed that PDMS-based SC ISEs are more sensitive to oxygen than those with PMHS because of higher defective site density.
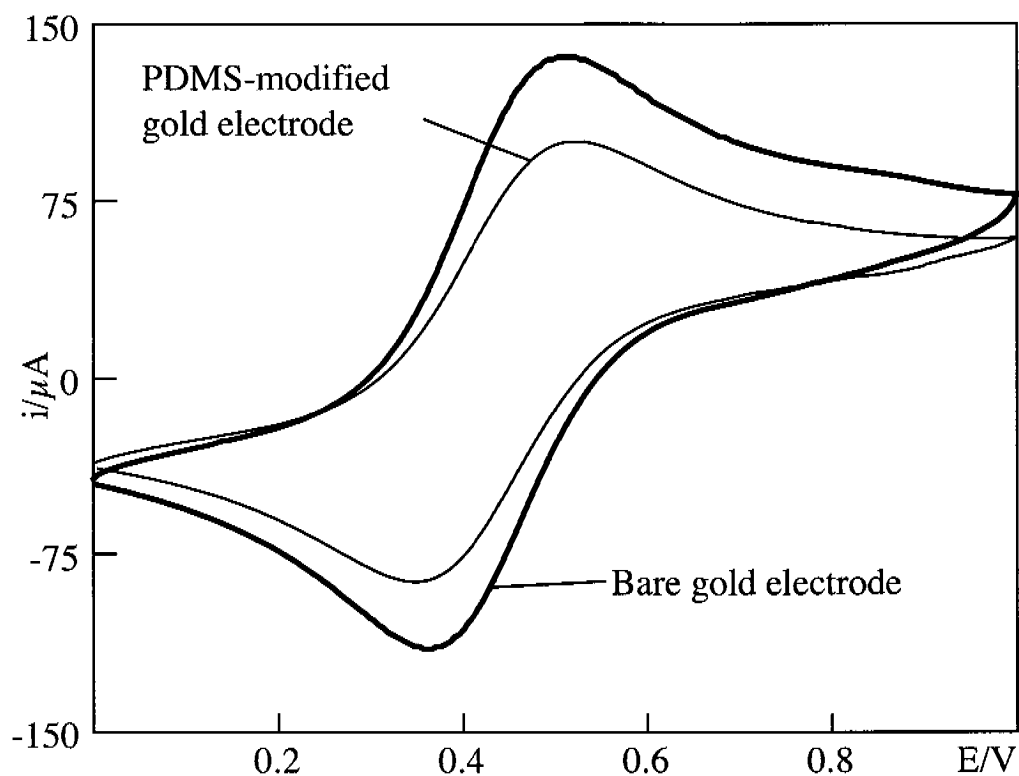
Figure 5.30. CVs of a bare gold bead electrode and of one modified with H-PDMS measured in 1 mM $K_4[Fe(CN)_6]$ in a 1 M KCl solution, scan rate 0.1 V s^{-1}.

To confirm the presence of a high fraction of pinholes, PDMS-modified electrodes were further treated with 1-octanethiol, which can form monolayers on gold surfaces, thus filling the holes. The corresponding CVs (results not given) showed an effectively reduced current compared with the electrodes modified only with PDMS and assumed a sigmoidal shape as observed for PMHS-covered gold electrodes.

5.7 Conclusions

With the aim of preparing redox-active polysiloxane layers that can be used as solid-contact materials in ISEs, several routes were explored including the covalent attachment of redox-active species to the polymer layer, the previous modification of the polysiloxane with a redox-active species, and the physical entrapment of the latter in the polymer layer. Various ferrocene derivatives were examined as redox-active centers. Stability and redox activity of the new solid-contact materials were carefully examined by means of cyclic voltammetry and advancing contact angles measurements on gold substrates modified with these polymers and soaked for different periods of time in organic solvents and water. Modification of gold with PMHS-1-ferrocenylundec-10-en-1-one polymer and entrapment of PVF in PMHS along with the covalent attachment of the latter to a gold surface were found to meet the requirements of lipophilicity and redox activity, both crucial for further applications of these polysiloxanes in SC ISEs. While the former requirement is dictated by the necessity of avoiding the formation of an inner water layer, the latter is directly connected with the stability of the ISE potential. For the two above mentioned solid-contact materials, the advancing contact angles of water measured on flat, modified gold substrates were above 80° corresponding to a high surface lipophilicity. The redox-active ferrocene centers were not (or very slowly) washed out of the polysiloxane layer during several days of soaking in toluene, methylene chloride, or water. In terms of lipophilicity and stability, the entrapment of PVF in PDMS layers was even more promising since this polymer, unlike PMHS layers, cannot undergo hydrolysis and cross-linking.

The polysiloxane-based polymers meeting the requirements of solid-contact materials were examined in Ca^{2+}-selective SC ISEs. Compared with coated-wire type electrodes, the PMHS-PVF SC ISEs did not show improved potential stabilities. The water layer and oxygen sensitivity tests performed in a three-

electrodes cell showed that an water layer was formed between solid contact and ISE membrane during the conditioning of the electrodes, pointing to an insufficient lipophilicity of the PMHS-PVF layer. By applying a flow-through cell setup, in which the membrane is strongly pressed against the solid-contact layer, the formation of an inner water layer was partly avoided. However, PMHS-PVF-modified electrodes examined in this cell turned out to be more sensitive to oxygen than the corresponding coated-wire type electrodes. Since for PDMS-PVF-modified electrodes the oxygen sensitivity was even stronger, both kinds of polysiloxane layers were examined for pinholes. Voltammetric pinhole tests clearly indicated the presence of pinholes in both PMHS and PDMS layers. While PMHS layers block the gold surface almost entirely, PDMS layers only slightly reduce the accessibility of redox-active species in solution to it and are, therefore, more sensitive toward oxygen than PMHS layers.

The overall performance of the SC ISEs examined here was not improved compared with SC ISEs already described in the literature (e.g., SC ISEs with redox-active SAMs [60,61,87]). Notwithstanding, the immobilization of ferrocene species with PMHS or H-PDMS on metal surfaces described in this chapter provides a simple route to ferrocene-containing polymer layers (for other examples, see [100,101]), which, unfortunately, cannot be used for the preparation of SC ISEs owing to the presence of pinholes in the polysiloxane layers.

5.8 Experimental

5.8.1 Reagents

All solvents were purchased from Fluka (Buchs, Switzerland) and were of UV quality grade except for toluene, which was puriss. absolute (over molecular sieve). Poly(methylhydrosiloxane) (PMHS, M_n = 2270) and Si–H-terminated poly(dimethylsiloxane) (H-PDMS, M_n = 28 000) were from ABCR (Karlsruhe, Germany). cis-[PtCl$_2$(PhCH=CH$_2$)$_2$] (Pt catalyst) was synthesized by Global Surface AG (Zürich, Switzerland). Vinylferrocene (97%,) was from Aldrich (Milwaukee, WI, USA), hydroxymethylferrocene (99%) from Strem Chemicals (Newburyport, MA, USA), and poly(vinylferrocene) (PVF) from Polyscience Inc. (Warrington, PA, USA). The calcium ionophore (N,N-dicyclohexyl-N',N'-dioctadecyl-3-oxapentanediamide, ETH 5234), potassium tetrakis-[3,5-bis-(trifluoromethyl)phenyl]borate (KTFPB), tetradodecyl-ammonium tetrakis(4-chlorophenyl)borate (ETH 500), Tecoflex®, bis-(2-ethylhexyl) sebacate (DOS), tetrahydrofuran (THF), and cyclohexanone (all Selectophore®), 1-pentene and 1-octanethiol (both purum), tetrabutylammonium hexafluorophosphate (Bu$_4$NPF$_6$, electrochemical grade), potassium hexacyanoferrate(II) trihydrate (K$_4$[Fe(CN)$_6$]•3H$_2$O, puriss. p.a.), CaCl$_2$, NaCl, and KCl (all p.a.) were from Fluka. Hydrochloric acid (1 mol L^{-1}, Titrisol®), sulfuric acid (95–97%, p.a.), and H$_2$O$_2$ (p.a.) were from Merck (Darmstadt, Germany). Aqueous solutions were prepared with deionized water (specific resistance, 18 MΩ cm; Nanopure; Barnstead, Basel, Switzerland).

1-Ferrocenylundec-10-en-1-one was synthesized at the ETH Zürich (all chemicals used for the synthesis were reagent grade from Fluka):

Methylene chloride (150 mL) was cooled to 0 °C in an ice bath under Ar. Ferrocene (20 mmol) and AlCl$_3$ (20 mmol) were added to the flask and mixed well by stirring under argon. 10-Undecenoyl chloride (20 mmol) in CH$_2$Cl$_2$ (50

mL) was added dropwise to the flask in 2 h. The reaction mixture was stirred for another 20 min and then poured into ice water (20 mL). The organic phase was washed with water until the aqueous phase had pH 7. The organic phase was dried over $MgSO_4$ and concentrated to 20 mL under vacuum. The residue was purified by column chromatography on silica gel with hexane acetic acid ethyl ester (7:3) as eluent. The solvent of the second fraction was removed under vacuum to give liquid 1-ferrocenylundec-10-en-1-one ($C_{21}H_{28}OFe$). Yield: 73%. ^{1}H-NMR (300 MHz, toluene-d_8): 4.95 (*t*, 2H), 5.80 (*m*, 1H), 4.75 (*s*, 2H), 4.45 (*s*, 2H), 4.18 (*s*, 5H), 3.80 (*t*, 2H), 2.17 (*m*, 2H), 1.70 (*m*, 2H), 1.38 (*m*, 10H). Elemental analysis, found: C, 70.93, H, 7.76 %; calc.: C, 71.60, H, 8.01 %.

5.8.2 Gold electrodes

Five types of gold electrodes were prepared as substrates for polysiloxane modifications as described in the following. *Gold beads* were formed at the tip of gold wires (Ø 0.5 mm, 99.995%, ChemPur, Karlsruhe, Germany) in a butane/propane flame. The wire was then insulated by melting a glass capillary onto it.

Gold wires (Ø 1 mm, 99.99%, ChemPur) were polished with 0.3 μm alumina (Metrohm AG, Herisau, Switzerland) and further cleaned by immersion in piranha solution (80% concentrated H_2SO_4 and 20% H_2O_2) at 80 °C for 1 h. Then, the wires were rinsed with water and dried in an Ar stream.

Gold disks for rotating disk electrode (Ø of gold disk, 3 mm; tip Ø, 10 mm) mounted in a Teflon® body (Metrohm) were polished with 0.3 μm alumina and further cleaned by sonication in piranha solution at room temperature, followed by washing with water and ethanol. After that, electrodes were dried in an Ar stream.

Microscope slides (glass, 7.54 cm x 2.54 cm) were cleaned by immersion in piranha solution at 80 °C for 1 h, rinsed with water and ethanol, and dried in a

stream of warm air. On the other hand *silicon wafers* (Philips Semiconductors) were rinsed with water and acetone and dried in an Ar stream. Gold substrates were received by thermal evaporation of gold (200 nm, 99.99%, Johnson Mattey, Zürich) with deposition rates of 2 nm s^{-1} onto the respective supports (slides, wafers) covered with a layer of Cr (6 nm, 99.99%, Balzers, Liechtenstein) using a Balzers MED 010 instrument at a pressure of ca. 10^{-3} Pa.

5.8.3 Surface modifications with PMHS and H-PDMS

Gold surfaces were immersed immediately after their preparation into adsorption solutions, previously deoxygenated by Ar bubbling and kept under Ar. After every reaction step, electrodes were rinsed with toluene or methylene chloride and dried in an Ar stream. Unless otherwise mentioned, modifications were done at room temperature.

Surface modification with PMHS and vinylferrocene or PMHS and hydroxymethylferrocene

For covalent attachment of PMHS, gold electrodes were first immersed for 10 min in a toluene solution of PMHS (0.17 mM) and *cis*-[PtCl$_2$(PhCH=CH$_2$)$_2$] (50 μM). For attachment of the ferrocene compound to the polysiloxane layer, electrodes were immersed during 2 h in a toluene solution containg either vinylferrocene or hydroxymethylferrocene (0.5 mM) and *cis*-[PtCl$_2$(PhCH=CH$_2$)$_2$] (50 μM).

Surface modification with PMHS-vinylferrocene polymer or PMHS-hydroxymethylferrocene polymer

Vinylferrocene or hydroxymethylferrocene (0.72 mM) was added to a solution containing PMHS (0.25 mM) and *cis*-[PtCl$_2$(PhCH=CH$_2$)$_2$] (50 μM) in toluene. The solution was stirred during 48 h. To assure covalent attachment of the thus

formed polymer to the gold surface, another 50 µM of Pt catalyst was added to the reaction solution (to give a total concentration of 100 µM) in which gold electrodes were immersed during 16 h.

Surface modification with PMHS and 1-ferrocenylundec-10-en-1-one

Gold electrodes were covered with a PMHS layer (for procedure see PMHS-vinylferrocene and PMHS-hydroxymethylferrocene modifications). To vary the thickness of PMHS layers, samples were immersed into the reaction solution for 30 min or 45 min. For further modification with the ferrocenyl compound, gold electrodes were immersed in a solution of 1-ferrocenylundec-10-en-1-one (0.73 mM) and cis-[PtCl$_2$(PhCH=CH$_2$)$_2$] (50 µM) in toluene for 24 h.

Surface modification with PMHS-1-ferrocenylundec-10-en-1-one polymer

To obtain the polymer, PMHS (0.13 mM) was added to a solution of 1-ferrocenylundec-10-en-1-one (1.4 mM) and cis-[PtCl$_2$(PhCH=CH$_2$)$_2$] (50 µM) in toluene. The solution was stirred for 3 h and then gold electrodes were immersed in it for 24 h.

For further modification with pentene, beads were immersed into a toluene solution of 1-pentene (7 mM) and cis-[PtCl$_2$(CH$_2$=CHPh)$_2$] (50 µM) for 20 h.

Surface modifications with poly(vinylferrocene)-polysiloxane

Gold surfaces were immersed into a methylene chloride solution containing poly(vinylferrocene) (2.4 mM relative to the monomer), cis-[PtCl$_2$(PhCH=CH$_2$)$_2$] (50 µM), and either PMHS or H-PDMS (1 mM) for 1 h.

5.8.4 NMR spectroscopy

NMR spectra were measured on a Bruker Avance DPX-300 MHz spectrometer. Chemical shifts are given in ppm relative to tetramethylsilane as internal

standard. The signal multiplicities are labeled as follows: *s,* singlet; *d,* doublet; *t,* triplet; *dd,* doublet of doublet; *m,* multiplet.

PMHS: ^{1}H-NMR (300 MHz, toluene-d_8): 5.04 (*d*, 1H), 0.28 (*m*, 3H).

Vinylferrocene: ^{1}H-NMR (300 MHz, toluene-d_8): 6.35 (*dd*, 1H), 5.30 and 4.98 (*dd*, 2H), 4.20 and 4.03 (*m*, 4H), 3.97 (*s*, 5H).

5.8.5 Surface characterisation

Contact angle measurements

Advancing contact angles of water were determined with a Ramé-Hart 100-00 Goniometer (Mountain Lakes, NJ, USA) at room temperature under atmospheric pressure. Nanopure water (3 μL) was dropped two times onto the same spot on the surface with a Hamilton syringe. Angles were read off on the right and left side of each drop (see Figure 4.4).

Cyclic voltammetry

Cyclic voltammetric measurements were performed either with an EG&G Princeton applied research model 263A potentiostat/galvanostat or a μAutolab Type II potentiostat/galvanostat (Eco Chemie, Utrecht, Netherlands). A Ag|AgCl|3 M KCl electrode (Bioanalytical Systems, West Lafayette, USA) was used as reference and a Pt wire as counter electrode. Scan rates for every measurement are specified in the text.

The surface coverage of Au beads with redox-active species was determined by CV measurements according to Equations 4.4 and 4.5. The electrode area was determined from the slope of a linear plot of the cathodic current vs. $v^{1/2}$ for the reversible reduction of $[Ru(NH_3)_6]^{3+/2+}$ (1 mM in 0.1 M NaCl, taking 7.5×10^{-6} cm^2 s^{-1} as its diffusion coefficient in this solution) according to Equation 4.6

after immersing modified beads in piranha solution at 80 °C for 1 h in order to remove the polysiloxane layer.

Voltammetric pinhole tests were performed in a solution of 1 mM $K_4[Fe(CN)_6]$ in aqueous 1 M in KCl.

5.8.6 ISE membranes and electrodes

The Ca^{2+}-selective polyurethane membrane (CaPuM) contained ETH 5234 (1.05 wt.%, 13.1 mmol kg^{-1}), KTFPB (0.54 wt.%, 6.0 mmol kg^{-1}), Tecoflex® (65.8 wt. %), and DOS (32.6 wt. %). The total weight of the mixture was 200 mg. It was dissolved in THF (2 mL). For silicon wafer electrodes used in the flow-through cell, a membrane solution of the same composition was prepared dissolved in a 1:1 mixture (2 mL) of THF and cyclohexanone.

The construction of SC ISEs varied strongly. Gold wires were insulated with a plastic pipette tip (see Figure 5.18 a). A piece of PVC tubing was fixed on this tip, the membrane solution (20 µL) was drop-cast onto the tubing, and the solvent allowed to evaporate during 4 h.

For gold disk electrodes, a piece of PVC tubing (2 cm long) was stuck over the electrode tip (see Figure 5.18 b) in which the membrane solution (100 µL) was drop-cast on the electrode surface, and the solvent was allowed to evaporate during 4 h.

Membranes with a diameter of about 1 cm were prepared on gold-coated glass slides as electrodes by casting the membrane solution (50 µL) on them, whereas other ones with a diameter of about 6 mm were obtained on gold-coated silicon wafer electrodes by casting 3 times 10 µL of membrane solution onto them.

For selectivity measurements with LC ISEs, a membrane solution of the same composition as mentioned above in THF (2 mL) was prepared and cast into a glass ring (inner diameter, 24 mm) fixed on a glass plate, the solvent being allowed to evaporate overnight. A disk of 5 mm diameter was then punched

from the master membrane and glued to a PVC tubing with a PVC/THF slurry. After that, the electrodes were assembled, filled with 10^{-2} M NaCl, and conditioned in 10^{-2} M NaCl overnight before starting selectivity measurements.

5.8.7 EMF measurements

Potentials were measured with a custom-made 14-channel electrode monitor at room temperature (23 °C) in stirred solutions. A double-junction Ag/AgCl/3 M KCl reference electrode (type 6.0729.100, Methrom) containing a 1 M NH_4NO_3 electrolyte bridge was used.

All EMF values were corrected for liquid-junction potentials according to the Henderson equation. Activity coefficients were calculated by the Debye-Hückel approximation.

For measurements in dilute solutions, membranes were conditioned in 10^{-3} M $CaCl_2$ solution for at least 20 h and after that in 10^{-6} M $CaCl_2$ overnight. A background of 10^{-4} M NaCl was used with all $CaCl_2$ sample solutions.

Seite Leer /
Blank leaf

6 Solid-contact ion-selective electrodes based on conducting polymers with nanomolar detection limits

6.1 Introduction

Organic conducting polymers (CPs) are polymers that have an extended conjugated π-orbital system. The conductivity is achieved by inducing a deficiency or an excess of π electrons in the polyconjugated chain. The latter is called doping in analogy to inorganic semiconductors [102]. The discovery of CPs is ascribed to the first doping of polyacetylene in 1976 [103-105] (Nobel Price 2000).

In their neutral state (undoped or semiconducting form), CPs are insulating, i.e., the π electrons are localized and cannot carry an electric current. The doping process is normally accompanied by a change in various properties of the polymer such as wettability and stability [106]. For example, polythiophene in its neutral state has a very hydrophobic surface that becomes more and more hydrophilic as the degree of oxidation increases. Depending on its oxidation state, the corresponding contact angles of water measured on it varied from 180 to 0° [107]. To compensate for the excess (or deficiency) of charge, a counterion (doping ion) penetrates the polymer film during the doping process. Therefore, CPs show both electronic and ionic conductivity. Due to this characteristic, CPs (especially polyheterocycles, see Figure 6.1) nowadays belong to the best established solid-contact materials for SC ISEs and are widely applied.
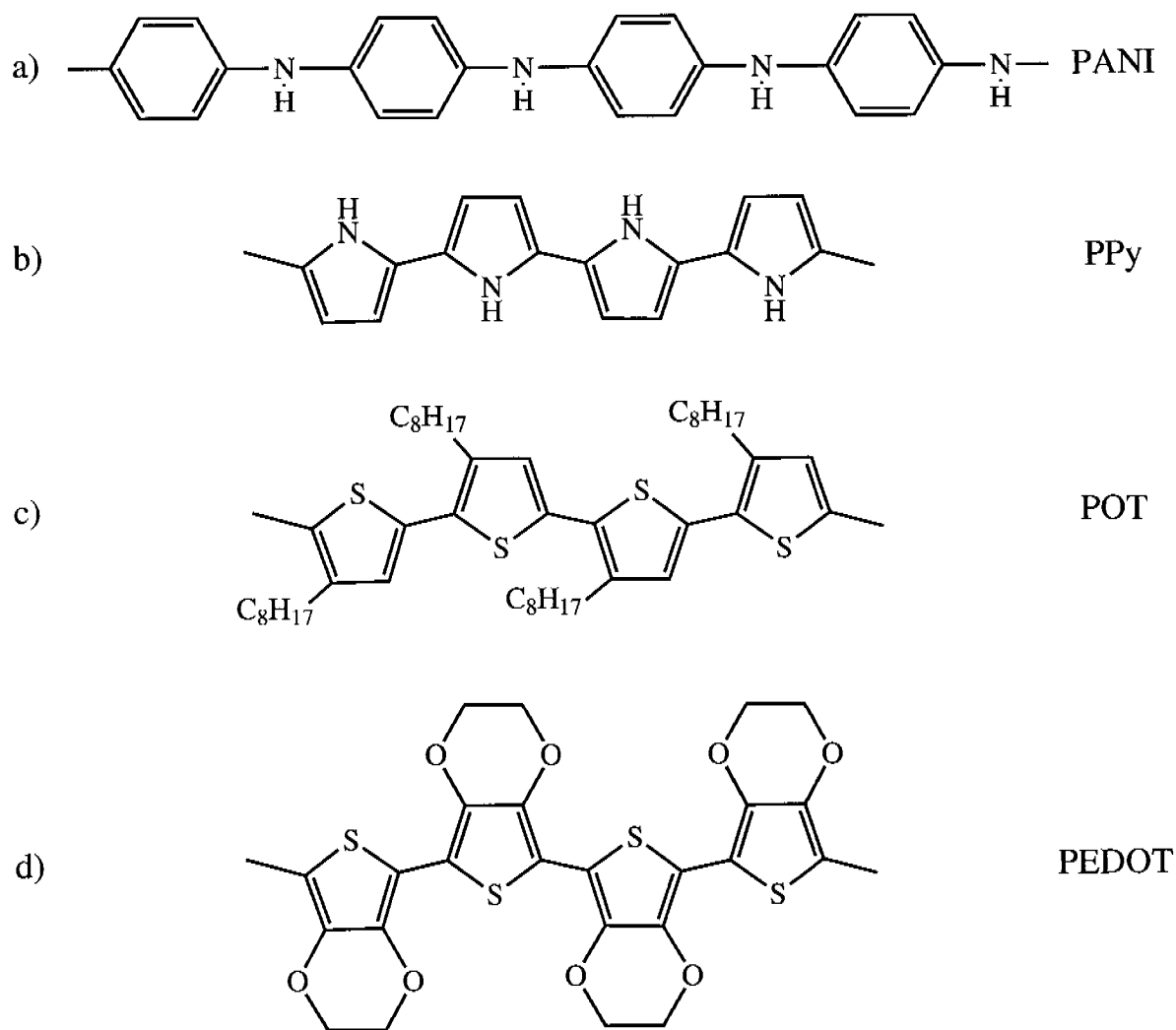
Figure 6.1. Examples of conducting polymers commonly used for SC ISEs: a) polyaniline (PANI), b) polypyrrole (PPy), c) poly(3-octylthiophene) (POT), and poly(3,4-ethylenedioxythiophene) (PEDOT) [108].

Conducting polymers are often produced by electrochemical polymerization, which allows to control the polymerization process instrumentally and to obtain a polymer film suitable for further electrochemical applications or modifications [102]. The electrochemical reaction scheme for the anodic coupling of pyrrole to polypyrrole is shown in Figure 6.2 and the corresponding reaction mechanism, a series of subsequent electrochemical and chemical steps, in Figure 6.3.
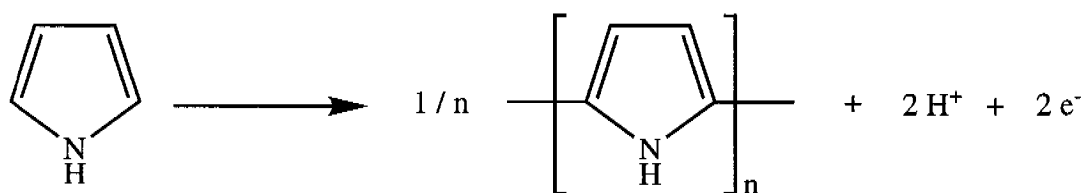
Figure 6.2. Reaction scheme of the electropolymerization (anodic coupling) of pyrrole to polypyrrole [102].
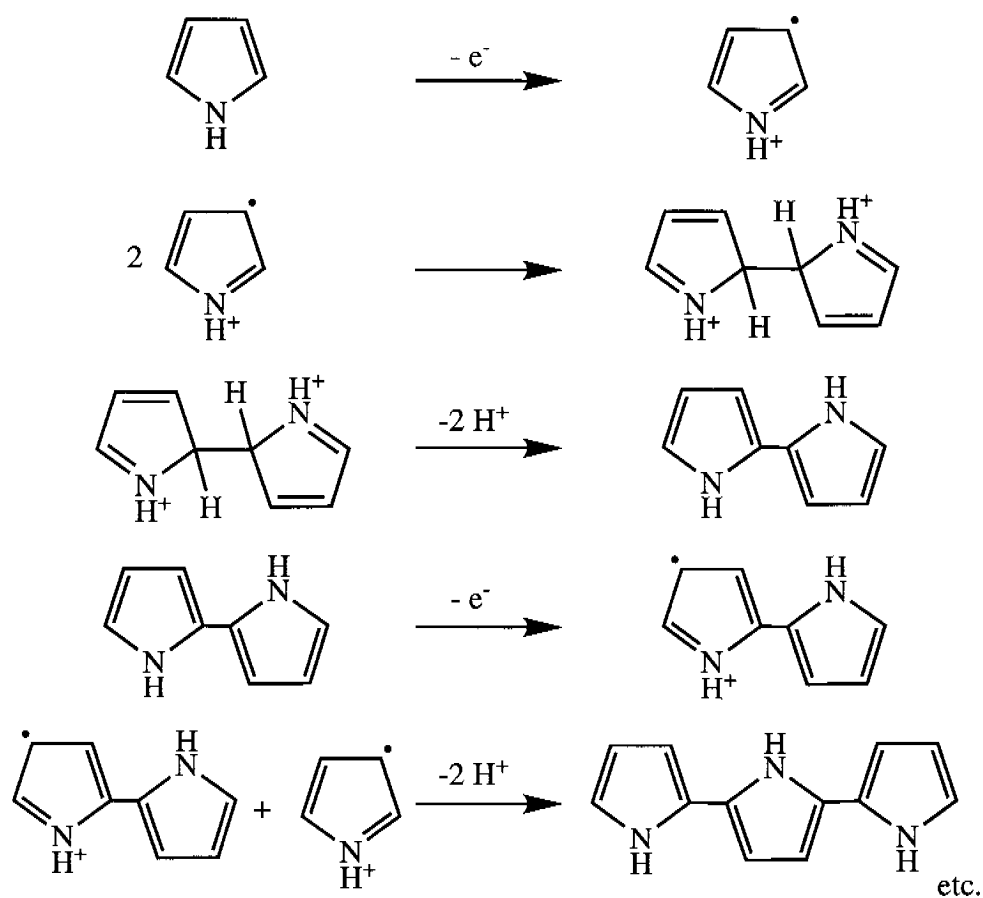
Figure 6.3. Scheme for reaction mechanism of anodic coupling of pyrrole to polypyrrole [102].

The deposition of the polymer occurs by precipitation as soon as the length of the oligomer attains a critical solubility. The reaction proceeds with an electrochemical stoichiometry of 2.2–2.3 Faraday, two of which are required for

95

the oxidation of the monomer. The excess of charge (0.2–0.3 Faraday) corresponds to the reversible oxidation (doping) of the polymer [102]. The properties of the resulting polymer film can be influenced by many experimental variables such as solvent, monomer concentration, type and concentration of electrolyte, temperature, electrode material, and applied electrical conditions [102,106,109,110].

A review of potentiometric ion sensors based on conducting polymers was recently published by Bobacka et al. [108]. The first ISEs based on CPs were reported in 1988 by Dong et al. who prepared anion-doped polypyrrole (PPy) films on glassy carbon electrodes and examined their potentiometric response to anions [111,112].

The potentiometric response of CPs varies from anionic to cationic depending on the mobility of the doping anion in the CP layer. Bulky doping anions such as poly(4-styrenesulfonate) or hexacyanoferrate induce a cationic or mixed (i.e., not only cations are exchanged but also anions can take part in the overall ion exchange) ionic response in PPy layers. They are entrapped in the CP layer and act as a cation exchanger. For small, mobile doping anions (i.e. chloride, perchlorate, nitrate) anion exchange between polymer and solution is observed [113] (see Figure 6.4). A cationic response over a larger range can be achieved for both types of PPy layers if a Nafion® layer (cation exchanger membrane on the basis of poly(perfluoroalkene)sulfonic acid) is applied on top [113,114]. Furthermore, the potentiometric response can be altered by the presence of a redox couple in the sample solution [108,115-117].

Some CPs as, e.g., polypyrroles [118-123] and polyanilines [124] were shown to possess pH sensitivity. Their selective response to protons was used to build pH electrodes [125,126] or biosensors where the conducting polymer acted as a pH transducer [127-129].

Bulky, multiply charged doping anions, e.g., poly(4-styrenesulfonate) or hexacyanoferrate

Small, mobile doping anions, e.g., chloride, nitrate, perchlorate
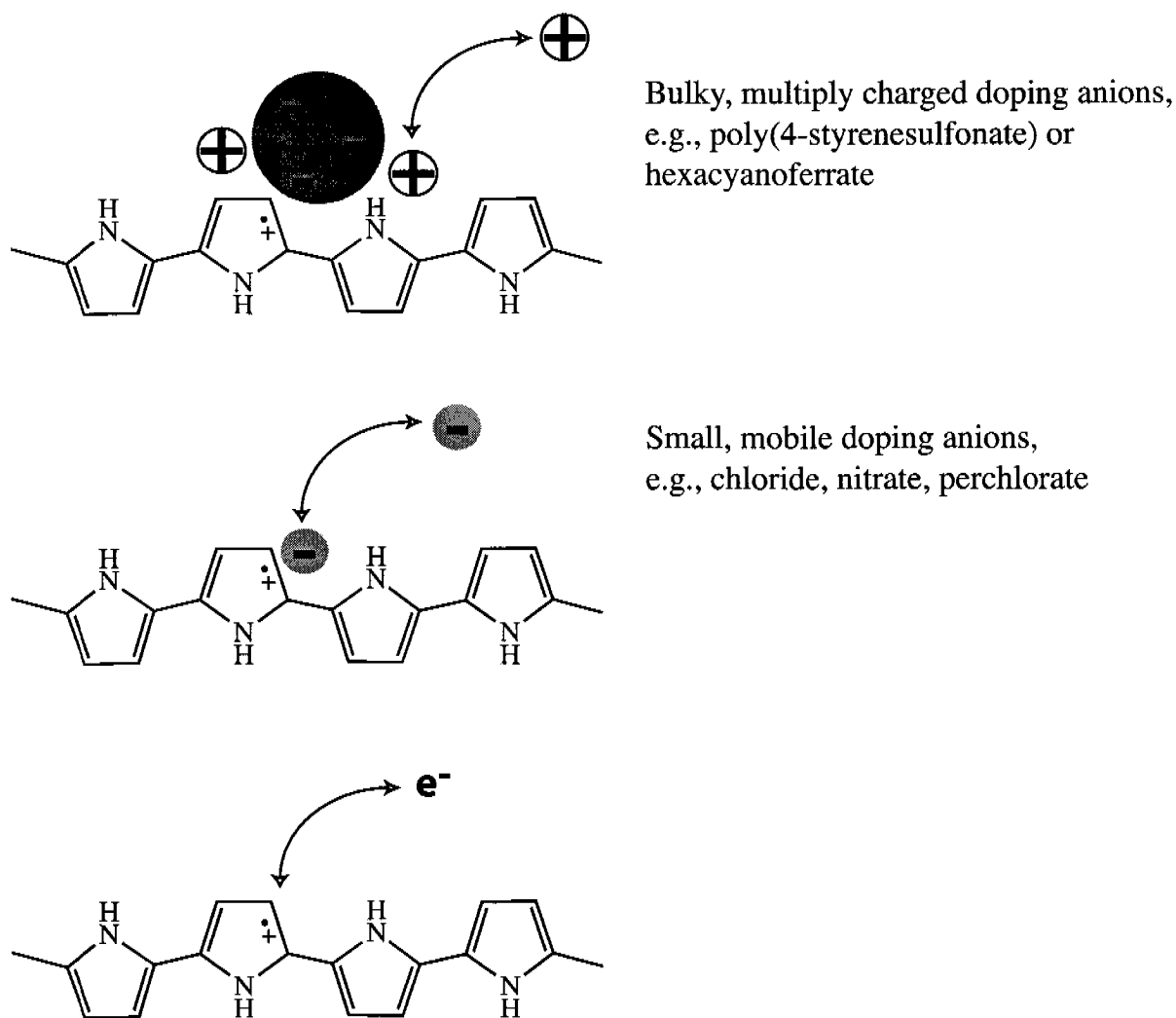
Figure 6.4. Anionic, cationic and redox response (from top to bottom) of PPy films [108].

Beside the pH sensitivity of some CPs, they usually do not show an ion-selective response unless complexing ligands and/or ion exchangers are included in the CP film as demonstrated for electropolymerized PPy [130], for solvent-processable polyaniline (PANI) [58], and for drop-cast poly(3-octylthiophene) (POT) [55,131,132].

Another approach to render CP-based electrodes ion-selective was to incorporate a solvent-processable CP (undoped POT or PANI doped with bis-[4-(1,1,3,3-tetramethylbutyl)phenyl]phosphoric acid) into an ion-selective liquid

polymer membrane [53,133,134]. However, so far, the most promising way to produce a potentiometric sensor on the basis of CPs is the application of a liquid ISE membrane on top of a CP layer. In such an ISE setup, the ion-selective membrane determines the ion selectivity of the sensor, whereas the CP transduces the ionic response of the membrane into an electronic signal.

The most frequently investigated material for this kind of SC ISEs [49,135-141] or for SC microelectrodes [50,51,86] is PPy. The response of such SC ISEs can be influenced by spontaneous charging and discharging processes, which mainly occur when PPy layers are in contact with aqueous solutions. This phenomenon, accompanied by proton release, renders the open-circuit potential of PPy-coated electrodes unstable [121,142,143].

Other CPs, which have been successfully applied as interface between ion-selective membrane and internal electrode are PANI [144,145], electropolymerized poly(3,4-ethylenedioxythiophene) (PEDOT) [56,146], PEDOT drop-cast from aqueous dispersion and doped with poly(4-styrenesulfonate) [147,148], electropolymerized POT [149-151], and solvent-processable POT in its undoped form together with silicone rubber membranes [57].

Only recently, the lower detection limit of SC ISEs based on CP interfaces has become a topic of interest. Previously, the potentiometric response was investigated only in the ion activity ranges required for clinical analysis. In a recent publication [152], the response of a Ca^{2+}-selective SC ISE could be varied from Nernstian with a lower detection limit of 10^{-5} M to super-Nernstian by impregnating the CP layer (poly(methylthiophene)) with EDTA. This shows that ion gradients can be generated in SC ISEs if a depletion of Ca^{2+} on the inner side of the ISE membrane is induced. Indirectly, this result indicates that the response of SC ISEs can be biased by the same leaching processes occurring in liquid-contact electrodes. The SC ISEs with an EDTA impregnated CP layer were not applicable for trace level measurements because a linear Nernstian

response could only be achieved over a small sample activity range. However, the lower detection limit was improve by applying an external current to PPy-based SC ISEs [153], in analogy to earlier experiments with LC ISEs [154,155].

6.2 Systematic comparison of Ca^{2+}-selective SC electrodes based on PPy and POT

The results of several working groups show that the lower detection limits of SC ISEs are biased by the same leaching processes as those of LC ISEs [60,61,152,153]. Generally, ion exchanges at the outer or inner membrane surface generates ion gradients in the membrane, which leads to inward or outward ion fluxes. In SC ISEs, ion exchange can take place at the interface between the inner membrane surface and an inner water layer, which is formed during the conditioning of the sensor. Additionally, in SC ISEs based on CPs having functional groups that can be protonated (e.g. PPy), the ion fluxes through the membrane can be influenced by proton release induced by spontaneous discharging processes. If no inner water layer is formed, only ion exchange at the outer membrane surface takes place.

The considerations mentioned above suggest that the water layer, which is formed between CP film and ISE membrane, plays an important role in the control of the lower detection limits. Up to the present, only one example of CP-based SC ISE has been published where the formation of an inner water layer was investigated [86]. Here, potentiometric water layer tests on K^+-selective SC ISEs using potassium hexacyanoferrate(II)/(III) doped PPy as a solid contact showed that no inner water layer was formed in the electrodes.

Thus, it was interesting to apply different CPs in SC ISEs and test them for the formation of an inner water layer. In this work, three CPs were examined and systematically compared with each other: polypyrrole doped with KCl

(PPy_KCl) or with potassium hexacyanoferrate(II)/(III) (PPy_FeCN), both electropolymerized, as well as drop-cast poly(3-octylthiophene) (POT). It is known from the literature that PPy_KCl films show anionic potentiometric responses, whereas PPy_FeCN films typically show a positive, sub-Nernstian slope, which indicates that not only cations but also anions take part in the overall ion-exchange process [113]. POT was chosen because it is the most lipophilic CP among those used for SC ISEs. In addition, in its undoped (uncharged) form, it is solvent-soluble and can be drop-cast.

Teflon

Au disk   POT or PPy   PVC tubing   Ion-selective membrane
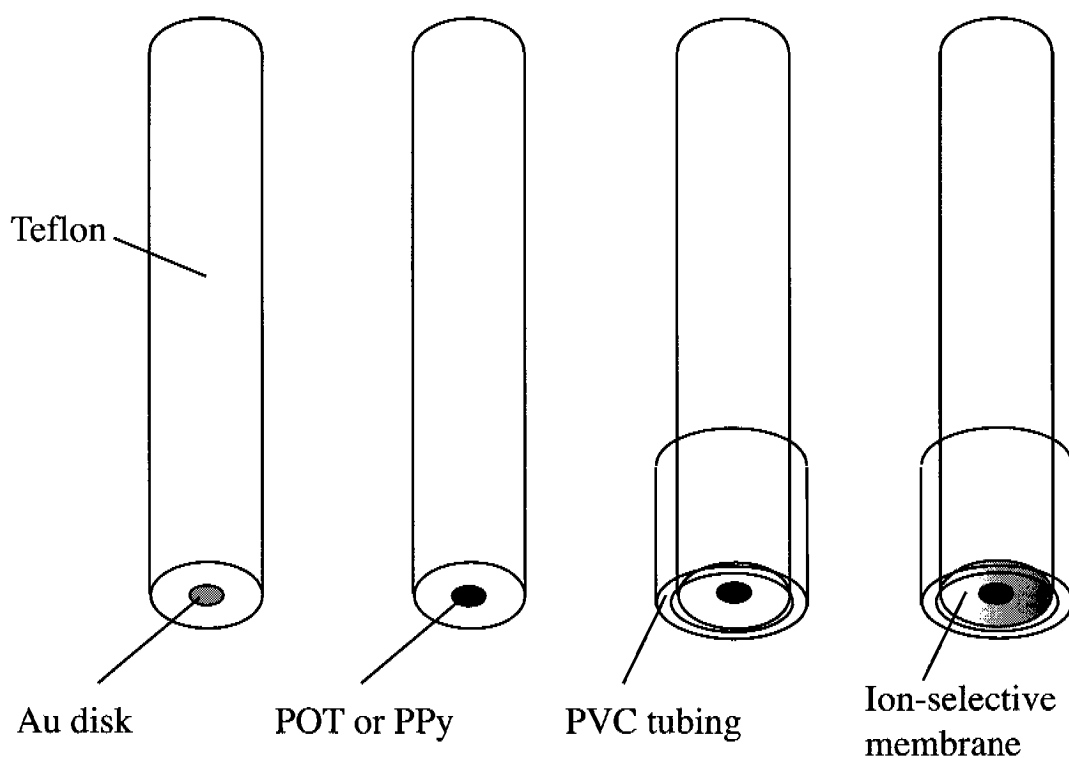
Figure 6.5. Construction of SC ISEs. A Au disk electrode was first covered with a CP film (electropolymerized or drop-cast), then a PVC tubing was stuck over the tip and the membrane cocktail was cast into this ring.

A simple electrode construction using a commercially available Au disk electrode was chosen for this study (Figure 6.5). Selectivities, slopes, lower detection limits, potential stabilities, and response times of ISEs with a CP solid

contact were compared to coated-wire type electrodes (SC ISEs without inner
CP layer) of the same membrane composition. Two different membrane
compositions were used (cf. paragraph 6.6.3), i.e. a conventional PVC
membrane with 66 wt% of DOS (CaPVCM) and a polyurethane (Tecoflex®)
membrane with only 33 wt% of DOS (CaPuM). Since initial experiments with
Ca^{2+}-selective POT SC ISEs showed light-dependent EMF responses (drift, ca. 2
mV h^{-1}), all electrodes were kept in the dark for the measurements shown here.

Table 6.1. Potentiometric selectivity coefficients, log K_{CaJ}^{pot}, and response slopes
(in parentheses, mV $decade^{-1}$; concentration range, 10^{-1}–10^{-3} M) of the CaPVCM
membrane obtained with the separate solution method [16]. Data shown for LC
ISEs [38] and SC ISEs (SD, n = 3)

Ion J	LC ISEs	SC ISEs			
		Au^a	Au/PPy_KCl^a	Au/PPy_FeCN	Au/POT
H^+	-3.8	—	—	-2.6 ± 0.1	-3.3 ± 0.2
	(56.8)			(53.4 ± 0.3)	(54.1 ± 0.3)
Na^+	-5.8	—	—	-5.2 ± 0.2	-6.5 ± 0.1
	(50.6)			(57.7 ± 0.6)	(57.3 ± 0.1)
K^+	-6.5	—	—	-6.0 ± 0.2	-7.5 ± 0.1
	(40.1)			(53.8 ± 0.3)	(52.6 ± 0.1)
Mg^{2+}	-9.5	—	—	-8.5 ± 0.2	-9.4 ± 0.2
	(29.4)			(31.6 ± 1.7)	(24.2 ± 1.6)

[a] Due to long-term EMF drifts of these electrodes, it was not possible to
determine their selectivity coefficients.

Table 6.1 and Table 6.2 show the most important selectivity coefficients of the
two ISE membranes described above, determined with LC ISEs and SC ISEs
(PPy_KCl, PPy_FeCN and POT). For PPy_KCl SC ISEs combined with
membrane CaPVCM and for coated-wire type electrodes (both membrane

compositions), selectivity coefficients could not be determined because of long-term potential drifts during the measurements.

Table 6.2. Potentiometric selectivity coefficients, log K_{CaJ}^{pot}, and response slopes (in parentheses, mV decade^{-1}; concentration range, 10^{-1}–10^{-3} M) of CaPuM membrane obtained with the separate solution method [16]. Data shown for LC ISEs and SC ISEs (SD, n = 3).

Ion J	LC ISEs	SC ISEs			
		Au[a]	Au/PPy_KCl	Au/PPy_FeCN	Au/POT
H$^+$	-2.0 ± 0.2	—	-2.2 ± 0.2	-2.0 ± 0.1	-2.8 ± 0.1
	(54.2 ± 0.9)		(49.1 ± 2.8)	(54.1 ± 1.3)	(45.3 ± 0.3)
Na$^+$	-5.9 ± 0.3	—	-5.7 ± 0.1	-5.6 ± 0.1	-7.5 ± 0.4
	(54.2 ± 0.9)		(54.2 ± 1.4)	(54.4 ± 0.3)	(53.7 ± 0.1)
K$^+$	-6.6 ± 0.3	—	-6.3 ± 0.2	-6.4 ± 0.2	-8.1 ± 0.3
	(54.2 ± 0.9)		(47.7 ± 1.8)	(47.2 ± 0.3)	(45.3 ± 0.3)
Mg^{2+}	-8.5 ± 0.1	—	-8.1 ± 0.3	-8.4 ± 0.1	-9.1 ± 0.1
	(26.9 ± 0.9)		(28.3 ± 2.2)	(27.6 ± 0.5)	(24.8 ± 0.6)

[a] Due to long-term EMF drifts of these electrodes, it was not possible to determine their selectivity coefficients.

Selectivities obtained for the PPy SC ISEs were, in general, comparable to, or only slightly worse than those of LC ISEs, whereas POT SC ISEs showed comparable or even better selectivities than LC ISEs. It was, therefore, assumed that POT diffuses into the membrane and partly influences its selectivity.

Calibration curves of the same SC ISEs as in Table 6.1 and Table 6.2, obtained by successively decreasing the Ca^{2+} activity of the sample are shown in Figure 6.6.
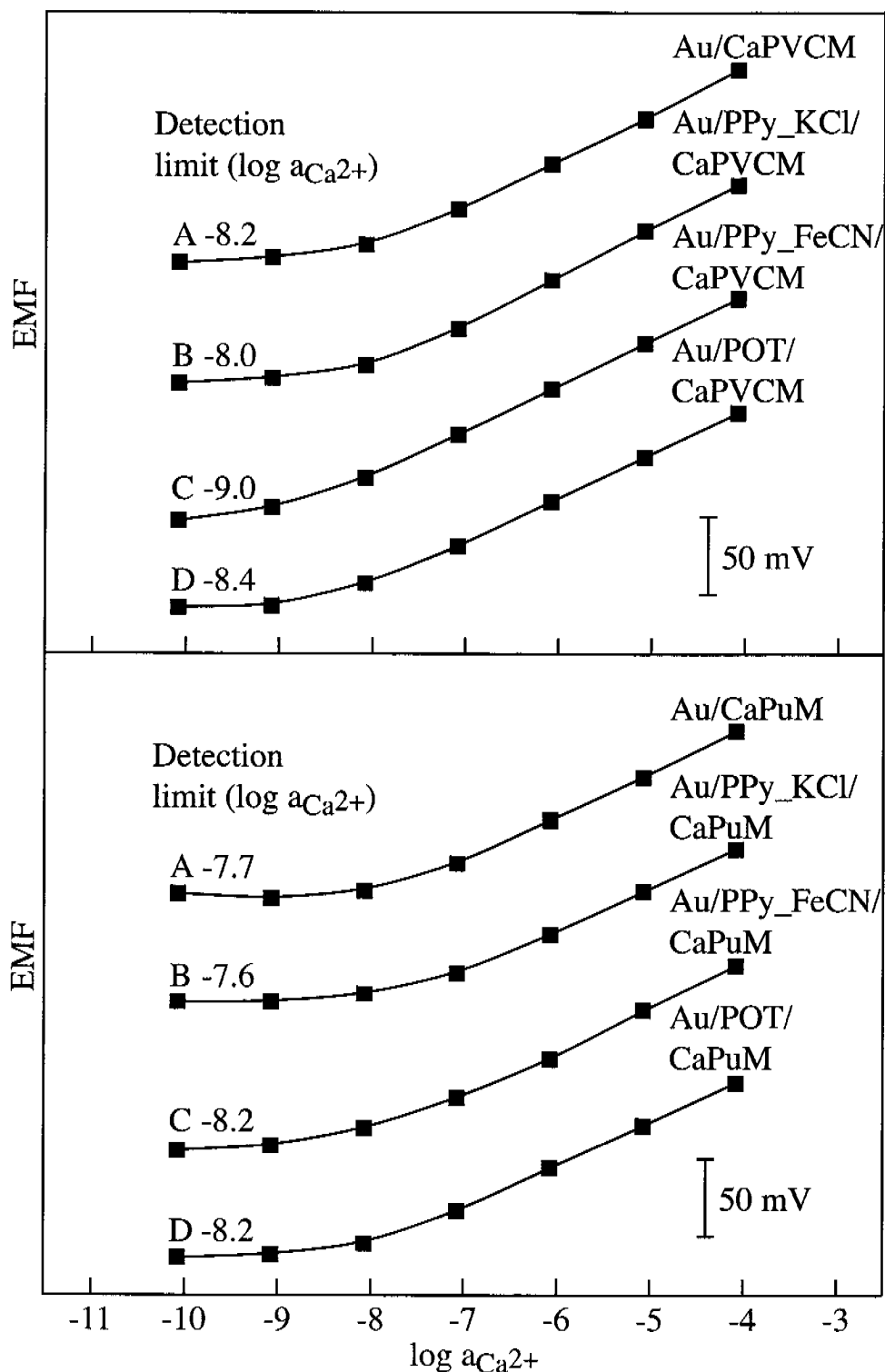
Figure 6.6. Calibration curves of SC ISEs without CP (A), with PPy_KCl (B), with PPy_FeCN (C), and with POT (D) obtained by successively decreasing the Ca^{2+} activity of the sample (background: 10^{-4} M NaCl). The curves were measured with membranes CaPVCM (top) and CaPuM (bottom).

Overall, the detection limits found with the PVC membrane electrodes were better than those with the polyurethane membrane electrodes. The difference can be explained by taking into account the H^+ selectivity of the two membranes (Table 6.1 and Table 6.2). The lower detection limit is determined by the H^+ interference, which is stronger for the polyurethane membranes. PPy_KCl ISEs and coated-wire type electrodes, generally, showed higher and less reproducible detection limits ($10^{-7.8}$–$10^{-8.3}$ M for CaPVCM, 10^{-7}–$10^{-8.3}$ M for CaPuM) than the PPy_FeCN- and POT-based ISEs.

With the polyurethane membrane CaPuM, no difference was observed between the detection limits of SC ISEs based on PPy_FeCN or POT ($10^{-8.2}$–$10^{-8.3}$ M), whereas SC ISEs with the PVC membrane CaPVCM and PPy_FeCN as solid contact showed a lower detection limit that was better by 0.1–0.6 logarithmic units ($10^{-8.8}$–10^{-9} M) than the corresponding POT-based SC ISEs ($10^{-8.4}$–$10^{-8.7}$ M).

Figure 6.7 shows water layer tests (compare Chapter 4, paragraph 4.3.2) for the SC ISEs under investigation. The PPy_KCl and coated-wire type ISEs showed positive EMF drifts upon changing from the Ca^{2+} conditioning solution to a Na^+ solution (respective initial drifts: CaPVCM: 5 and 24 mV h^{-1}; CaPuM: 8 and 10 mV h^{-1}) and negative drifts when the sample was exchanged again for the initial Ca^{2+} solution (respective initial drifts: CaPVCM: -17 and -28 mV h^{-1}; CaPuM: -7 and -27 mV h^{-1}). This behavior implies the formation of an inner water layer. The potential drifts observed for PPy_FeCN SC ISEs with CaPVCM were very small (initial drifts, ca. 2 mV h^{-1} in both interfering and primary ion solutions), but only if the PPy_FeCN solid contact was thoroughly washed before being coated with the ISE membrane. Otherwise, the drifts observed during the water layer test were much larger (results for Ca^{2+}-selective electrodes not shown; for an example of a Pb^{2+}-selective PPy_FeCN SC ISE, see Figure 6.13, top).

Solid-contact ion-selective electrodes based on conducting polymers with nanomolar detection limits
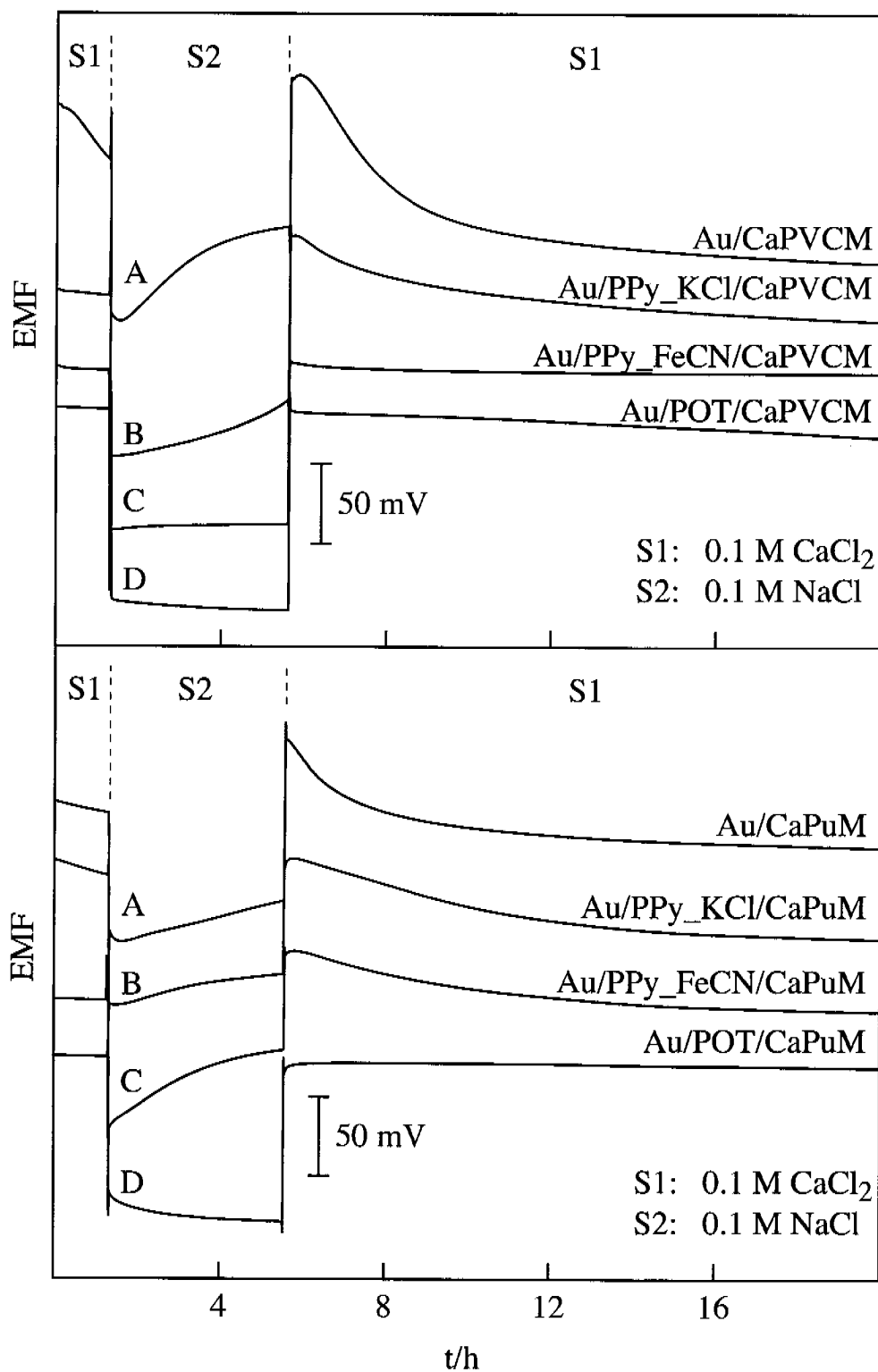
Figure 6.7. Results of the water layer tests for Ca^{2+}-selective SC ISEs without CP (A), with PPy_KCl (B), with PPy_FeCN (C), and with POT (D). The curves were measured with membranes CaPVCM (top) and CaPuM (bottom).

On the other hand, the initial potential drifts of PPy_FeCN electrodes with the polyurethane membrane were around 20 and 10 mV h^{-1} in Na^+ and Ca^{2+} solutions, respectively, and thus comparable to the drifts of PPy_KCl and coated-wire type electrodes.

Interestingly, PPy_FeCN SC ISEs both with PVC and polyurethane membrane showed better detection limits than PPy_KCl and coated-wire type ISEs. This was explained by the presence of K^+ ions in the inner water layer, which were released from the potassium hexacyanoferrate(II)/(III) doping in the PPy_FeCN solid contact. These K^+ can replace some of the Ca^{2+} on the internal membrane side, creating a small Ca^{2+} gradient toward the inner side of the membrane. This gradient partly compensates the Ca^{2+} gradient in direction of the sample, which is generated by ion-exchange processes on the outer membrane side. The ion exchange on the inner membrane side could also explain why PPy_FeCN SC ISEs with CaPVCM have better detection limits than the corresponding POT electrodes, whose solid contact is undoped.

An astonishing result of the water layer tests was that the EMF drifts were larger for PPy_FeCN SC ISEs with CaPuM than for those with CaPVCM. In fact, in previous works, polyurethane membranes with low plasticizer content were found to have better adhesion properties than PVC membranes containing approximately 66 wt% of plasticizer [60]. Apparently however, in the above case, a high amount of plasticizer improved the adhesion of the membrane to the PPy_FeCN layer.

Oxygen tests were conducted with the four kinds of SC ISEs combined with PVC or polyurethane membranes. Changes in the oxygen concentration of the sample were induced by alternately bubbling argon and oxygen through it. The results are shown in Figure 6.8. Overall, potential drifts observed for electrodes with CaPuM were smaller than for those with CaPVCM. This can be attributed to the smaller diffusion coefficient of oxygen in the polyurethane membrane due

to its higher viscosity. As expected, the biggest response to oxygen was observed for the coated-wire type ISEs without CP interface. Of the three SC ISEs with an inner CP layer, only POT electrodes (with both PVC or polyurethane membrane) showed no reaction to changes in the oxygen concentration of the sample. The two kinds of PPy solid contacts could not completely prevent the sensitivity to oxygen of the respective electrodes. The PPy_KCl SC ISEs, generally, showed a smaller potential step than the PPy_FeCN electrodes, even though the responses strongly varied among the electrodes of the same type (differences of up to 10 mV).

Figure 6.9 shows the response times of PPy_FeCN-based SC ISEs with CaPVCM or CaPuM, for stepwise dilutions of the Ca^{2+} activity from 10^{-4} to 10^{-10} M. Electrodes with CaPuM, in general, had slower response times in the concentration range of 10^{-6}–10^{-8} M Ca^{2+} (EMF drift between 10^{-6} and 10^{-7} M: < 0.4 mV min^{-1} after 1 min for CaPVCM, after 5 min for CaPuM). At lower concentrations, the response times of the two membranes were comparable (drift between 10^{-8} and 10^{-9} M: < 0.4 mV min^{-1} after 7 min for CaPVCM, after 6 min for CaPuM). A similar behavior was observed for all other types of SC ISEs investigated in this study.
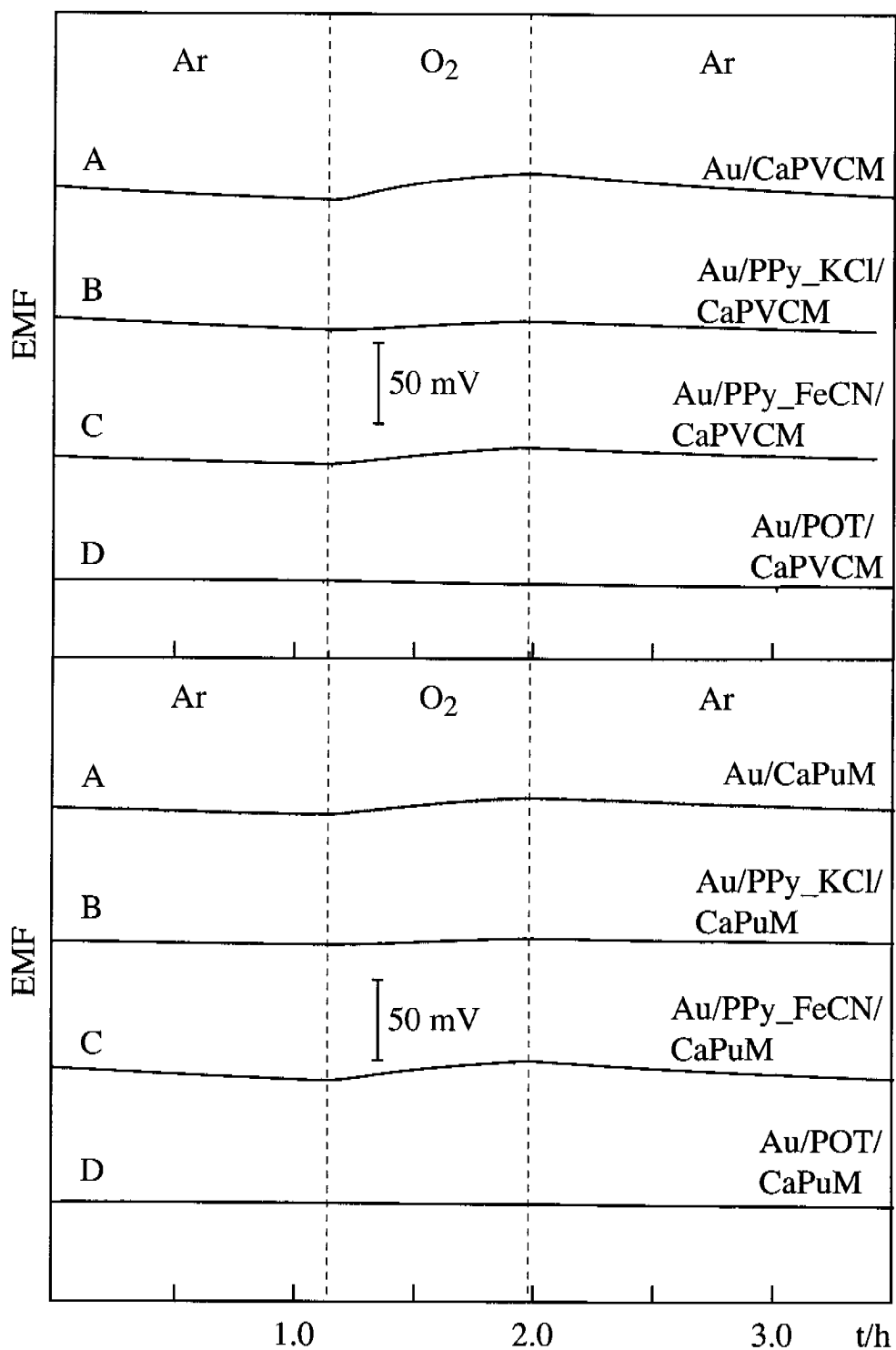
Figure 6.8. Influence of oxygen on the EMF of Ca^{2+}-selective SC ISEs without CP (A), with PPy_KCl (B), with PPy_FeCN (C), and with POT (D). The curves were measured with membranes CaPVCM (top) and CaPuM (bottom). Sample solution: 0.1 M $CaCl_2$.
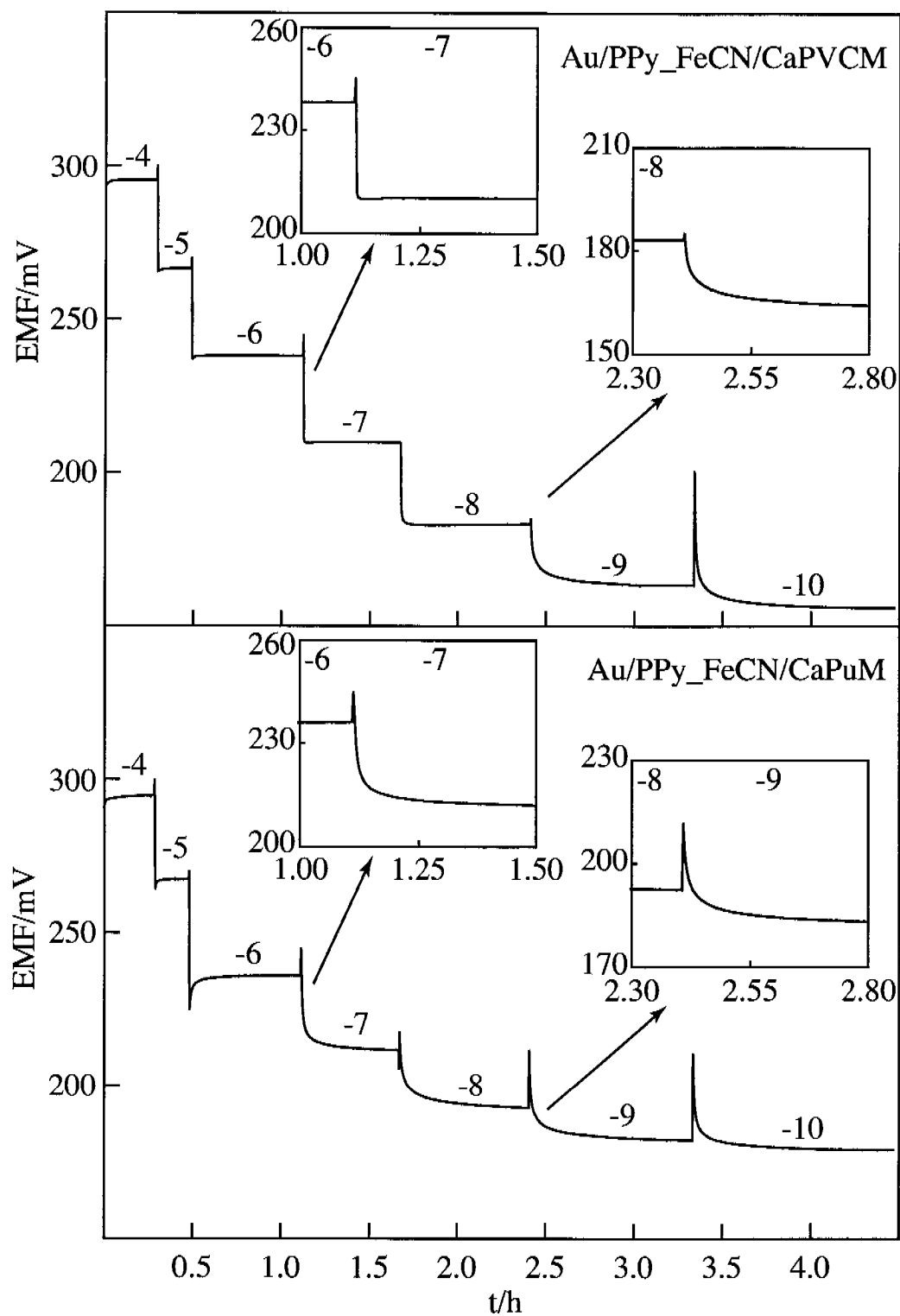
Figure 6.9. Time traces of EMF responses of SC ISEs based on PPy_FeCN with membranes CaPVCM (top) and CaPuM (bottom). The values given above the curves indicate the respective logarithmic molar Ca^{2+} concentrations in the sample.

6.3 Optimization of Pb^{2+}-selective SC electrodes based on PPy

The study on Ca^{2+}-selective ISEs with CP solid contacts has shown that it is possible to achieve low detection limits for SC ISEs if an appropriate CP is chosen that avoids the formation of an inner water layer. To further investigate the behavior of SC ISE at low ion concentrations, Pb^{2+}-selective membranes were chosen since the characteristics of the analogous LC ISEs are well studied [7,32].

In the present work, in addition to measurements in the batch mode with Au disk SC ISEs (Figure 6.5), a flow-through cell (Figure 6.10) was used in combination with screen-printed Pt electrodes as supports for CP layers. The same flow-through cell was already used to investigate PMHS- and PDMS-based SC ISEs (see Chapter 5) and for the study of K^+-selective SC ISEs with a PPy solid contact doped with potassium hexacyanoferrate(II)/(III) [86].
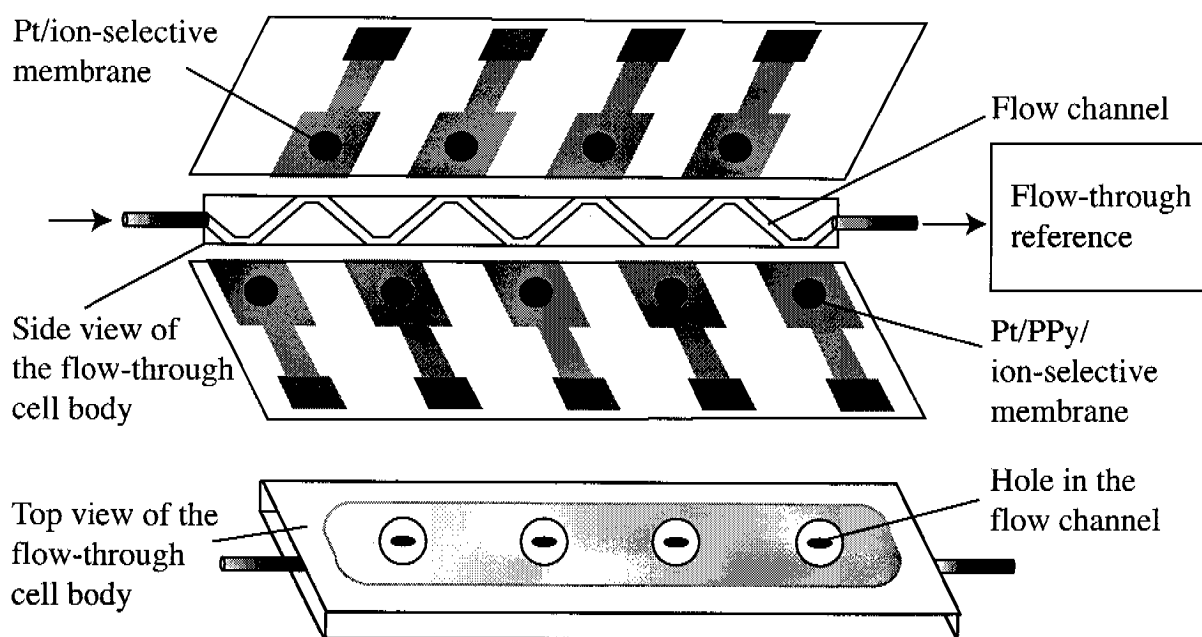
Figure 6.10. Schematic illustration of the flow-through cell with screen-printed Pt electrodes (the cell is also described in [86]).

Preliminary measurements in the flow-through cell with Pb^{2+}-selective POT-based PVC/DOS membrane ISEs showed that this CP used as solid contact diffused into the membrane and deteriorated its selectivity. Initially colorless membranes showed the same orange color as POT when the cell was disassembled after measurements. Therefore, all experiments described here were done with potassium hexacyanoferrate(II)/(III)-doped polypyrrole (PPy_FeCN) as solid contact.

The Pb^{2+}-selective PVC/DOS membranes used had two different compositions: PbPVCM_1 was the same as in [7]. It contained low concentrations of ionophore (0.7 mmol kg^{-1}) and ionic sites (0.3 mmol kg^{-1}) in order to reduce ion fluxes in the membrane. In PbPVCM_2, these concentrations were increased to 9.6 mmol kg^{-1} for the ionophore and to 5 mmol kg^{-1} for the ionic sites in order to improve the selectivity over H^+ relative to that of PbPVCM_1 (see Table 6.3).

Table 6.3. Potentiometric selectivity coefficients, log K_{PbJ}^{pot}, and response slopes (in parentheses, mV $decade^{-1}$; concentration range, 10^{-1}–10^{-4} M) of LC ISEs with PbPVCM_1 [7] and PbPVCM_2 obtained with the separate solution method [16] (SD, n = 5).

Ion J	PbPVCM_1	PbPVCM_2
H^+	-3.5 ± 0.3 (43.7 ± 2.0)	-7.3 ± 0.3 (46.3 ± 0.3)
Na^+	-6.3 ± 0.2 (58.2 ± 3.5)	-6.3 ± 0.1 (58.1 ± 0.1)
K^+	-6.3 ± 0.1 (56.8 ± 1.1)	-6.6 ± 0.1 (56.9 ± 0.2)
Ca^{2+}	-12.3 ± 0.1 (23.7 ± 0.8)	-13.6 ± 0.2 (23.7 ± 0.2)

Figure 6.11 shows calibration curves obtained with Pb^{2+}-SC ISEs of the two different types of electrode assemblies. Since the ionic strength of the sample solutions was kept constant during measurements (background: 10^{-3} M $CaCl_2$, 10^{-4} M HNO_3), the EMF values in this case were not corrected for the liquid

junction potential and Pb^{2+} activities were assumed to be proportional to the concentrations.
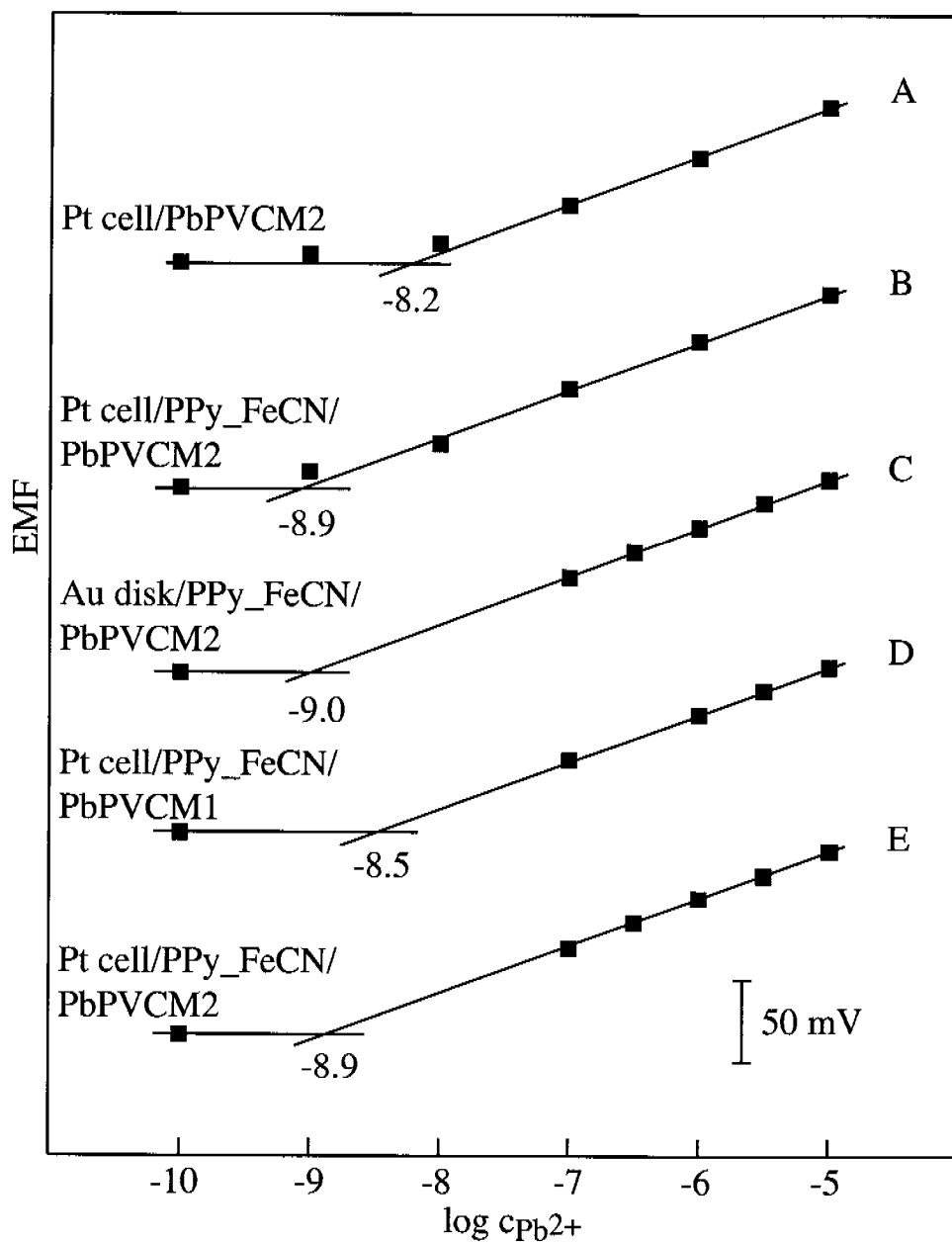
Figure 6.11. Calibration curves obtained with four kinds of SC ISEs by decreasing (A, B) or increasing (C, D, E) the Pb^{2+} concentration of the sample having a constant background of 10^{-3} M $CaCl_2$ and 10^{-4} M HNO_3.

After conditioning in 10^{-5} M for 2 days and then, in 10^{-6} M Pb^{2+} overnight, the ISEs were checked for their Nernstian response by stepwise decreasing the Pb^{2+} sample concentration (curves A and B). Afterwards, the ISEs were conditioned again, this time in 10^{-10} M Pb^{2+} overnight. The next day, the response was measured from low to high concentrations (curves C, D, and E), in order to determine the lower detection limit. Solutions of 10^{-9} and 10^{-8} M Pb^{2+} were skipped since the ISE responses at these concentrations were very slow, especially when measured in the flow-through cell. The results showed that the use of a PPy_FeCN solid contact improved the lower detection limit of SC ISEs by at least 0.7 logarithmic units compared with electrodes lacking such a CP layer (Figure 6.11, curves A and B). In addition, owing to a better H^+ selectivity, the lower detection of SC ISEs with PbPVCM_2 was better than that of electrodes with PbPVCM_1 (curves D and E).

The reproducibility of the lower detection limit was investigated too. Already after 3 days of repeated measurements, the lower detection limit of ISEs based on PbPVCM_1 was shifted towards higher concentrations by approximately half a logarithmic unit. This was supposed to be due to a deterioration in the ISEs' selectivity behavior because in the flowing system membrane components are eluted more rapidly. The PPy_FeCN electrodes with PbPVCM_2, on the other hand, showed very reproducible responses (Figure 6.12, bottom). The detection limit was still approximately 10^{-9} M Pb^{2+} after 14 days of repeated measurements, the intercept of the calibration curve was shifted only slightly, and the slope had not changed at all. In the same period of time, the lower detection limit of the corresponding coated-wire type electrodes lost 0.3 logarithmic units, the slope of the calibration curve decreased significantly and the absolute electrode potential had shifted by more than 100 mV (see Figure 6.12, bottom). The results suggest that a CP film between membrane and internal electrode stabilizes the SC ISE response when measured over a long time period.
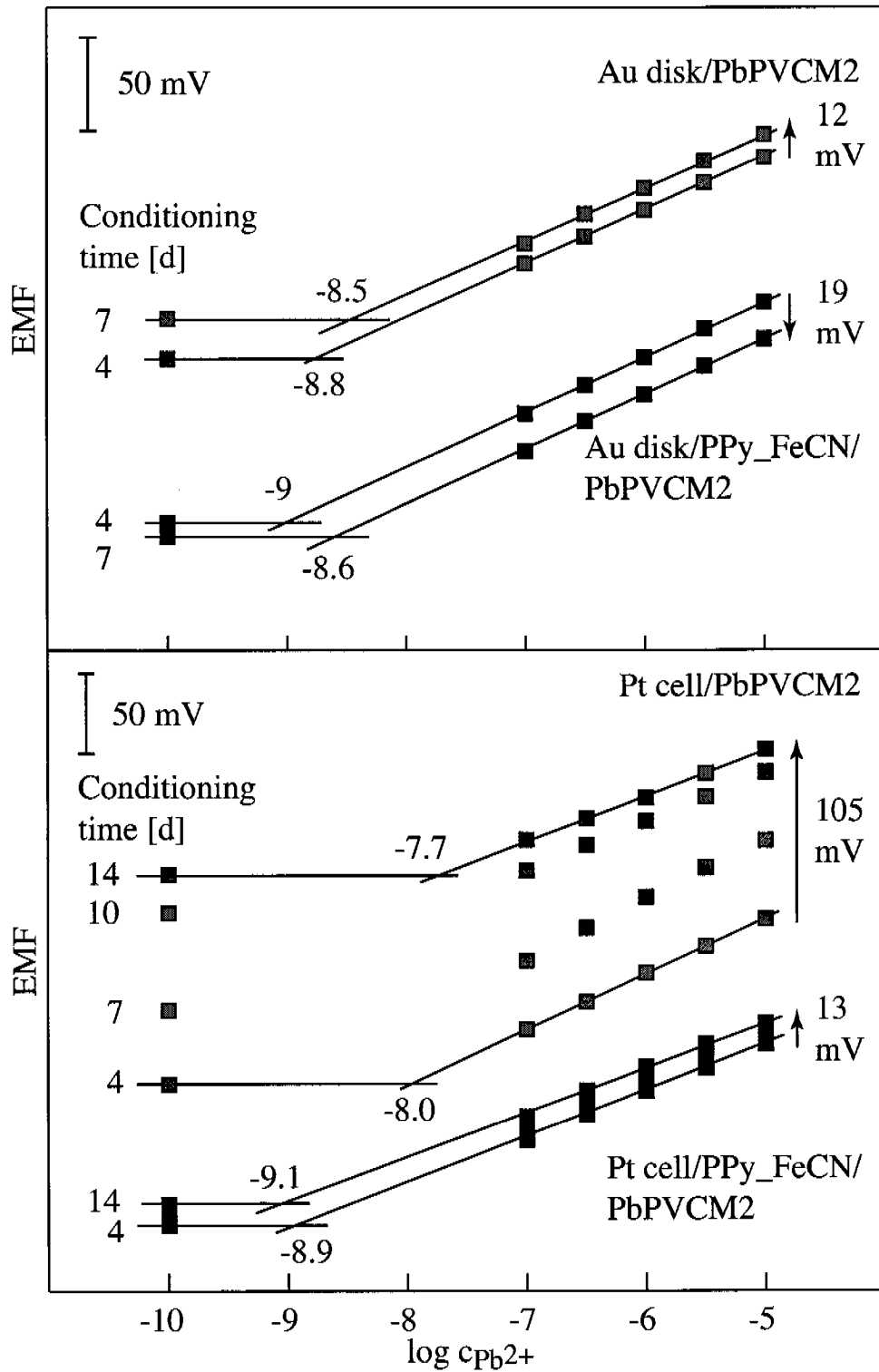
Figure 6.12. Long-term response reproducibility of Au-based (top) and Pt-based SC ISEs (bottom), both without (▨) and with (■) internal PPy_FeCN layer.

The lower detection limits of Au disk electrodes with a PPy_FeCN solid contact measured in the batch mode were initially comparable to those of Pt screen-printed electrodes in the flow-through cell (compare curves C and E in Figure 6.11), but lost 0.4 logarithmic units within 3 days of repeated measuring (see Figure 6.12, top). This difference most probably occurs due to a better adhesion of the ISE membrane in the flow-through cell assembly, where the membrane is tightly pressed onto the internal electrode.

Screen-printed Pt- and Au disk-based ISEs were tested for the formation of an inner water layer by replacing the $Pb(NO_3)_2$ conditioning solution with $CaCl_2$. Surprisingly, electrodes with an inner PPy_FeCN layer initially showed large potential drifts, whereas coated-wire type electrodes did not (Figure 6.13, top). In order to eliminate the EMF drifts, the excess of potassium hexacyanoferrate(II)/(III) present in the PPy layer had to be washed thoroughly with water (Figure 6.13, bottom). Between the two types of electrode construction, no difference was observed.

However, the importance of the PPy_FeCN layer was demonstrated by the results of the oxygen test (Figure 6.14). The oxygen concentration of the sample solution was varied by alternately bubbling argon or oxygen through it. Electrodes without a CP layer (curves A and B) showed potential steps of more than 30 mV when oxygen was bubbled into the sample, whereas for electrodes with an internal PPy layer, the EMF changes were much smaller (curves C and D). On screen-printed Pt electrodes, thicker PPy layers could be prepared than on Au disk electrodes (see paragraph 6.6.2), which explains the difference in sensitivity of the two ISE setups toward oxygen.
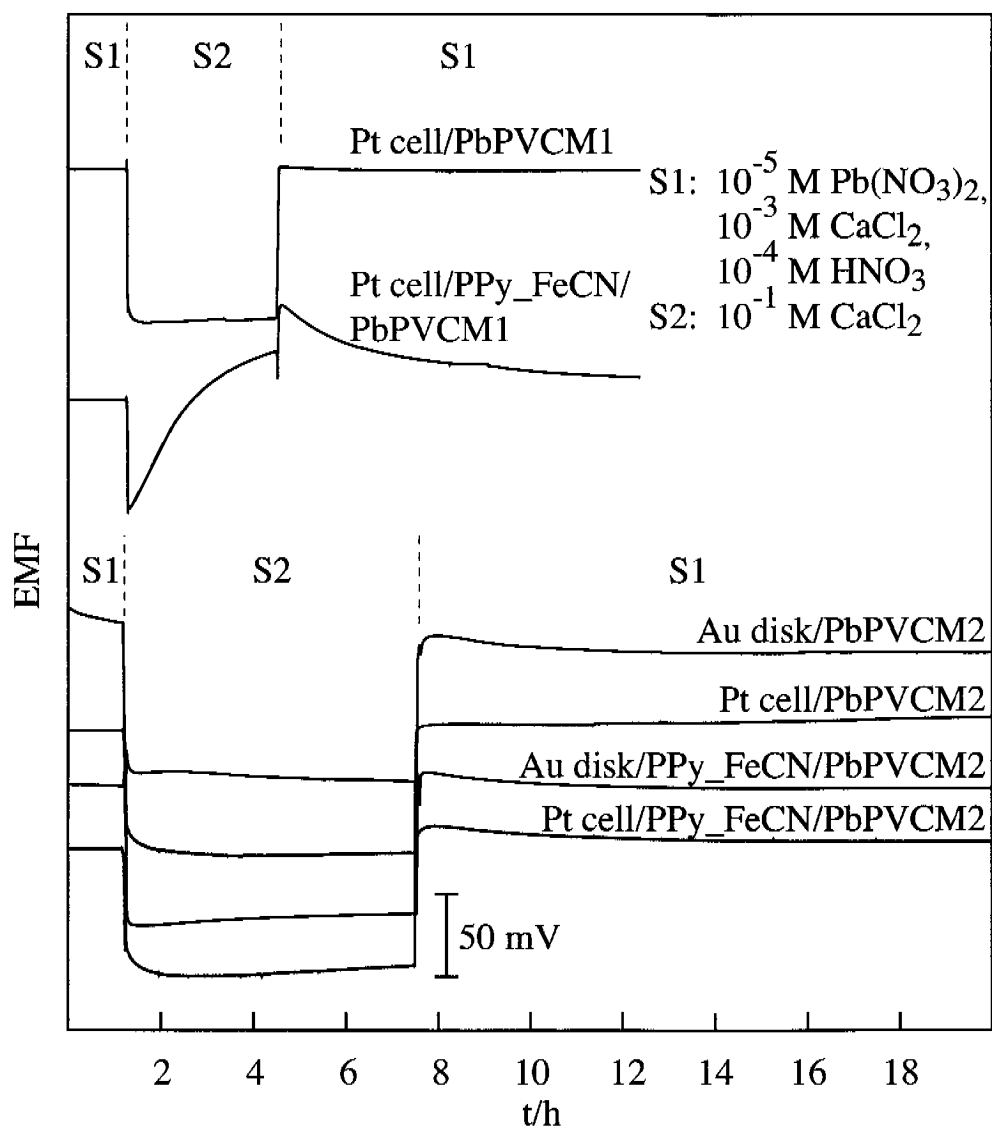
Figure 6.13. Water layer tests on SC Pb^{2+}-ISEs without and with PPy layer. A significant water layer was only observed with PPy-based SC ISEs that had only been rinsed briefly with water after electropolymerization (top). All other PPy layers were soaked in water for 4 h before the membrane was applied (bottom).
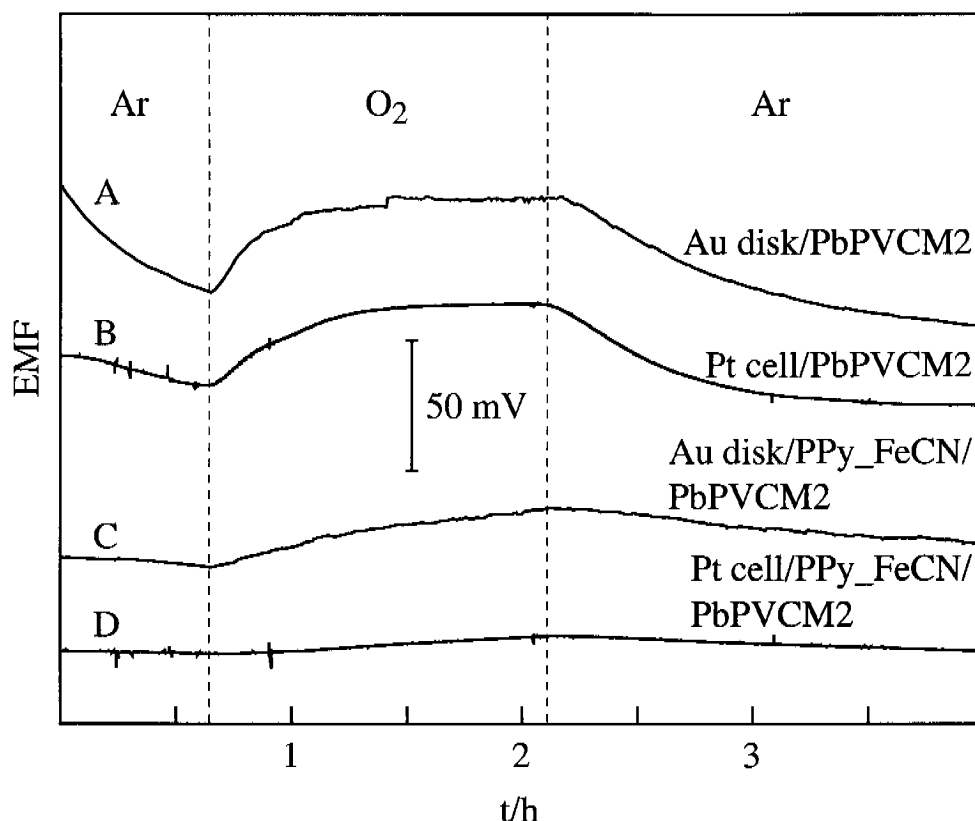
Figure 6.14. Influence of O_2 on the EMF of Pb^{2+}-selective SC ISEs without (A,
B) and with (C, D) inner PPy layer. Sample solution: 0.1 M $CaCl_2$.

Response times of one Au disk and two screen-printed Pt-based ISEs are shown
in Figure 6.15. At low concentrations, Pt electrodes showed slower responses
than Au disk electrodes. Upon changing the sample concentration from 10^{-10}
directly to 10^{-7} M, the potential drifts for Pt-based SC ISEs were < 0.4
mV min^{-1} after 11 min for the second- and 18 min for the last-placed electrode
in the flow-through cell; for the Au disk-based electrode it was < 0.4 mV min^{-1}
after 6 min.
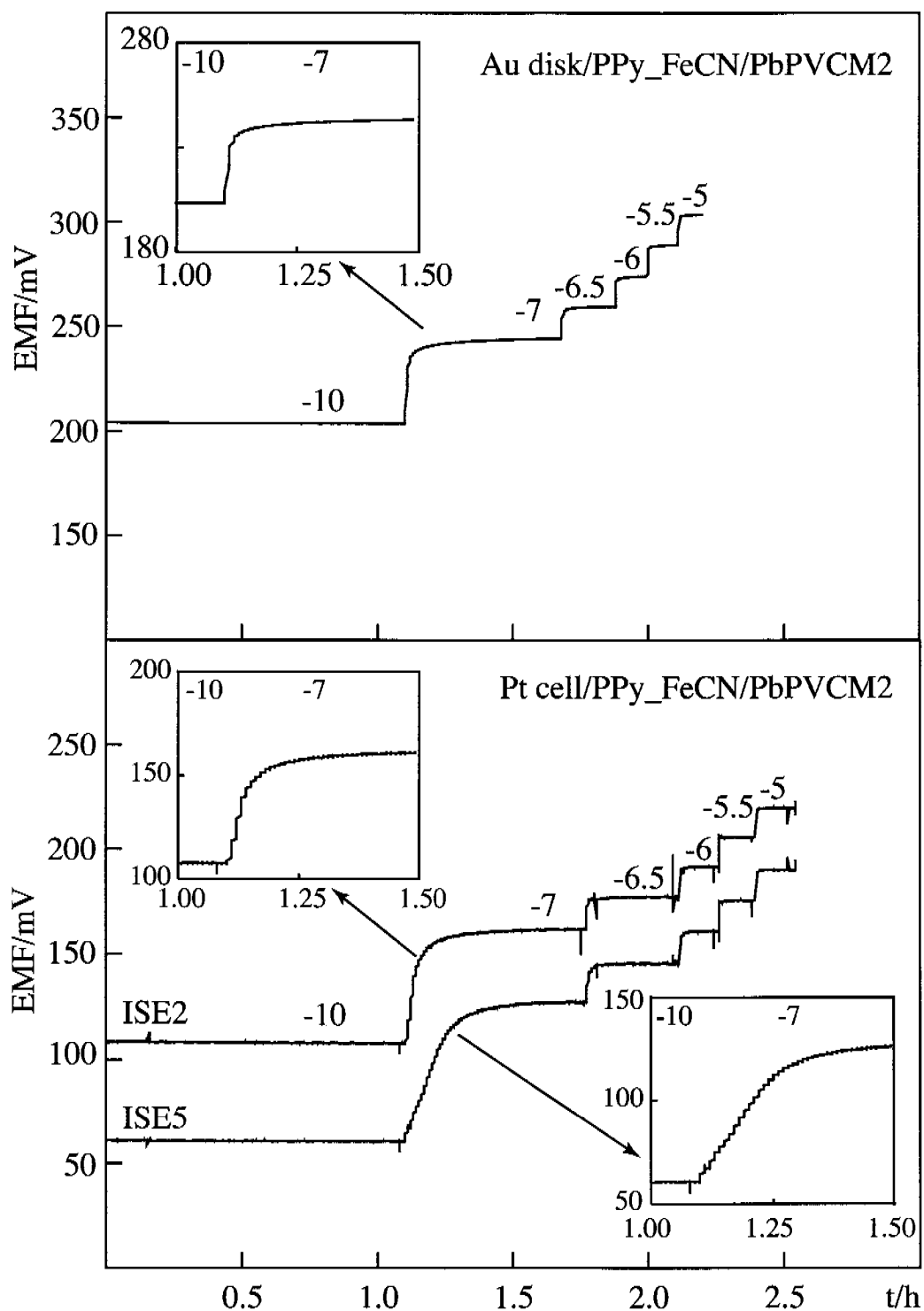
Figure 6.15. Time traces of EMF response of Pb^{2+}-selective Au-disk (top) and Pt-based (bottom) SC electrodes, both with an inner PPy layer. ISE2 is placed in the second, ISE5 in the last position of the flow-through cell (compare Figure 6.10). The values given above the curves indicate the respective logarithmic molar Pb^{2+} concentrations in the sample.

At concentrations above 10^{-7} M, no difference between the two ISE setups was observed. At low sample concentrations in the flow-through cell, however, it takes longer until enough Pb^{2+} ions are transported to the membrane surface since only small sample volumes come into contact with the membrane (flow rate, 0.2 mL min^{-1}, as a comparison, the sample volume in the batch mode was 500 mL). Consequently, the membrane interface requires more time to equilibrate with the sample. The longer response time of the SC ISE in position five compared with that in position two of the flow-through cell supports this hypothesis. When the sample solution reaches the ISE in position five, its Pb^{2+} content is already depleted because of the contact with the other ISE membranes before.

6.4 Optimization of Pb^{2+}-selective SC electrodes based on POT and plasticizer-free methacrylic copolymer membranes

From earlier experiments, it is known that beside the solid contact also the membrane composition can influence the membrane adhesion and, therewith, the formation of an inner water layer between internal electrode and liquid membrane [60]. It was found that PVC membranes with a lower plasticizer content have better adhesion properties than those with a higher plasticizer/PVC ratio [60]. Recently, plasticizer-free methacrylic-acrylic copolymers [73,74,76] and methacrylic copolymers [79] have been introduced as matrices for LC ISE membranes. The diffusion coefficients of ion-ionophore complexes in these copolymers were found to be approximately three orders of magnitude lower than in conventional plasticized PVC membranes [81]. Considering the biocompatibility as well as the possibility of miniaturization of the sensor, such membranes have the advantage that the plasticizer cannot be washed out from the membrane.

The absence of plasticizer makes this membrane material especially attractive for SC ISEs. So far, only one example of a PPy-based SC ISE with a methacrylate-acrylate copolymer membrane matrix has been published [82]. Hence, it was decided to further investigate such plasticizer-free membranes with CP-based SC ISEs, focusing especially on their lower detection limits and the possible formation of an inner water layer. Owing to the good mechanical and potentiometrical properties of a series of LC ISEs [79], a methyl methacrylate-decyl methacrylate (MMA-DMA) copolymer was selected as membrane matrix.

Table 6.4. Potentiometric selectivity coefficients, log $K_{Ca,J}^{pot}$, and response slopes (in parentheses, mV decade^{-1}; concentration range, 10^{-1}–10^{-4} M) obtained with the separate solution method [16] for optimized Ca^{2+}-selective LC electrodes based on a conventional PVC/DOS membrane [38] and for Ca^{2+}-selective MMA-DMA SC electrodes with drop-cast POT as inner layer (CaMDM; SD, n = 5).

Ion J	Ca^{2+}-selective PVC/DOS membrane	CaMDM
H^+	-3.8 (56.8)	-4.0 ± 0.1 (54.3 ± 0.7)
Na^+	-5.8 (50.6)	-5.1 ± 0.1 (51.6 ± 0.8)
K^+	-6.5 (40.1)	-6.2 ± 0.1 (52.7 ± 1.7)
Mg^{2+}	-9.5 (29.4)	-6.2 ± 0.1 (28.9 ± 1.8)

In preliminary experiments, polypyrrole and drop-cast poly(3-octylthiophene) (POT dc) layers were tested as solid-contact layer between a Ca^{2+}-selective MMA-DMA membrane (CaMDM) and an Au disk electrode (for construction, see Figure 6.5). PPy layers were found to be incompatible with MMA-DMA membranes since no Nernstian response was obtained for the corresponding

sensors. In contrast, SC ISEs prepared with drop-cast POT showed Nernstian responses with detection limits of 10^{-9} M Ca^{2+} and selectivity coefficients comparable to those of a conventional PVC/DOS membrane of similar composition (Table 6.4). Because the EMF of these electrodes was influenced by light, all experiments were conducted in the dark.
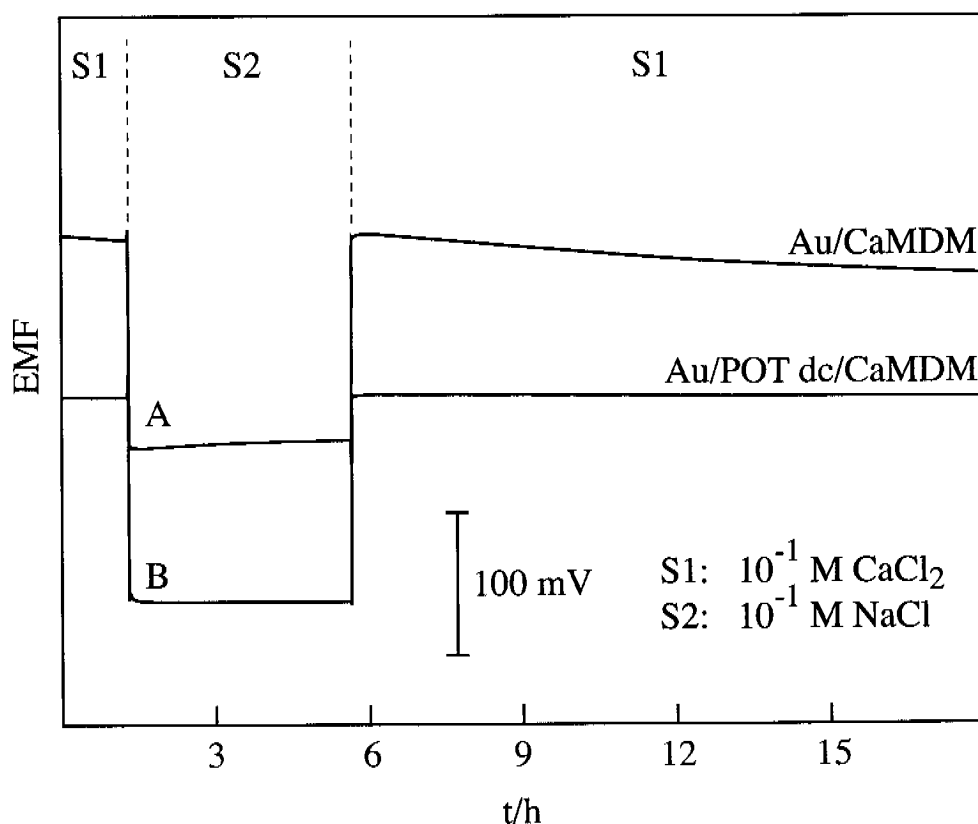
Figure 6.16. Water layer tests on Ca^{2+}-selective SC ISEs without (A) and with a drop-cast POT (POT dc) layer (B).

Coated-wire type ISEs with the same MMA-DMA membrane had comparable detection limits but showed small potential drifts (initial drifts, 3 mV h^{-1} in solutions of interfering or primary ion) during the water layer test, whereas SC ISEs with the drop-cast POT layer were perfectly stable (Figure 6.16). A similar behavior was observed in the oxygen test: Upon alternately bubbling argon and oxygen through the sample solution, coated-wire type electrodes gave EMF

steps of ca. 7 mV, whereas POT electrodes showed stable potentials (Figure not shown). Thus, it was concluded that an inner water layer had formed in the coated-wire type electrodes, but not in the POT-based SC ISEs.

As for the Ca^{2+}-selective membranes, the selectivity coefficients obtained for the Pb^{2+}-selective MMA-DMA membrane (PbMDM) in drop-cast POT-based electrodes were comparable to those of LC ISEs with a PVC/DOS membrane of similar composition (see Table 6.5). Again, no difference in selectivities was found between coated-wire type and POT-based electrodes with the MMA-DMA membrane.

Table 6.5. Potentiometric selectivity coefficients, log K_{PbJ}^{pot}, and response slopes (in parentheses, mV decade^{-1}; concentration range, 10^{-1}–10^{-4} M) obtained with separate solution method [16] for optimized Pb^{2+}-selective LC electrodes based on a conventional PVC/DOS membrane [156] and for Pb^{2+}-selective MMA-DMA SC electrodes with drop-cast POT as inner layer (PbMDM; SD, n = 10).

Ion J	Pb^{2+}-selective PVC/DOS membrane	PbMDM
H^+	-7.5 (57.1)	-7.9 ± 0.2 (52.9 ± 2.3)
Na^+	-7.5 (61.4)	-8.7 ± 0.2 (59.0 ± 1.0)
K^+	-6.9 (58.1)	-8.7 ± 0.2 (54.6 ± 2.2)
Ca^{2+}	-13.1 (27.1)	-14.3 ± 0.2 (26.6 ± 2.7)

It has to be mentioned, however, that the solvent used to dissolve the membrane components was of crucial importance for obtaining good selectivities. When the membrane components were dissolved in tetrahydrofuran (THF), which has the advantage of drying slowly and giving smooth membrane surfaces, the selectivity coefficients of POT SC ISEs were much worse than those of the

corresponding coated-wire type electrodes. Apparently, during the longer time required for THF to evaporate, POT diffused into the membrane and deteriorated its selectivity. A similar effect had already been observed for Pb^{2+}-selective PVC/DOS membranes (cf. paragraph 6.3). Thus, in all further experiments with drop-cast POT-based SC ISEs, the membrane components were dissolved in methylene chloride.
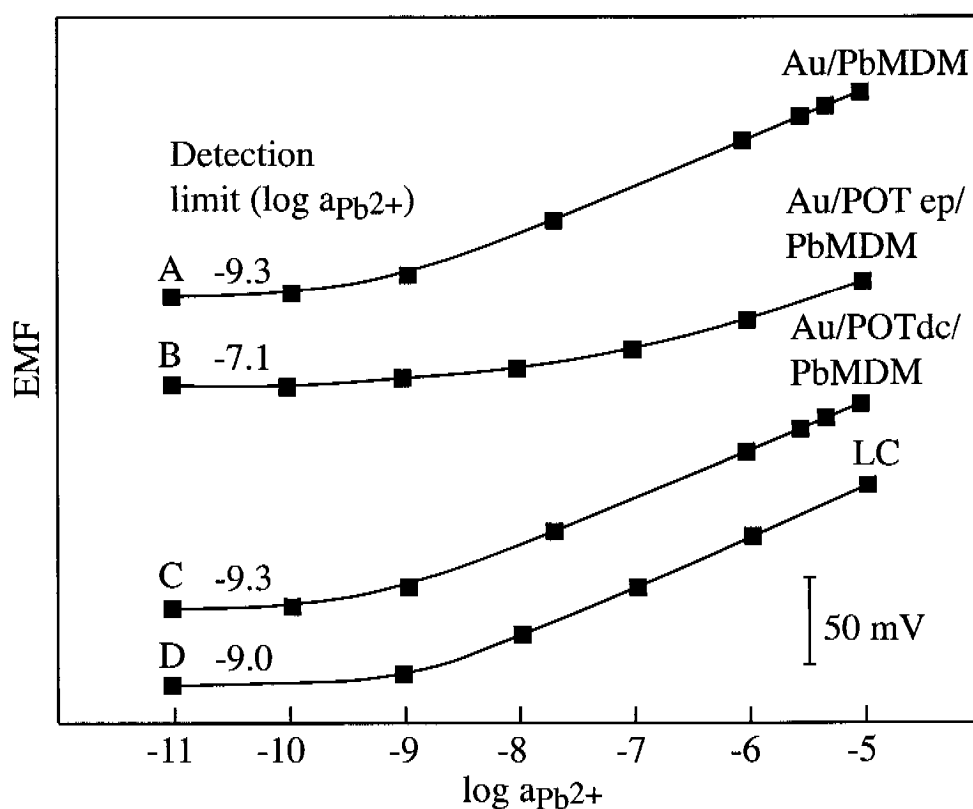
Figure 6.17. Calibration curves obtained by successively increasing the Pb^{2+} activity of the sample (background: 10^{-4} M HNO_3) for SC ISEs without (A), with electropolymerized (B), and with drop-cast (C) inner POT layer, as well as for a LC ISE of the same membrane composition (D).

The deterioration of the membrane selectivities observed with drop-cast POT led to the idea to test electropolymerized POT (POT ep) as an inner CP layer, which has a higher charge density than the drop-cast form and, therefore, a

lower solubility in THF. The selectivity coefficients of such electrodes having ISE membranes whose components had been dissolved in THF were, indeed, comparable to those of coated-wire type electrodes prepared analogously. Below 10^{-5} M Pb^{2+}, however, their calibration curves showed sub-Nernstian slopes and detection limits that were worse by at least two orders of magnitude than those of drop-cast POT (Figure 6.17, curves B and C) and of coated-wire type electrodes (curve A). Detection limits in the range of 10^{-9} M Pb^{2+} were also achieved with LC ISEs based on the same membrane (curve D), if the internal filling solution was buffered to a very low Pb^{2+} activity (log $a_{Pb^{2+}_{free}}$ = -11.45).

Water layer tests gave an explanation for the worse lower detection limit obtained with ISEs having electropolymerized POT as solid contact (see Figure 6.18). A positive potential drift in the interfering ion solution, followed by a negative drift in the primary ion solution, indicating the formation of an inner water layer, was only observed for electrodes based on electropolymerized POT. As already explained in the previous chapters, the presence of a water layer increases the lower detection limit. Apparently, either the porosity or/and the higher charge density of electropolymerized POT facilitated the formation of an inner water layer. The fact that for coated-wire type electrodes, there was no indication of an inner water layer being formed, is rather astonishing but can be attributed to the good adhesion of the membrane to the Au disk.
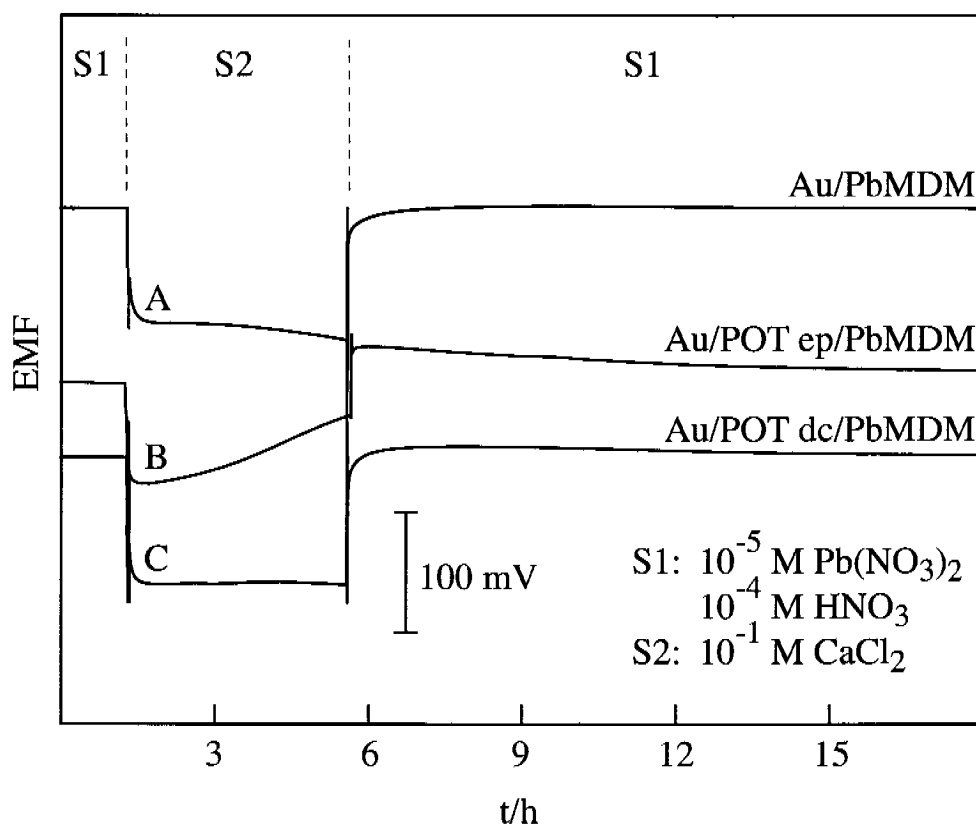
Figure 6.18. Water layer tests on Pb^{2+}-selective SC ISEs without (A), with electropolymerized (B), and with drop-cast (C) inner POT layer.

However, the oxygen tests shown in Figure 6.19 demonstrate the importance of having a CP layer between membrane and Au disk. When oxygen was first removed and then added again by alternately bubbling argon and oxygen through the sample solution, coated-wire type electrodes showed an EMF step of ca. 30 mV, whereas both types of POT electrodes gave stable EMF responses. Drop-cast POT is applied in its undoped, semi-conducting form, which is more stable than the oxidized, charged form. Therefore, it is not clear why it is capable of stabilizing the EMF of SC ISEs upon oxygen fluctuation in solution. It must be assumed that a very small part of the CP is charged and a redox couple POT/POT^{n+} or POT/POT^{m-} is present, which stabilizes the potential at the metal/POT interface. Additionally, an ion exchange at the POT/ISE membrane interface must take place.
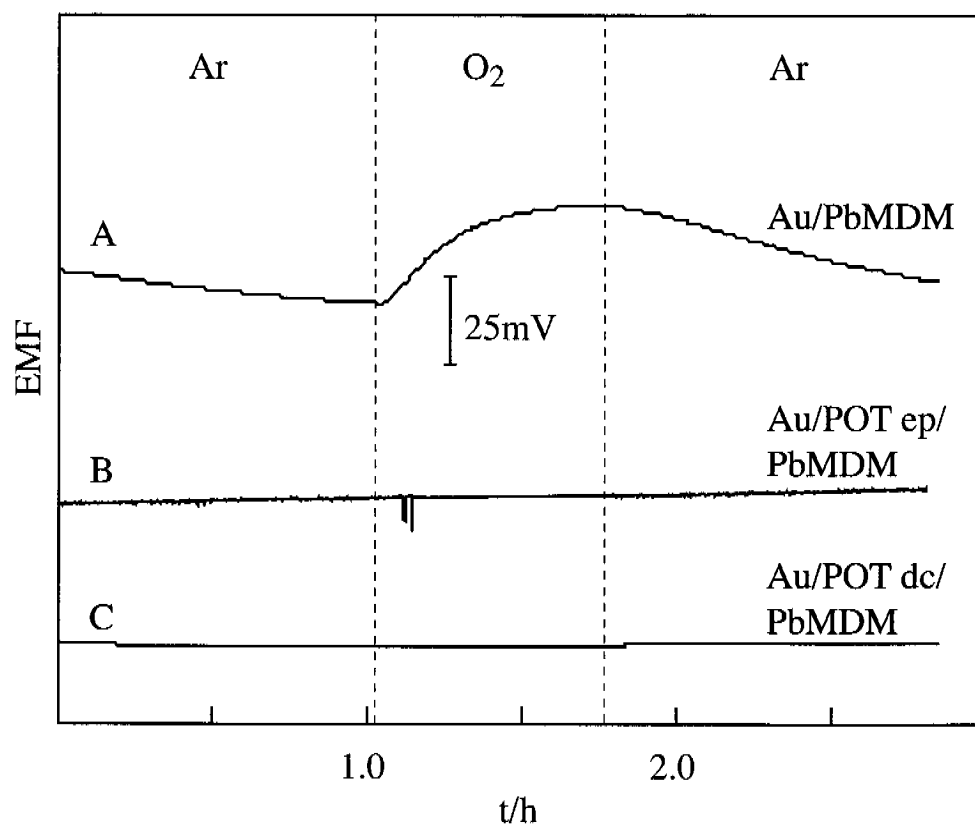
Figure 6.19. Influence of oxygen on the EMF of Pb^{2+}-selective SC ISEs without (A), with electropolymerized (B), and with drop-cast (C) inner POT layer. Sample solution: 0.1 M $CaCl_2$.

An important advantage of the MMA-DMA membrane SC ISEs compared to the corresponding LC ISEs is shown in Figure 6.20. They have much faster response times at low concentrations than LC ISEs (e.g. 2 min after changing sample from 10^{-9} to $10^{-7.7}$ M, drift < 0.4 mV min^{-1}). At concentrations above 10^{-7} M, the response times of both electrode types were similar. The higher noise of LC ISEs is a consequence of a higher membrane thicknesses and thus, higher electrical resistance.
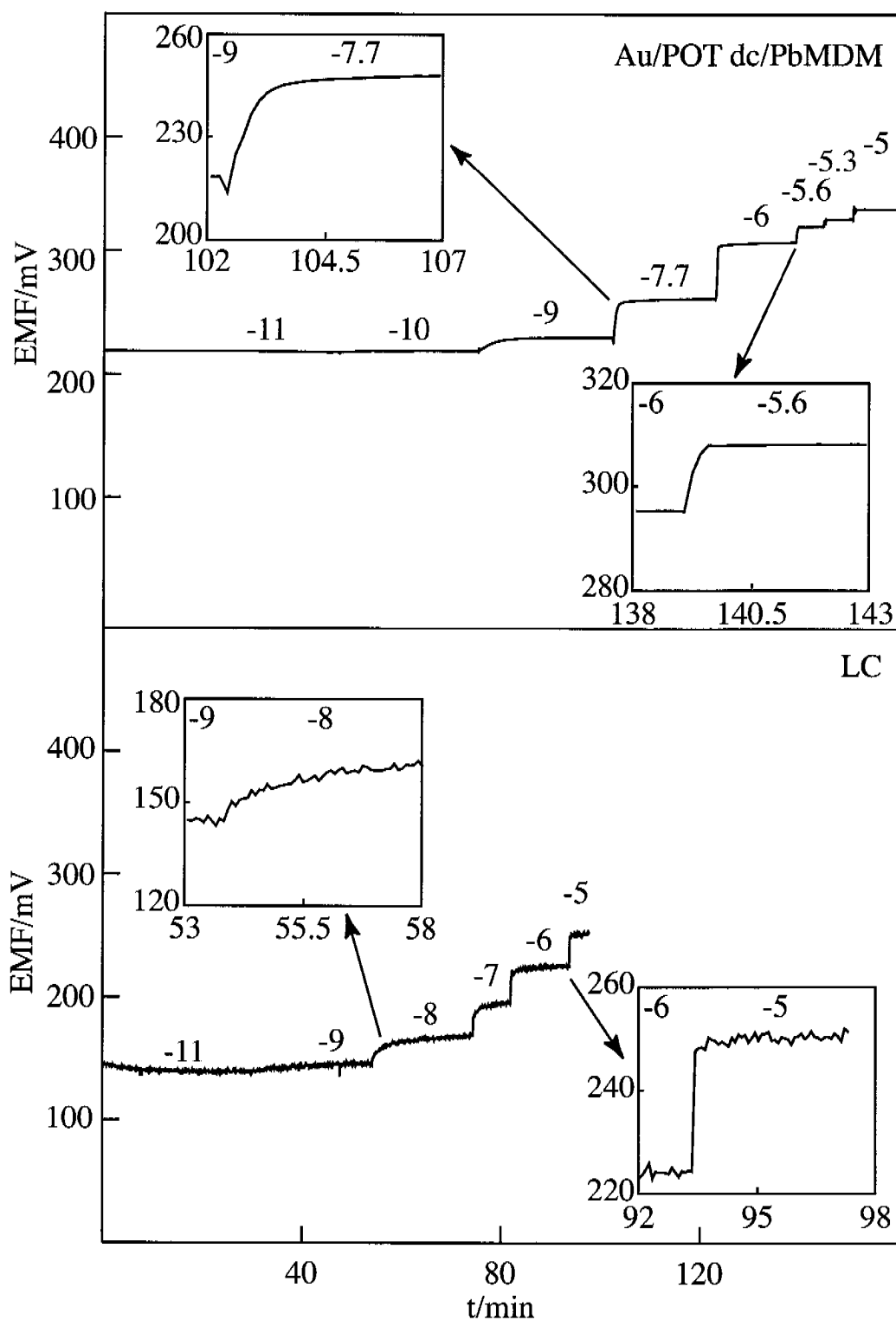
Figure 6.20. EMF time traces of Pb^{2+}-selective SC electrodes based on a MMA-DMA membrane with an inner drop-cast POT layer (top) and of LC ISE with the same membrane (bottom). The values given above the curves indicate the respective logarithmic molar Ca^{2+} concentrations in the sample.

6.5 Conclusions

Overall, the results of the present study showed that SC ISEs based on conducting polymers are a very promising platform to reach low detection limits. If the CP and the membrane matrix are chosen carefully, it is possible to obtain reproducible and stable EMF responses and very good selectivities with such sensors. In addition, their lifetime is significantly improved.

Since a variety of different conducting polymers and membrane materials were investigated in view of their application in SC ISEs, an overview of the results are shown in Table 6.6 for Ca^{2+}-SC ISEs and in Table 6.7 for Pb^{2+}-SC ISEs. In these Tables, LDL stands for the lower detection limit (-log a), the + sign for significant EMF drifts observed in the water layer test (H_2O) and the oxygen test (O_2) indicating the presence of an inner water layer and oxygen sensitivity, respectively, and the − sign means that the EMF responses were stable. Gaps in the Tables signify that the corresponding solid-contact material was not examined in combination with this membrane composition.

A preliminary study on Ca^{2+}-selective SC electrodes with various CPs in view to their use as solid contacts showed that PPy doped with potassium hexacyanoferrate(II)/(III) (PPy_FeCN) and drop-cast, undoped POT (POT dc) are better solid-contact materials than PPy doped with potassium chloride (PPy_KCl). The use of the latter as a solid contact did not improve the performance of the ISEs compared with that of analogous coated-wire type electrodes, whereas solid contacts based on PPy_FeCN or POT had beneficial effects. Their use improved the ISEs' lower detection limits, stabilized their EMF response, and reduced their sensitivity to oxygen.

Table 6.6. Main characteristics of Ca^{2+}-selective CP-based SC ISEs.

SC layer	PVC (66 wt % plasticizer)			Polyurethane (33 wt % plasticizer)			MMA-DMA (plasticizer-free)		
	LDL	H_2O	O_2	LDL	H_2O	O_2	LDL	H_2O	O_2
none	7.8–8.3	+	+	7.0–8.3	+	+	9.0	+	+
PPy_KCl	7.8–8.3	+	+	7.0–8.3	+	+			
PPy_FeCN	8.8–9.0	–	+	8.3–8.4	+	+	*		
POT dc	8.4–8.7	–	–	8.2–8.3	–	–	9.1	–	–

* PPy_FeCN was tested in combination with the Ca^{2+}-selective MMA-DMA membrane but no Nernstian response was obtained

Experiments with Pb^{2+}-SC ISEs showed that the choice of the appropriate CP solid contact strongly depended on the membrane composition. For PVC/DOS membranes, it was not possible to use drop-cast POT since it diffused into the membrane and deteriorated the selectivity behavior, but the same membrane could be used in combination with potassium hexacyanoferrate(II)/(III)-doped PPy. Especially in the flow-through cell, where the membranes are tightly pressed against the internal electrode, CP-based SC ISEs with high potential stabilities and very low detection limits were obtained. On the other hand, solid contacts based on polypyrrole were not compatible with MMA-DMA membranes; whereas drop-cast POT could be used instead. Electropolymerized POT (POT ep) was also tested in combination with MMA-DMA membrane but without success.

Table 6.7. Main characteristics of Pb^{2+}-selective CP-based SC ISEs.

SC layer	PVC (66 wt % plasticizer)			MMA-DMA (plasticizer-free)		
	LDL	H_2O	O_2	LDL	H_2O	O_2
none	7.8–8.5		+	9.3	–	+
PPy_FeCN	9–9.3	–	+			
POT ep				7.1	+	–
POT dc	*			9.3	–	–

* POT dc was tested in combination with a Pb^{2+}-selective PVC/DOS membrane but it diffused into the membrane and deteriorated its selectivity behavior.

The static detection limit, which is dictated only by the membrane's selectivity behavior, was not reached with any of the SC ISEs under study. The observed detection limits of ca. 10^{-9} M for Ca^{2+}- and Pb^{2+}-sensors indicate that the primary ion concentration at the membrane surface was still influenced by ion-exchange processes at the membrane/sample interface. A further improvement of the lower detection limits can only be achieved by drastic miniaturization of the ISEs combined with the synthesis of new ionophores showing better selectivities.

6.6 Experimental

6.6.1 Reagents

Poly(3-octylthiophene) (POT) was obtained from Applications Chemistry & Technologies (AC&T, Saint-Egrève, France). Pyrrole purum (Fluka AG, Buchs, Switzerland) was distilled prior to use and kept under Ar at low temperature in the dark. Propylene carbonate (anhydrous, 99.7%) and lithium tetrafluoroborate (98%) were from Sigma-Aldrich (Milwaukee, USA), and 3-octylthiophene from Acros Organics (New Jersey, USA). The MMA-DMA polymer was synthesized as described previously [79] by applying a somewhat higher reaction temperature (95 °C instead of 85 °C). The calcium ionophore N,N-dicyclohexyl-N',N'-dioctadecyl-3-oxapentanediamide (ETH 5234), and the lead ionophore, $tert$-butylcalix[4]arene-tetrakis(N,N-dimethylthioacetamide) as well as potassium tetrakis[3,5-bis(trifluoromethyl)phenyl]borate (KTFPB), sodium tetrakis[3,5-bis(trifluoromethyl)phenyl]borate (NaTFPB), tetradodecyl-ammonium tetrakis-(4-chlorophenyl)borate (ETH 500), bis(2-ethylhexyl) sebacate (DOS), poly(vinyl chloride) (PVC), Tecoflex$^®$, tetrahydrofuran (THF), and cyclohexanone (all Selectophore$^®$), potassium hexacyanoferrate(II) trihydrate ($K_4Fe(CN)_6 \cdot 3H_2O$), ethylenediaminetetraacetic acid disodium salt dihydrate ($Na_2EDTA \cdot 2H_2O$), Nitrilotriacetic acid (NTA), $MgCl_2 \cdot 6H_2O$, methylene chloride, and chloroform (all puriss. p.a.), and $Pb(NO_3)_2$ (lead ion chromatography standard solution, 1.0 g L^{-1} in HNO_3) were from Fluka. Hydrochloric acid (1 M) and sodium hydroxide (0.1 M) were Titrisol$^®$, $CaCl_2$, NaCl, and KCl, and nitric acid (65%) were Suprapur$^®$ from Merck (Darmstadt, Germany). Aqueous solutions were prepared with deionized water (specific resistance: 18 MΩ cm; NANOpure; Barnstead, Basel, Switzerland).

6.6.2 Preparation of solid contacts

Three types of electrodes were prepared for solid-contact ISEs. Gold tips for rotating disk electrodes (Au disk of 3 mm Ø; type 6.1204.020, Metrohm AG, Herisau, Switzerland, see Figure 6.5) were polished with 0.3 μm alumina (Metrohm) and rinsed with water and methylene chloride. Silicon wafers were rinsed with water and acetone and dried in an Ar stream. Gold electrodes designed for the use in a flow-through cell as described elsewhere [86] (see also Chapter 5) were obtained by thermal evaporation of 200 nm of Au (99.99 %, Johnson Mattey, Zürich) with deposition rates of 2 nm/s onto the wafers covered with a layer of 6 nm of Cr (99.99 %, Balzers, Liechtenstein) using a Balzers MED 010 instrument at a pressure of ca. 10^{-3} Pa. Screen-printed Pt electrodes described elsewhere [86] (see Figure 6.10) for use in the flow-through cell were cleaned in O_2 plasma (pressure, 1.7 x 10^{-2} mbar; MCS 020 instrument, Balzers) before further treatment.

Electrochemical polymerization of pyrrole and 3-octylthiophene was performed in a one-compartment three-electrode electrochemical cell with a μAutolab Type II potentiostat/galvanostat (Eco Chemie, Utrecht, Netherlands). A Ag/AgCl/3 M KCl electrode (Bioanalytical Systems, West Lafayette, USA) was used as reference and a Pt wire as counter electrode.

Polypyrrole (PPy) films were deposited on Au disk and Pt electrodes by potentiostatic electropolymerization, PPy films doped with potassium hexacyanoferrate(II)/(III) (PPy_FeCN) in an aqueous solution of 0.5 M $K_4Fe(CN)_6$ and 0.5 M pyrrole, (cf. ref. [86]), and those doped with potassium chloride (PPy_KCl) in an aqueous solution of 0.1 M KCl and 0.2 M pyrrole. Solutions were purged with Ar before electropolymerization. To prepare PPy_FeCN films, a potential of 1 V was applied during 90 s for the Pt electrodes and only the 40 s for Au disk electrodes since after 90 s, the thick and porous PPy film used to come off easily from the Au disk. For PPy_KCl films on Au

disk electrodes, 1 V was applied during 60 s. On the 5-site Pt electrode arrays the deposition was performed simultaneously on 3–5 electrically connected individual electrodes. After electropolymerization, the electrodes were rinsed with water. Based on preliminary experiments with PPy_FeCN, they were generally left soaking in water for 4 h and rinsed again with water in order to remove any excess of doping electrolyte. Then, the PPy films were dried at room temperature and rinsed with small aliquots of THF to remove residual traces of water.

Poly(3-octylthiophene) (POT) films were deposited on Au disk electrodes by galvanostatic electropolymerization of 0.1 M 3-octylthiophene in a solution of 0.1 M lithium tetrafluoroborate in propylene carbonate purged with Ar. A constant current of 0.4 A was applied for 80 s. The electropolymerization was performed in the hood since propylene carbonate is irritating to the eyes. The electrodes were, first, rinsed with propylene carbonate and, then, with THF and dried at room temperature.

Solvent-soluble POT was applied on Au disks and on Au-coated silicon wafers by drop-casting 2 x 10 μL of a 25 mM solution (calculated relative to the monomer) in chloroform yielding a layer of ca. 5 mm diameter, which was dry after 2 min.

6.6.3 ISE membranes and electrodes

The plasticized Ca^{2+}-selective membranes for SC ISEs contained Ca^{2+} ionophore (1 wt %, 13 mmol kg^{-1}), KTFPB (0.6 wt %, 6.2 mmol kg^{-1}), DOS (65.9 wt %), and PVC (32.5 wt %) for CaPVCM, and Ca^{2+} ionophore (1 wt %, 13 mmol kg^{-1}), KTFPB (0.5 wt %, 6.0 mmol kg^{-1}), DOS (33.1 wt %), and Tecoflex® (65.4 wt %) for CaPuM. The membranes were prepared by dissolving the membrane components (202.2 mg for CaPVCM and 201.8 mg for CaPuM) in THF (2 mL). For selectivity measurements with LC ISEs, a membrane solution of the same

composition as CaPuM was cast into a glass ring (i.d., 2.4 cm). Overnight evaporation yielded a transparent membrane. A disk of 5 mm Ø was punched from this master membrane and glued to PVC tubings with a PVC/THF slurry. The internal solution contained 10^{-3} M $CaCl_2$ and 5 x 10^{-2} M Na_2EDTA adjusted to pH 9.0 with 10^{-1} M NaOH giving log $a_{Ca^{2+}_{free}}$ = -10.3.

The plasticized Pb^{2+}-selective membranes for SC ISEs contained Pb^{2+} ionophore (0.07 wt %, 0.7 mmol kg^{-1}), NaTFPB (0.03 wt %, 0.3 mmol kg^{-1}), ETH 500 (1.3 wt %, 11.5 mmol kg^{-1}), DOS (62.1 wt %), and PVC (36.5 wt %) for PbPVCM1 (membrane with low concentrations of ionophore and ionic sites, cf. [7]), and Pb^{2+} ionophore (1.0 wt %, 9.6 mmol kg^{-1}), NaTFPB (0.44 wt %, 5.0 mmol kg^{-1}), ETH 500 (1.1 wt %, 9.6 mmol kg^{-1}), DOS (61.8 wt %), and PVC (35.6 wt %) for PbPVCM2. The membranes were prepared by dissolving the components in cyclohexanone (418.4 mg in 2.8 mL for PbPVCM1 and 208.6 mg in 1.4 mL for PbPVCM2). The corresponding solutions for the Pb^{2+}-selective membranes for POT SC ISEs (i.e. Au slide electrodes used in the flow-through cell) and in LC ISEs used for selectivity measurements were poured into glass rings (i.d., 7 cm for PbPVCM1 and 5 cm for PbPVCM2). Overnight evaporation yielded transparent membranes. For LC ISEs, disks of 5 mm Ø were punched from this master membrane and glued to PVC tubings with a PVC/THF slurry. The internal filling solution was 10^{-2} M NaCl.

The plasticizer-free Ca^{2+}-selective MMA-DMA membrane for SC ISEs contained Ca ionophore (1.6 wt %, 20.1 mmol kg^{-1}), NaTFPB (0.5 wt %, 5.1 mmol kg^{-1}), and MMA-DMA copolymer (97.9 wt %). The membrane was prepared by dissolving the membrane components (202.2 mg) in methylene chloride (1.5 mL). The Pb^{2+}-selective MMA-DMA membrane for the solid-contact ISE contained Pb ionophore (1.1 wt %, 9.9 mmol kg^{-1}), NaTFPB (0.5 wt %, 5.2 mmol kg^{-1}), ETH 500 (1.1 wt %, 9.8 mmol kg^{-1}), and MMA-DMA copolymer (97.4 wt %). The membrane was prepared by dissolving the membrane components (199.6 mg) in methylene chloride (2 mL). Before drop-

casting, the membrane solution was degassed by sonication for 10 min. The corresponding Pb^{2+}-selective MMA-DMA membrane for LC ISEs contained Pb ionophore (1.0 wt %, 9.5 mmol kg^{-1}), NaTFPB (0.5 wt %, 5.2 mmol kg^{-1}), ETH 500 (1.2 wt %, 10.1 mmol kg^{-1}), MMA-DMA copolymer (97.3 wt %), and aqueous 10^{-2} M $Pb(NO_3)_2$ (36.5 µL) solution. The components totaling 140 mg were dissolved in THF (1.0 mL) and poured into a glass ring (i.d., 2.2 cm). Overnight evaporation yielded a transparent membrane of about 200 µm thickness. After casting, the membrane was immersed for about 1 h in distilled water in order to detach the glass ring with the membrane more easily from the glass plate. Then, the glass ring together with the membrane was put into a plastic beaker containing the internal solution, and the membrane was conditioned overnight. From this membrane, an appropriate amount to give, in the end, a layer of ca. 2 mm thickness, was cut and stuffed into a small piece of PVC tubing (1.6 mm i.d. and 3.1 mm o.d.) previously inserted into one end of a wider PVC tubing (3.1 mm i.d. and 6.3 mm o.d.). This kind of assembly was necessary to keep the highly sticky membrane material, which, at the same time, has a tendency to flow, in place. In the thus assembled tubing, a plastic pipette tip was inserted and, then, the tubing and the tip were filled with the internal solution containing 10^{-5} M $Pb(NO_3)_2$ and 10^{-2} M NTA adjusted to pH 7.4, giving $\log a_{Pb^{2+}_{free}} = -11.45$. On top of it, a second pipette tip was mounted with 10^{-3} M NaCl as a bridge electrolyte.

The preparation of Au disk SC electrodes is shown in Figure 6.5. Once the CP coatings were dry, a piece of PVC tubing (ca. 2 cm long) was placed over the tip. This tight PVC surrounding of the tip allowed to cast 100 µl of membrane solution on top of the CP-covered electrode leading to a an estimated membrane thickness of 100–130 µm. It was dried at room temperature overnight for PVC/DOS- and Tecoflex®/DOS-based membranes and during 15 min for MMA-DMA-based membranes. Au disk electrodes without CP layer were prepared analogously.

Once the PPy coatings on the Pt electrodes were dry, 7 μL of the respective membrane solution were drop-cast onto the sensing area, also spreading around it (cf. [86]). As soon as it was dry, an additional 7 μL of membrane solution were applied. For ISEs of the coated-wire type, the membrane solution was directly drop-cast onto the Pt electrodes. Once dry, a 5-site array of Pt/PPy electrodes and a 4-site array of coated-wire type ISEs were assembled in the flow-through cell (see Figure 6.10) in a way that the membranes were pressed from both sides onto the holes in the zig-zag flow channel of the plexiglass cell. Mechanical fixation was provided by silicon rubber springs pressing against the cell walls.

For POT/Au electrodes also applied in the flow-through cell, a disk of 4 mm Ø was punched from the PbPVCM1 master membrane and placed on the POT layer. Coated-wire type electrodes were prepared by placing the membrane directly onto the Au surface. Then, 5 POT SC-ISEs and 4 coated-wire type ISEs were assembled in a 5-site array and a 4-site array, respectively. These two arrays were then assembled in the flow-through cell in the same way as for the Pt/PPy SC-ISEs (see Figure 6.10).

6.6.4 EMF measurements

Potentials were measured with a custom-made 14-channel electrode monitor at room temperature (22 °C). Solid-contact electrodes were kept in darkness. For measurements with Au disk electrodes and LC ISEs, a double-junction Ag/AgCl/3 M KCl reference electrode (type 6.0729.100, Metrohm) containing a 1 M NH_4NO_3 electrolyte bridge was used. Experiments were performed in 500-mL polyethylene beakers. For Pb^{2+} measurements, the beakers were pretreated overnight with 10^{-4} M nitric acid.

The flow-through cell was connected to a peristaltic pump (type ISM597A V.10, Ismatec SA, Zürich, Switzerland) letting the solution pass at a flow rate of 0.21

mL min^{-1}. A flow-through Hg/Hg$_2$Cl$_2$/sat. KCl reference electrode with 3 M KCl as bridge electrolyte (type OP-0829P-S, Radelkis, Budapest, Hungary) was placed downstream from the cell. The bridge electrolyte was continuously pumped through the salt bridge compartment of the reference block, its stream joining with sample effluent from the flow-through cell.

If not mentioned otherwise, EMF values were corrected for liquid-junction potentials according to the Henderson equation. Activity coefficients were calculated by the Debye-Hückel approximation. For measurements in dilute solutions, Ca^{2+}-selective electrodes were conditioned, first, for 2 d in 10^{-4} M and, then, overnight in 10^{-6} M CaCl$_2$ (background: 10^{-4} M NaCl). This same background was used with all CaCl$_2$ sample solutions. The Pb^{2+}-selective electrodes were conditioned, first, during at least 2 d in 10^{-5} M Pb(NO$_3$)$_2$ for PVC/DOS membranes and in 10^{-4} M Pb(NO$_3$)$_2$ for MMA-DMA membranes and then, overnight in 10^{-6} M or 10^{-10} M Pb(NO$_3$)$_2$ for measurements from high to low concentrations or for measurements from low to high concentrations, respectively. The background used with Pb(NO$_3$)$_2$ sample solutions was either 10^{-3} M CaCl$_2$ with 10^{-4} M HNO$_3$ or 10^{-4} HNO$_3$ alone.

For selectivity measurements, the solid- and liquid-contact ISEs were conditioned during 24 h either in 10^{-2} M NaCl for membranes containing KTFPB or in 10^{-2} M KCl for those with NaTFPB.

Seite Leer /
Blank leaf

7 Current responses of ion-selective solvent polymeric membranes at controlled potential

7.1 Introduction

In nearly all applications reported so far, ISEs based on liquid polymeric membranes have been used as potentiometric sensors, i.e., for potential measurements under zero-current conditions. Nevertheless, experiments on ISEs under the influence of electrical current have a long tradition. Early investigations were often performed to elucidate response mechanisms of ion-selective liquid polymeric membranes [157-159] but in some cases, the purpose was to extend the sensors' measuring range [160,161]. Also more recent experiments on ISEs performed under a constant applied current aimed at the optimization of the sensor response. A current-induced modulation of ion fluxes in the membrane permitted an improvement of the lower detection limit by several orders of magnitude [154,162,163]. This effect was in close analogy to that achieved with conventional ISEs in potentiometric experiments, where zero-current ion fluxes in the membrane were suppressed by using an ion buffer in the internal filling solution [6,36,37]).

Recently, the voltammetric and amperometric behavior of ion sensors based on liquid polymeric membrane was further explored in order to expand their applicability [164-170]. It has been demonstrated that the selectivity of these sensors can be altered by varying the magnitude and sign of the applied potential or current [166,168]. Experiments showed that mass transport in the membrane is the limiting diffusion process because diffusion coefficients of ions in the membrane are smaller than in the aqueous phase. To avoid current or potential drifts, a pulsed mode was preferred to a linear sweep mode since ions extracted into the membrane during the measuring pulse can be quantitatively removed by

applying a baseline potential pulse in the interval between two measuring pulses [164,165,168].

A different group of fundamental studies focused on the electrochemical processes at the interface between two immiscible electrolyte solutions (ITIES), consisting of an aqueous sample solution and an organic solvent that contains an ionophore [171-175]. This measuring setup was used in place of the ISE- analog three-phase arrangement (aqueous phase/organic phase/aqueous phase) [176]. The ITIES showed voltammetric and amperometric responses that depended linearly on the primary ion concentration of the sample [175,177], this was the case when polymer-free organic phases [178] or membranes containing a very low amount of PVC were used [179-181] as well as for polymer-free organic phases supported by thin polymeric membranes with microholes [182]. In contrast, in similar experiments conducted with conventional PVC-based ISE membranes, current responses proportional to the logarithm of the primary ion activity (or concentration) of the sample were observed [160,161,166,167].

Practical applications of ionophore membranes in the controlled-potential mode may have been impeded because their above-mentioned current response behavior seemed to be quite contradictory. Here, new results on the current response of ionophore-based ISEs at controlled potential are reported. A theoretical approach is presented to explain the puzzling electrochemical behavior of polymer ISE membranes and related systems.

7.2 Theory

The theoretical model derived here is valid for cation-selective electrodes. A schematic representation of the applied model is shown in Figure 7.1. The membrane is considered as an electroneutral phase containing immobile, monovalent, anionic sites ("fixed" sites) [4,158,163,183]. Together with the

uncharged ionophore (ligand, L), the anionic sites (S) ensure a highly selective transfer of primary cations (I) into and through the membrane. The current flow within the membrane is then found to follow the ohmic law [4,163]:

$$i = AFz_I J_I = -\frac{1}{R_M}\Delta\Phi_M \qquad (7.1)$$

$$R_M = \frac{RT}{z_I F}\frac{d}{AFD_I(org)c_S(org)} \qquad (7.2)$$

where

i	electrical current [A]
J_I	total flux [mol cm^{-2} s^{-1}] of primary ions I of charge number z_I
$\Delta\Phi_M$	electric potential drop within the membrane [V]
R_M	inner membrane resistance [Ω]
A	active membrane area [cm^2]
d	membrane thickness [μm]
D_I(org)	average diffusion coefficient of primary ion (complexed with ionophore) in the organic phase (i.e., membrane phase) [cm^2 s^{-1}]
c_S(org)	given total concentration of anionic sites S in the membrane [mol L^{-1}]
F	Faraday constant (96 485 C mol^{-1})
R	universal gas constant (8.314 J K^{-1} mol^{-1})
T	absolute temperature [K]

Sample solution   ISE membrane   Internal solution

Diffusion layer   Diffusion layer
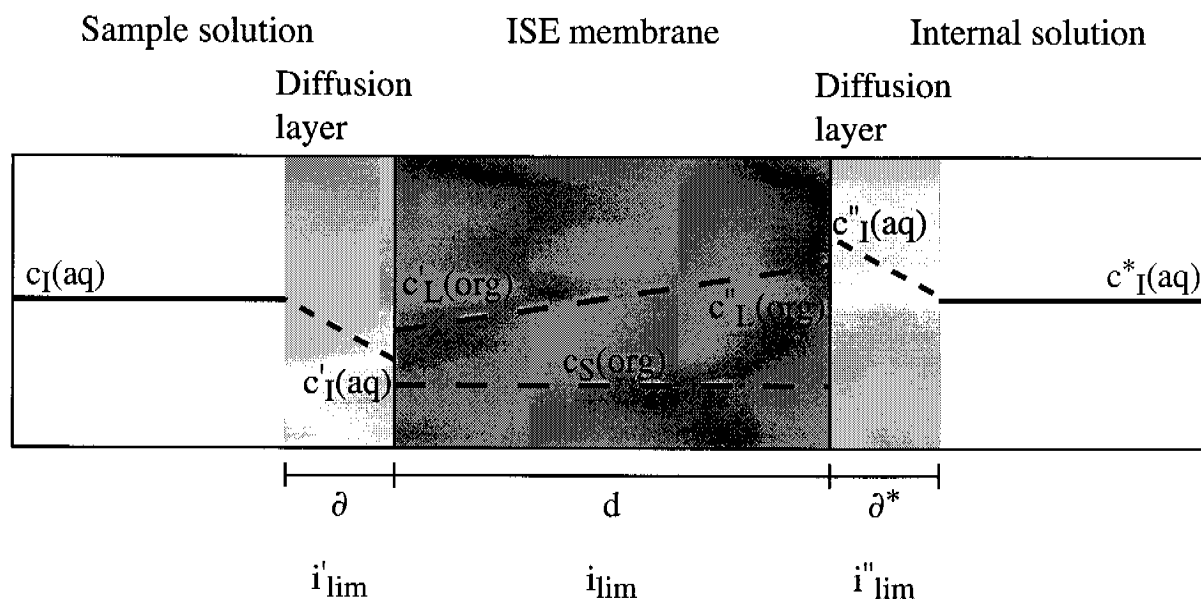
Figure 7.1. Schematic representation of the applied model. The concentration gradients of primary ions (I) in the aqueous diffusion layers (∂ of the sample and ∂^* of the internal solution) and of the free ionophore (L) in the organic membrane phase (thickness d) are shown for a hypothetic situation of a negative potential applied to the system (causing a positive current).

The transmembrane flux of primary ions is coupled with an equivalent diffusion flux through the Nernstian boundary layers of the aqueous (aq) sample (∂) and internal solution (∂^*), respectively. Hence, a current-induced gradient arises between the primary ion concentrations in the bulk of the sample solution, $c_I(aq)$, and at the sample solution/membrane phase boundary, $c_I'(aq)$:

$$i = i'_{lim} \frac{c_I(aq) - c_I'(aq)}{c_I(aq)} \tag{7.3}$$

$$i'_{lim} = \frac{AFz_I D_I(aq) c_I(aq)}{\delta} \tag{7.4}$$

where i'_{lim} is the diffusion-limited current reached for $c'_I(aq) \rightarrow 0$ and $D_I(aq)$ is the diffusion coefficient of the primary ion in aqueous solutions.

In complete analogy, a gradient arises in the internal part of the electrode between the primary ion concentrations in the bulk of the internal solution, $c_I^*(aq)$, and at the internal solution/membrane phase boundary, $c_I''(aq)$:

$$i = -i''_{lim} \frac{c_I^*(aq) - c_I''(aq)}{c_I^*(aq)} \qquad (7.5)$$

$$i''_{lim} = \frac{AFz_I D_I(aq) c_I^*(aq)}{\delta^*} \qquad (7.6)$$

where i''_{lim} is the diffusion-limited current reached for $c_I''(aq) \rightarrow 0$.

After replacing the concentration ratios in Equations 7.3 and 7.5 by the corresponding activity ratios, the boundary activities, $a_I'(aq)$ and $a_I''(aq)$, can be expressed in terms of the respective bulk activities, $a_I(aq)$ and $a_I^*(aq)$:

$$a_I'(aq) = a_I(aq) \frac{i'_{lim} - i}{i'_{lim}} \qquad (7.7)$$

$$a_I''(aq) = a_I^*(aq) \frac{i''_{lim} - i}{i''_{lim}} \qquad (7.8)$$

Another consequence of the current flow in an ionophore membrane is that the (here positively) charged ion-ionophore complexes move in the direction of the current, leading to a concentration gradient of the free ionophore in the opposite

direction [4,158,159]. At steady state, conservation of the ionophore in the membrane requires that

$$J_L + n_I J_I = 0 \qquad (7.9)$$

where J_L is the diffusion flux of uncomplexed ionophore. It is assumed that the primary ion is transported as ion-ionophore complex of a given $1:n_I$ stochiometry. By combining Equations 7.1 and 7.9, it follows that

$$i = -\frac{1}{n_I} AFz_I J_L = i_{lim} \frac{c_L''(org) - c_L'(org)}{2c_L(org)} \qquad (7.10)$$

$$i_{lim} = \frac{2}{n_I} \frac{AFz_I D_L(org) c_L(org)}{d} \qquad (7.11)$$

with

$$c_L(org) = 0.5 \, (c_L'(org) + c_L''(org)) \qquad (7.12)$$

where

$c_L'(org)$, $c_L''(org)$ phase boundary concentrations of the ionophore at the membrane/sample solution interface (′) and at the membrane/internal solution interface (″) [mol L^{-1}]

$D_L(org)$ diffusion coefficient of the free ionophore in the membrane [$cm^2 \, s^{-1}$]

i_{lim} limiting current related to the maximum diffusion flux of ionophore within the membrane [A]

$c_L(org)$ average concentration of the ionophore in the membrane [mol L^{-1}]

From Equations 7.10 and 7.12 follows:

$$c_L'(org) = c_L(org)\frac{i_{lim} - i}{i_{lim}} \tag{7.13}$$

$$c_L''(org) = c_L(org)\frac{i_{lim} + i}{i_{lim}} \tag{7.14}$$

The activities of the primary ion and the concentration of the ionophore at the phase boundaries of membrane/aqueous phases (Equations 7.7, 7.8, 7.13, and 7.14) as well as the concentration of the ionic sites (assumed to be constant in the whole of the membrane) enter into the description of the two interfacial Galvani potential differences, $\Delta\Phi'$ and $\Delta\Phi''$, arising at the membrane/aqueous solution phase boundaries [4,158,163,183]:

$$\Delta\Phi' = \frac{RT}{z_I F}\ln\left[\frac{z_I K_I' a_I'(aq)}{c_S(org)}\right] \quad \text{with} \quad K_I' = k_I \beta_{I,n_I}(c_L'(org))^{n_I} \tag{7.15}$$

$$\Delta\Phi'' = \frac{RT}{z_I F}\ln\left[\frac{z_I K_I'' a_I''(aq)}{c_S(org)}\right] \quad \text{with} \quad K_I'' = k_I \beta_{I,n_I}(c_L''(org))^{n_I} \tag{7.16}$$

where

K_I', K_I'' overall distribution coefficients of primary ions at the respective

         interfaces, related to the standard free Gibbs energy of ion transfer and

including the influence of ion complexation in the membrane

k_I distribution coefficient of the free primary ion between aqueous phase and membrane

β_{I,n_I} stability constant of the predominant $1:n_I$ ion-ionophore complex

After recalling Equation 7.1 for $\Delta\Phi_M$ and substituting the boundary activities (Equations 7.7, 7.8) and concentrations (Equations 7.13, 7.14) in Equations 7.15 and 7.16, the final result for the total membrane potential (E_M) is obtained:

$$E_M = \Delta\Phi_M + \Delta\Phi' - \Delta\Phi'' \tag{7.17}$$

$$E_M = \frac{RT}{z_I F}\ln\left|\frac{a_I(aq)}{a_I^*(aq)}\right| - R_M i + \frac{RT}{z_I F}\ln\frac{1 - i/i'_{lim}}{1 + i/i''_{lim}} + \frac{n_I RT}{z_I F}\ln\frac{1 - i/i_{lim}}{1 + i/i_{lim}} \tag{7.18}$$

where E_M is the potential difference between the bulks of the internal and the sample solutions and i is the current flowing from the sample to the internal solution (for negative signs, vice versa). The first term in Equation 7.18 is the expression for the zero-current membrane potential, the second term is characteristic of an ohmic resistor, and the last two terms are analogous to the formal description of polarographic waves accounting for the influence of current-induced concentration polarizations in the phase boundary regions. The ambivalent amperometric and voltammetric responses of ionophore-based ISEs, evidently, strongly depend on the various experimental parameters of the system. Earlier amperometric experiments on ISEs and ITIES indicated that the current i, generally, is a function of the sample activity $a_I(aq)$. This also becomes obvious from our theoretical approach if Equation 7.18 is rearranged:

$$\frac{i}{i_o} - \ln\frac{1-i/i'_{lim}}{1+i/i'_{lim}} - n_I \ln\frac{1-i/i_{lim}}{1+i/i_{lim}} = \ln\frac{a_I(aq)}{a_I^*(aq)} - \frac{z_I F}{RT}E_M \qquad (7.19)$$

with

$$i_o = \frac{1}{R_M}\frac{RT}{z_I F} = \frac{AFD_I(org)c_S(org)}{d} \qquad (7.20)$$

where i_o is a unit current corresponding to the current established for $\Delta\Phi_M = -25.7$ mV/z_I at 25 °C. The exact type of the activity dependence in Equation 7.19 is, evidently, dictated by the magnitude of the current relative to the parameters i_o, i'_{lim}, i''_{lim}, and i_{lim}.

For the practical relevance of ISEs as amperometric sensors, R_M must be sample-independent and invariant, which is not the case for thin liquid membranes [184]. However, for plasticized PVC membranes used in this work, it was found in hundreds of consecutive measurements [185] that the membrane resistance did not change significantly for sample concentrations above 10^{-6} M and can, therefore, be considered as constant. In analogy, it was assumed that this is also the case for the two other membrane types used in this work, which were not examined experimentally.

The general result in Equation 7.20 can also be considered as an extended description of ITIES systems. However, since diffusion coefficients in the organic phase of ITIES systems are comparable to those in the aqueous sample phase, limitations by mass transport in the organic phase as well as by the ohmic resistance are either nonexistent or may be excluded. For ISE systems, on the other hand, these limiting terms may play a substantial role depending on the magnitude of the various experimental parameters (see below).

7.3 Current responses of ion-selective solvent polymeric membranes at controlled potential in comparison with their theoretical description

In the theoretical paragraph, it was shown that three diffusion processes may limit the current measured on ISE membranes at controlled potential. The diffusion-controlled limiting currents in the two aqueous phases are related to the respective maximum values of the concentration gradients of the primary ion, while the maximum migration current through the membrane is determined by the back-diffusion process of the free ionophore (see Figure 7.1). In the next paragraphs, several ISE systems are discussed in which one or two of the three diffusion processes dominate over others (see also [186]). Since these descriptions are, obviously, restricted to special cases or limited concentration ranges of the primary ion in the aqueous solutions and of the ionophore and ionic sites in the membrane, the full theory has to be applied to an adequate analysis of the complete current response.

In the case of plasticized polymer membranes used for conventional ISEs (containing 33 wt % of PVC), the diffusion coefficients of ionophores and of complexed primary ions are of the order of $1\text{--}5 \times 10^{-8}$ cm s^{-1} [187-192] and are at least 2 orders of magnitude lower than in the aqueous phase [193]. Thus, the membrane resistance is high and the value of i_o comparatively low. It follows that $i_o \ll i'_{lim}$ and $i_o \ll i''_{lim}$ hold as long as both aqueous solutions contain adequate concentrations of primary ions (cf. Equations 7.4, 7.6, and 7.20). If the membrane contains an excess of free ionophore, i.e., $c_L(org) \gg c_S(org)$, the condition $i_o \ll i_{lim}$ is also fulfilled (cf. Equations 7.11 and 7.20). Accordingly, the second and third term on the left of Equation 7.19 can be neglected except for extremely high values of the applied voltage, and the current response reduces to the simple Equation 7.21:

$$i = \frac{1}{R_M} \frac{RT}{z_I F} \ln \frac{a_I(aq)}{a_I^*(aq)} - \frac{E}{R_M} = const + \frac{1}{R_M} \frac{RT}{z_I F} \ln a_I(aq) \qquad (7.21)$$

Evidently, this type of ISE system behaves as an ohmic resistor that yields a current response to the actual overpotential. The current response perfectly mimics the potentiometric response curve of the respective ISE at zero current. It is a linear function of the logarithm of the sample ion activity if the composition of the internal solution and the applied potential are constant. It should be noted that Equation 7.21 can also readily be derived from the Nernstian zero-current potential plus the ohmic potential drop (Equation 7.18 without the last two terms).

Contrasting response behavior is expected for an ISE with a polymer-free organic phase (of type ITIES) containing a relatively high concentration of dissolved electrolyte. Since the diffusion coefficients in an organic solvent of low viscosity are much higher than in a plasticized PVC membrane (e.g., in o-NPOE in the range of 0.5–5 x 10^{-6} cm^2 s^{-1} [171,194]), the conditions $i'_{lim} \ll i_o$ and $i'_{lim} \ll i_{lim}$ may hold. In this case, the sample concentration must be fairly low, which also guarantees that $i'_{lim} \ll i''_{lim}$. Finally, the second term on the left of Equation 7.19 becomes decisive, leading to

$$i = i'_{lim}\left[1 - e^{z_I FE/RT} \frac{a_I^*(aq)}{a_I(aq)}\right] = \frac{AFz_I D_I(aq)c_I(aq)}{\delta} \qquad \text{(for } z_I E \rightarrow -\infty) \qquad (7.22)$$

Such systems reflect the characteristics of ion transfer across the interface between two immiscible electrolyte solutions [171-175]. Accordingly, at sufficiently high voltages, a diffusion-limited current is reached that is directly proportional to the sample ion concentration.

An intermediate case is encountered with polymeric ISE membranes at very low sample activities. Here, the conditions $i_o \ll i'_{lim}$ and $i_o \ll i_{lim}$ still hold but also $i_o \approx i'_{lim}$. Therefore, the first two terms on the left of Equation 7.19 must be considered, which finally yields the following result:

$$i = \frac{1}{R_M}\frac{RT}{z_I F}\ln\left[\frac{a_I(aq)(1-i/i'_{lim})}{a_I^*(aq)}\right] - \frac{E}{R_M} = const + \frac{1}{R_M}\frac{RT}{z_I F}\ln\left[a_I(aq)+\Delta a_{I,el}\right]$$

$$(7.23)$$

with

$$\Delta a_{I,el} = -i\frac{a_I(aq)}{i'_{lim}} = -\frac{i\delta\gamma_I(aq)}{AFz_I D_I(aq)},$$

$$(7.24)$$

where $\gamma_I(aq)$ is the activity coefficient of the primary ion in the sample solution. In comparison with Equation 7.21, the modified response function in Equation 7.23 contains an additional activity increment, $\Delta a_{I,el}$, which stands for the electrical contribution to the lower detection limit [163]. As shown in Equation 7.24, this term is directly related to the current density, i/A, through the membrane, but is independent of other membrane parameters. These equations demonstrate that the useful current-response range of ISE membranes at constant potential differs from the analytical range of the corresponding potentiometric sensors. The observed effects depend on the sign and the magnitude of the current signal established in the region of the lower detection limit.
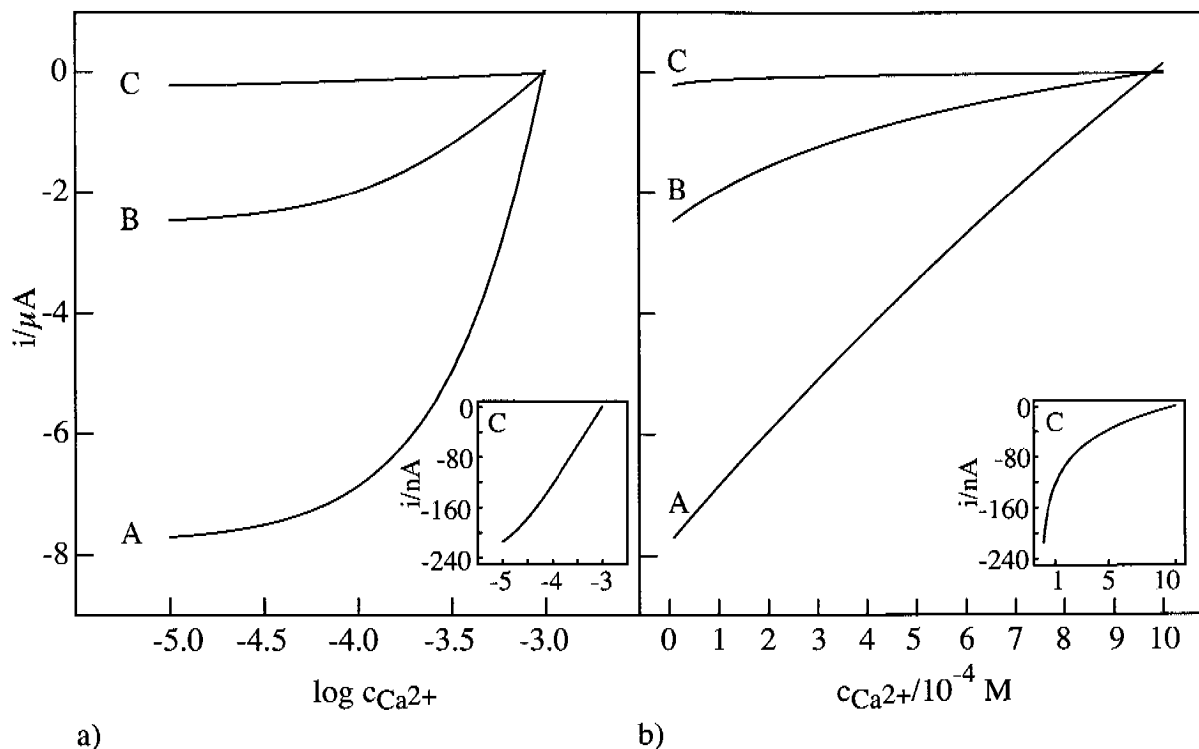
Figure 7.2. Theoretical current response, i vs. $\log c_{Ca^{2+}}$ (left) and i vs. $c_{Ca^{2+}}$ (right) calculated for an external potential of E = -0.3 mV applied to a membrane with an area of A = 0.64 cm^2. The other parameters were chosen as follows: $\partial = \partial^* = 500$ μm, c_I^*(aq) = 10^{-3} M Ca^{2+}, and D_I(aq) = 7.92 x 10^{-6} cm^2 s^{-1} [193]. Curve A: membrane thickness, d = 20 μm, D_I(org) = D_L(org) = 5 x 10^{-7} cm^2 s^{-1} (R$_M$ = 0.42 kΩ). Curve B: d = 60 μm, D_I(org) = D_L(org) = 10^{-7} cm^2 s^{-1} (R$_M$ = 6.24 kΩ). Curve C: d = 120 μm, D_I(org) = 6 x 10^{-9} cm^2 s^{-1}, D_L(org) = 3 x 10^{-8} cm^2 s^{-1} (R$_M$ = 210.0 kΩ).

Theoretical current responses to the sample Ca^{2+} concentration calculated from the general Equation 7.19 are shown in Figure 7.2. The values for the membrane area, A, and the diffusion layers in the sample and internal solutions, ∂ and ∂^*, as well as the concentration of the inner filling solution were chosen so that they matched the experimental conditions used afterwards for potentiometric and amperometric measurements (see below).

151

The diffusion coefficients used for the curves A in Figure 7.2 mimic the situation encountered with ITIES systems. Indeed, the response is almost linear if the current is plotted against the concentration (right side) but curved if it is shown as a function of the logarithmic concentration (left side). The opposite behavior is illustrated by curves C, which are based on experimentally obtained parameters for a plasticized Ca^{2+}-selective PVC membrane (see below). Here, the response on the logarithmic Ca^{2+} concentrations is practically linear and the response to the linear concentration scale is distinctly curved (see inserts with 100 times enlarged scale of the y axis). An intermediate case is shown by curves B calculated with parameters obtained in this work for PVC-free ISE membranes (see below).

Two kinds of PVC-free ISE membranes were investigated in this work in addition to the conventional PVC membrane. The first one was based on a microporous polypropylene matrix (Celgard® 2500, 25 μm thickness). The elliptical pores (0.057 x 0.22 μm² pore size) formed by extrusion, annealing, and stretching were shown to be oriented with their major axes parallel to the film surface [195]. It has also been reported that a thin surface layer has a slightly smaller pore size and a lower two-dimensional pore area than the interior of the film [195]. The other matrix was a track-etched Poretics® polycarbonate membrane having a thickness of 6 μm and pore diameters of 14 μm. The ISE membranes were obtained by impregnating these matrices with a solution of the ISE components (ionophore and ionic sites, see paragraph 7.5) in o-NPOE, which was also used as plasticizer in the corresponding conventional PVC membranes.
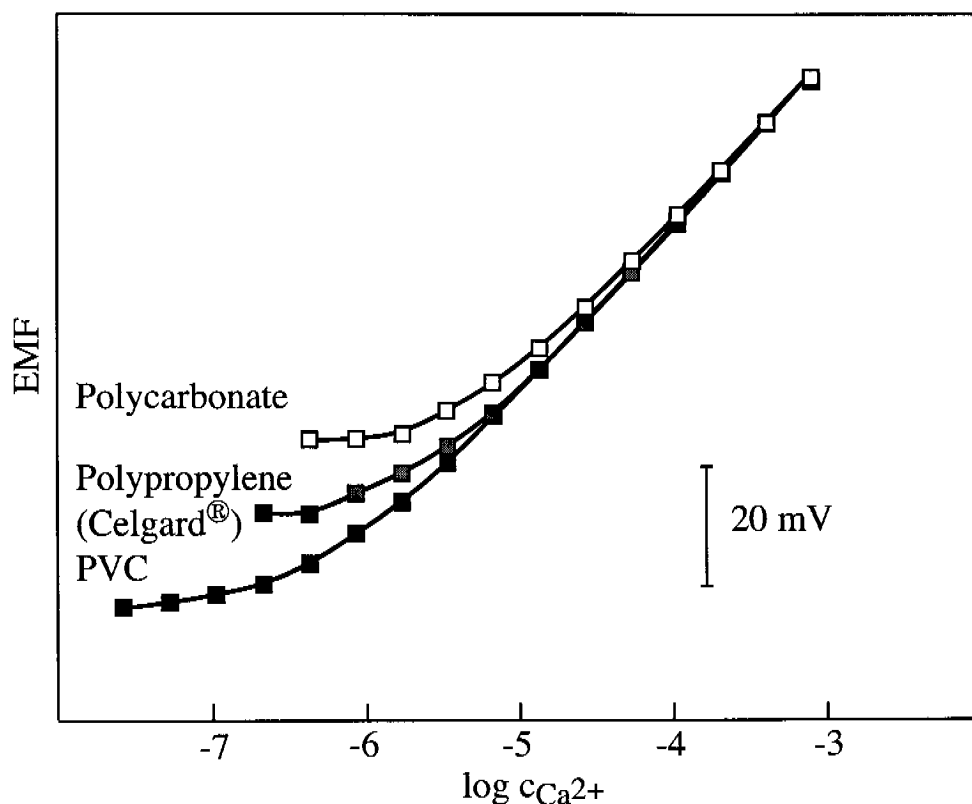
Figure 7.3. Potentiometric response of a PVC-supported and two PVC-free Ca^{2+}-ISE membranes, the latter being based on microporous polypropylene (Celgard®) or on track-etched polycarbonate as matrices. Internal solution: 10^{-3} M $CaCl_2$ with 10^{-3} M KCl and 10^{-4} M HCl; sample background: 10^{-3} M KCl with 10^{-4} M HCl. For better comparison, the curves were shifted to show the same EMF at a sample concentration of 10^{-3} M Ca^{2+}.

First, the response of the three types of membranes was investigated potentiometrically using 10^{-3} M $CaCl_2$ with 10^{-3} M KCl and 10^{-4} M HCl as the internal solution (see Figure 7.3). Owing to the coextraction of a small amount of $CaCl_2$ from the internal solution into the membrane and because of ion exchange, zero-current transmembrane ion fluxes arise. They are known to influence the lower detection limit of such ISEs, which therefore shifts to higher values with increasing diffusion coefficients in, and decreasing thickness of, the membrane phase [21,37,183]. Indeed, the PVC membrane shows the most

favorable lower detection limit (lowest ion fluxes), whereas the PVC-free membranes based on microporous polypropylene or track-etched polycarbonate matrices turn out to be worse by about half or one order of magnitude, respectively (Figure 7.3). Based on these results, it was expected that the amperometric response of the PVC-free membranes may differ from those of PVC membranes and approach the behavior of ITIES systems.

The current response of the three kinds of ISE membranes at a constant potential of E = -0.3 mV is shown in Figure 7.4 together with the theoretical response curves (drawn lines) calculated from Equation 7.19 with the parameters listed in the Figure caption. On the logarithmic concentration scale (Figure 7.4, left), the PVC membrane shows a perfectly linear current response as reported earlier [186]. In contrast, curved responses are obtained for the PVC-free polycarbonate and polypropylene membranes. As shown in Figure 7.4, right, the response behavior of the latter two membrane systems is also curved if plotted as a function of the concentration. The fitted responses show that the membrane resistance (212.0 kΩ for the PVC membrane) is lowered to 13.8 and 10.5 kΩ when using PVC-free polycarbonate and polypropylene (Celgard$^{\circledR}$) membranes, respectively. The calculated response of the Celgard$^{\circledR}$ membrane is based on the same diffusion coefficients as for curves B in Figure 7.2. The reversed order of the potentiometric (Figure 7.3) and current responses (Figure 7.4) of the two PVC-free membranes can be explained by the fact that the limiting diffusion processes are not the same in the two cases. The heterogeneous structure of Celgard$^{\circledR}$ (see above) apparently favors the back-diffusion of the free ionophore, which partly determines the limiting current in amperometric experiments.

a)   b)
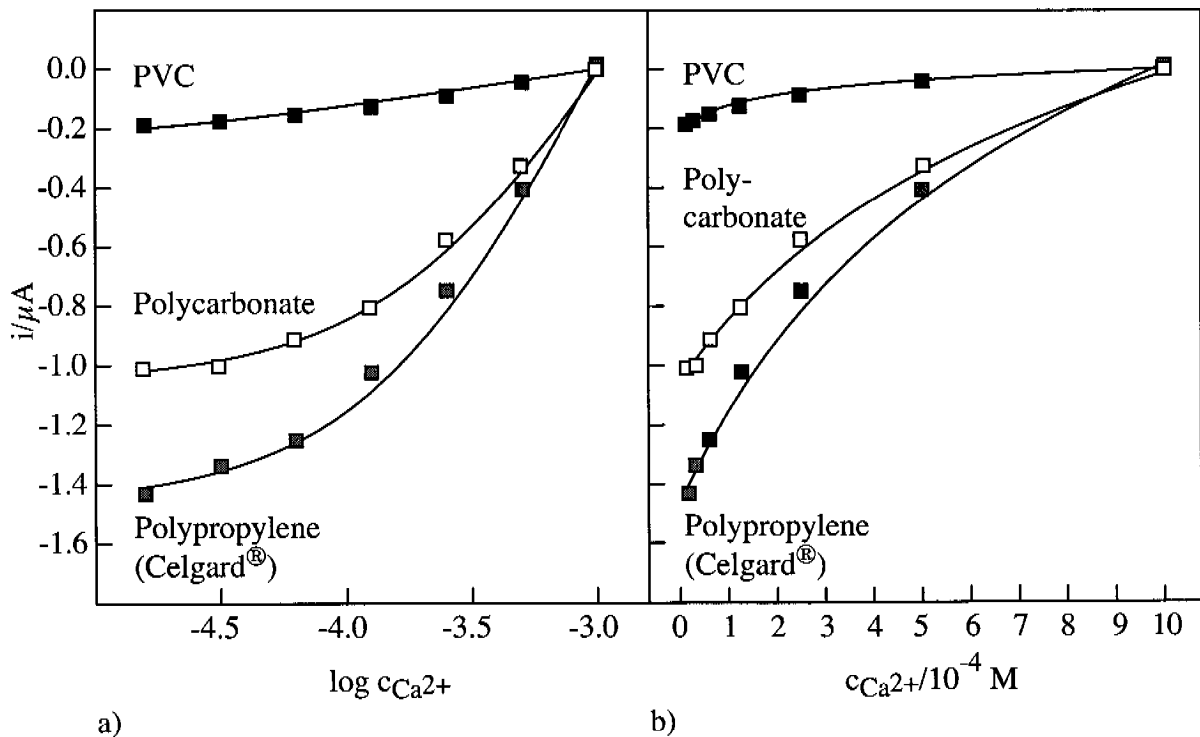
Figure 7.4. Current response at constant external potential (E = -0.3 mV) of a PVC-supported and two PVC-free Ca^{2+}-ISE membranes (for details, see Figure 7.3). Curves were calculated from Equation 7.19 with the following parameters: PVC membrane: d = 120 μm, A = 0.64 cm^2, $D_I(org)$ = 6 x 10^{-9} cm^2 s^{-1}, $D_L(org)$ = 3 x 10^{-8} cm^2 s^{-1} (R_M = 212.0 kΩ); polycarbonate membrane: d = 42 μm, A = 0.23 cm^2, $D_I(org)$ = $D_L(org)$ = 9 x 10^{-8} cm^2 s^{-1}, (R_M = 13.8 kΩ); microporous polypropylene (Celgard®) membrane: d = 58 μm, A = 0.35 cm^2, $D_I(org)$ = $D_L(org)$ = 1.05 x 10^{-7} cm^2 s^{-1} (R_M = 10.5 kΩ). The thickness of the stagnant layer in the sample and internal solutions was $\partial = \partial^* = 500$ μm in all cases.

Since various parameter combinations for the membrane phase may result in similar response curves, further experiments were carried out with Celgard® membranes, for which the current limitation by the ion transport in the membrane is relatively small. In one set of experiments (Figure 7.5), the effective thickness of the unstirred layer was varied by fixing an inert hydrophilic polycarbonate membrane with holes of about 1 mm diameter (ca. 40

holes cm^{-2}) in the sample compartment of the cell, about 3 mm apart from the membrane surface. The two calculated amperometric response curves were based on the same parameters, except for the apparent thickness of the stagnant layer.
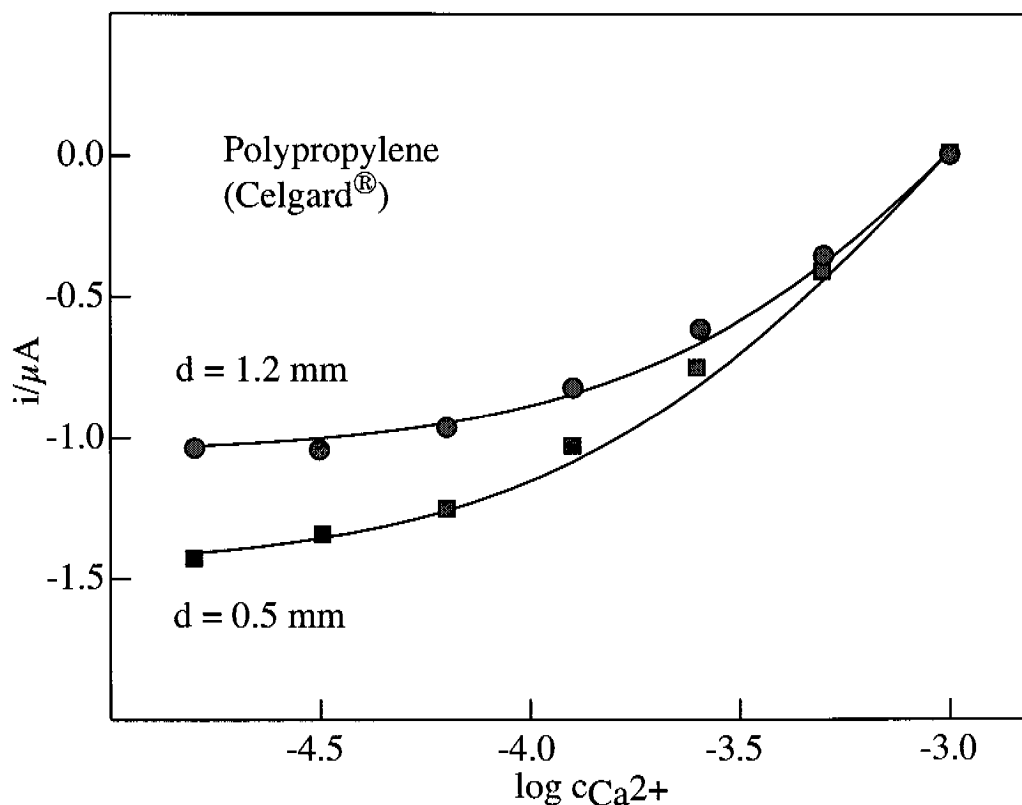
Figure 7.5. Current response at constant external potential (E = -0.3 mV) of a Ca^{2+}-ISE membrane based on a microporous polypropylene (Celgard®) matrix (for details, see Figure 7.3). The thickness of the stagnant layer was increased in one experiment by placing an inert, perforated polycarbonate membrane in front of the ISE membrane. The calculated curves are based on the same parameters as for Figure 7.4 except for the thickness of the stagnant layer indicated in the Figure.

Based on the same set of parameters, it was also possible to describe the current responses at three different potentials (E = -0.3, -30.0, and +30.0 mV, see Figure

7.6). These results clearly indicated that the quantitative model according to Equation 7.19 is sound and can be applied to various experimental setups.
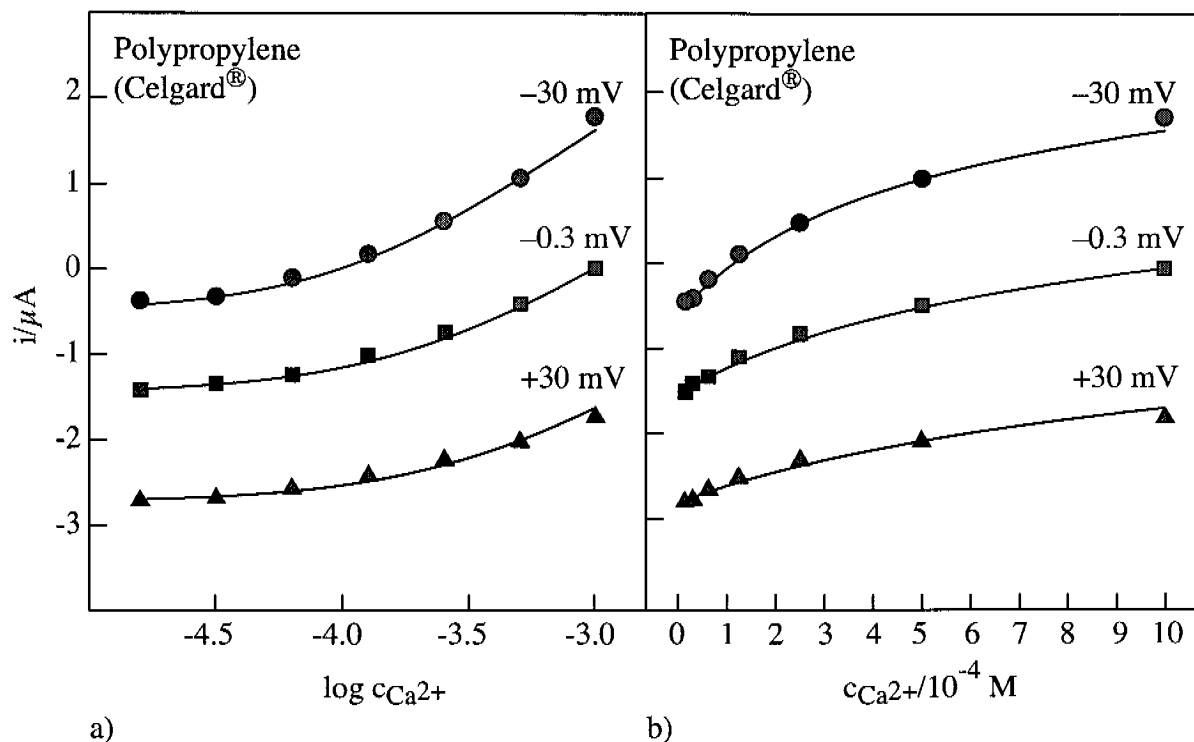
Figure 7.6. Current response at different external potentials (E = -0.3, -30.0, or +30.0 mV) of a Ca^{2+}-ISE membrane based on a microporous polypropylene (Celgard®) matrix (for details, see Figure 7.3). The curves are calculated from Equation 7.19 using the same parameters as in Figure 7.4.

All measurements discussed so far were based on steady-state current values. Depending on the type of membrane, this steady state was achieved after different equilibration times. As shown by the time traces in Figure 7.7, the Celgard® membranes exhibited fast responses and the respective steady states were reached within a few minutes.
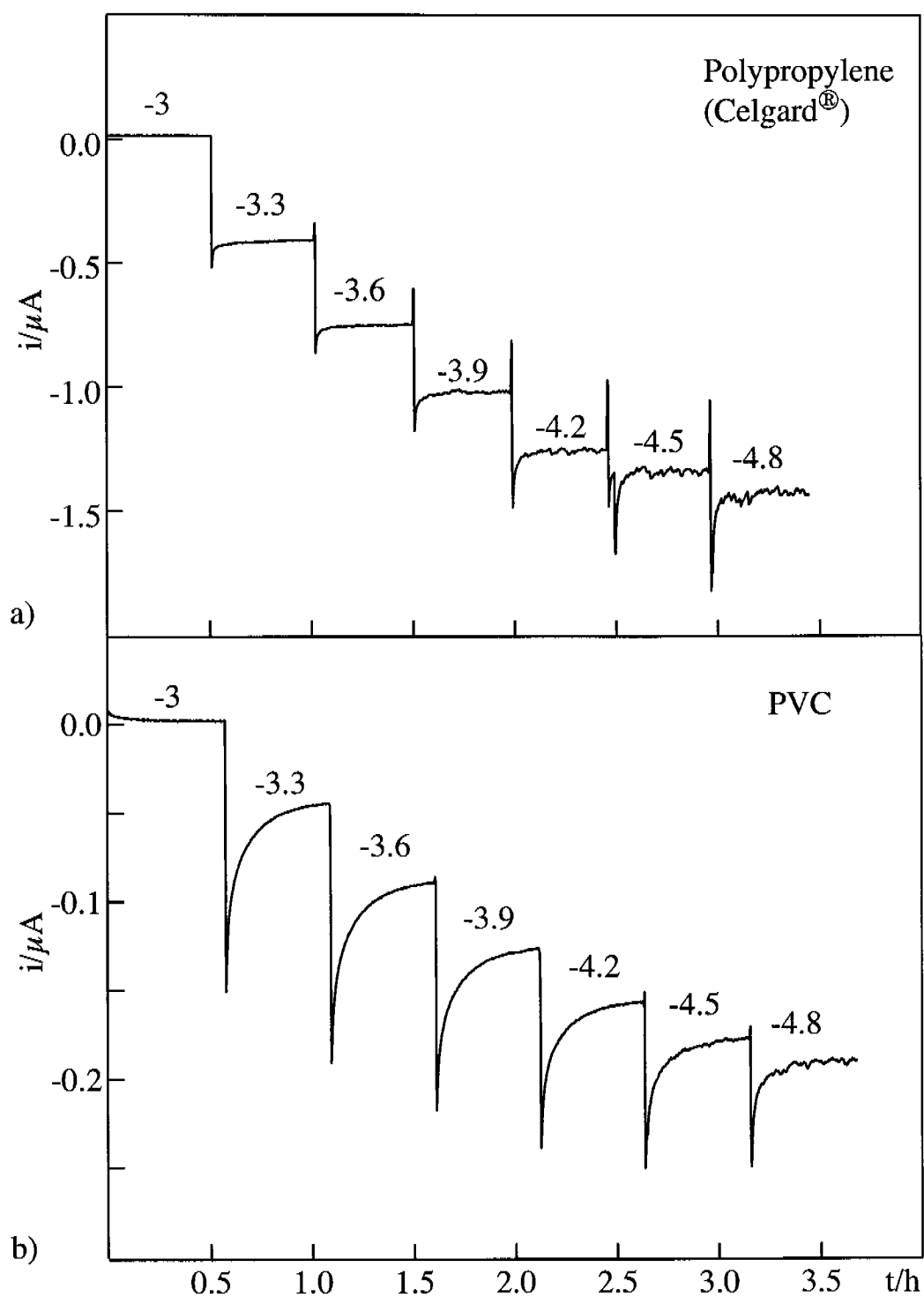
Figure 7.7. Time traces of the current response at E = -0.3 mV of a PVC-supported and a PVC-free Ca^{2+}-ISE membrane, the latter being based on a microporous polypropylene (Celgard®) matrix (for details, see Figure 7.3). The values given above the curves indicate the respective logarithmic molar Ca^{2+} concentrations in the sample.

As expected, PVC-based membranes responded much more slowly and the steady-state current value was achieved only about half an hour after sample changes. Due to their fast response behavior, Celgard® membranes are highly attractive candidates whenever fast transmembrane processes are required for potentiometric or amperometric sensing with liquid membrane electrodes.

7.4 Conclusions

The current response of ISE membrane assemblies at controlled potential was treated on a theoretical basis and studied in a series of experiments. The apparently contradictory amperometric response behavior obtained with ITIES and ion-selective PVC membranes was shown to originate from different kinetic limitations. For PVC-free liquid membranes based on inert microporous matrices (e.g., Celgard® or track-etched polycarbonate membranes), the response is not a linear function, neither when plotted vs. the logarithmic concentration, nor the concentration itself. Hence, the behavior of these membranes is intermediate between that of PVC membranes and ITIES systems. Although potentiometric measurements with ISEs are still widely preferred for the determination of ion activities (concentrations), the new amperometric method was shown to be an equivalent choice and may also find future applications in routine analysis.

7.5 Experimental

7.5.1 Reagents

Celgard® 2500 microporous flat sheet polypropylene membranes of 0.057 x 0.22 μm^2 pore size, 25 μm thickness, and 55 % porosity were purchased from Celgard Inc. (Charlotte, North Carolina, USA). Poretics® polycarbonate membranes without wetting agent (PVPF, poly(vinylpyrrolidone)-free) of 14 μm pore diameter and 6 μm thickness were obtained from Osmonics Inc. (Minnetonka, Minnesota, USA).

Poly(vinyl chloride) (PVC), the calcium ionophore, N,N-dicyclohexyl-N',N'-dioctadecyl-3-oxapentanediamide (ETH 5234), potassium tetrakis-[3,5-bis-(trifluoromethyl)phenyl]borate (KTFPB), and tetrahydrofuran (THF) were Selectophore® and 2-nitrophenyl octyl ether (o-NPOE) was puriss. p.a., all from Fluka AG (Buchs, Switzerland). Aqueous solutions were prepared with freshly deionized water (18.0 $M\Omega$ cm specific resistance) obtained with a NANOpure reagent-grade water system (Barnstead, 4009 Basel, Switzerland); $CaCl_2$, NaCl, and KCl were Suprapur® from Merck (Darmstadt, Germany).

7.5.2 Membranes

Celgard®-based membranes contained ETH 5234 (2.3 wt %, 28.6 mmol kg^{-1}), KTFPB (0.3 wt %, 2.9 mmol kg^{-1}), and o-NPOE (97.4 wt %). A total of 270.4 mg of these components was dissolved in THF (2 mL) and a Celgard® membrane disk of 2.0 cm diameter was impregnated with 40 μL of this solution. The membrane was then immediately mounted in a symmetrical plexiglass cell allowing an exposed area of 0.64 cm^2 and with compartments of 20 mL on each side. Before starting potentiometric or amperometric measurements, the

membrane was symmetrically conditioned in a solution of 10^{-3} M $CaCl_2$, 10^{-3} M KCl and 10^{-4} M HCl for ca. 30 min.

Polycarbonate-based membranes contained ETH 5234 (2.4 wt %, 30.2 mmol kg^{-1}), KTFPB (0.3 wt %, 3.2 mmol kg^{-1}), and o-NPOE (97.3 wt %). A total of 272.4 mg of these components was dissolved in THF (2 mL).

After evaporating the THF under air, a polycarbonate membrane disk of 2.0 cm diameter was impregnated with 2 µL of the solution. The membrane was then immediately mounted in the symmetrical plexiglass cell and conditioned for ca. 30 min as described above for the Celgard® membranes.

The PVC-based membranes contained ETH 5234 (1.6 wt %, 20.1 mmol kg^{-1}), KTFPB (0.2 wt %, 2.2 mmol kg^{-1}), o-NPOE (65.5 wt %), and PVC (32.7 wt %). Membranes of ca. 120 µm thickness were obtained by casting a solution of 404.4 mg of these components dissolved in THF (ca. 4 mL) into a glass ring (4.4 cm i.d.) fixed on a glass plate. After evaporation of the solvent overnight, a disk of 2.0 cm diameter was punched from this master membrane, mounted in the symmetrical plexiglass cell and conditioned as described above but in this case for 48 h.

7.5.3 EMF measurements

Potentials were measured with a custom-made 16-channel electrode monitor in the symmetrical plexiglass cell, the solutions in both compartments being stirred during measurements. Two identical reference electrodes (Metrohm type 6.0726.100, Ag/AgCl in 3 M KCl, Metrohm AG, 9101 Herisau, Switzerland) with a bridge electrolyte of 1 M KCl were used as reference and working electrodes.

7.5.4 Controlled potential measurements

Current measurements at controlled potential were performed on all ISE membranes with the same symmetrical cell as described above. For these measurements a four-electrode setup was used. The cell was equipped with a working and a counter electrode, both Ag/AgCl (0.64 cm^2), and two identical reference electrodes having a bridge electrolyte of 1 M KCl as mentioned under paragraph 7.5.3. The external potential difference was controlled with an SI 1287 Electrochemical Interface (Solartron Instruments, Farnborough, UK) using CorrWare software (Scribner Associates, Inc., Southern Pines, USA). The same instrument was used to measure the current response. For each concentration, current readings were taken after 30 min. In order to guarantee a direct and true comparison between potentiometric and amperometric ISE responses, one and the same experimental set-up was utilized for all measurements in this work. The membrane electrode cell basically conforms to the arrangement used for most practical ISE applications.

8 Structures

8.1 Plasticizers

Bis(2-ethylhexyl) sebacate (DOS), $C_{26}H_{52}O_4$, M_r 426.69

$$H_3C(H_2C)_2H_2C - \underset{\underset{CH_2CH_3}{|}}{CH} - CH_2 - O - \overset{\overset{O}{\|}}{C} - (CH_2)_8 - \overset{\overset{O}{\|}}{C} - O - CH_2 - \underset{\underset{CH_2(CH_2)_2CH_3}{|}}{CH} - CH_2CH_3$$
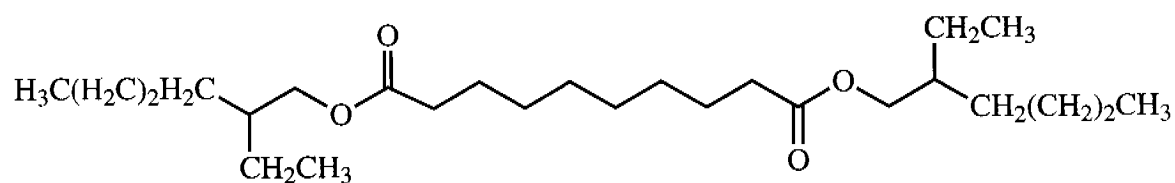
2-Nitrophenyl octyl ether (o-NPOE), $C_{14}H_{21}NO_3$, M_r 251.33

$$\text{(benzene ring with)} \quad O-CH_2(CH_2)_6CH_3 \quad \text{and} \quad NO_2$$
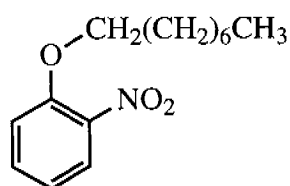
8.2 Lipophilic salt

Tetradodecylammonium tetrakis(4-chlorophenyl)borate, (ETH 500),

$C_{72}H_{116}BCl_4N$, M_r 1148.29

$$H_3C(H_2C)_{10}H_2C, \quad CH_2(CH_2)_{10}CH_3$$
$$N^+$$
$$H_3C(H_2C)_{10}H_2C \quad CH_2(CH_2)_{10}CH_3$$

$$\left[Cl - \text{(benzene ring)} - B^- \right]_4$$
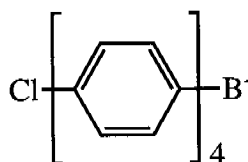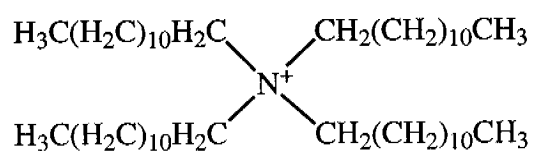
8.3 Ionic sites

Potassium tetrakis[3,5-bis(trifluoromethyl)phenyl]borate, (KTFPB),

$C_{32}H_{12}BF_{24}K$, M_r 902.32

Sodium tetrakis[3,5-bis(trifluoromethyl)phenyl]borate, (NaTFPB),

$C_{32}H_{12}BF_{24}Na$, M_r 886.21

K^+ or Na^+
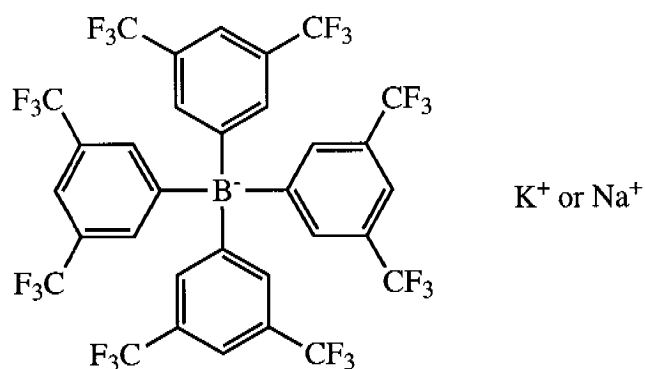
8.4 Ionophores

N,N-Dicyclohexyl-N',N'-dioctadecyl-3-oxapentanediamide (ETH 5234),

$C_{52}H_{100}N_2O_3$, M_r 801.37
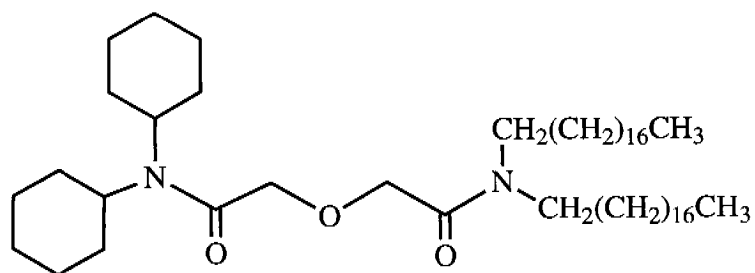
tert.-Butylcalix[4]arene-tetrakis(*N,N*-dimethylthioacetamide),

$C_{60}H_{84}N_4O_4S_4$, M_r 1054.59
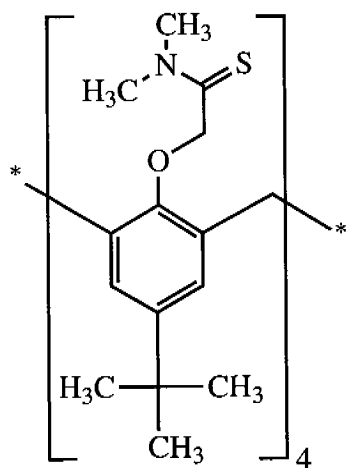
Seite Leer /
Blank leaf

9 Glossary

o	standard conditions
'	membrane/sample solution phase boundary
"	membrane/inner filling solution phase boundary
*	bulk of internal solution
A	active membrane area $[cm^2]$
a_J	activity of ion J $[mol\ L^{-1}]$
aq	aqueous phase
c_J	concentration of ion J $[mol\ L^{-1}]$
$c_L(org)$	average concentration of ionophore within the membrane $[mol\ L^{-1}]$
CP	conducting polymer
$c_S(org)$	total concentration of ionic sites in the membrane $[mol\ L^{-1}]$
CV	cyclic voltammogram
d	membrane thickness $[\mu m]$
D_J	diffusion coefficient of ion J $[cm^2\ s^{-1}]$
$D_L(org)$	diffusion coefficient of the ionophore in the membrane $[cm^2\ s^{-1}]$
DOS	bis(2-ethylhexyl) sebacate
$E°$	includes all constant terms of E_M
E_{const}	sum of all sample-independent contributions to the EMF
$E_{D,ref}$	liquid-junction potential of reference electrode
$E_J°$	intercept of linear response function of an ISE responding to ion J
E_M	potential difference between the bulks of the internal and sample solutions

$E_{M,const}$	sum of the phase boundary potential at the internal filling solution/membrane interface and of the diffusion potential in the membrane
EDTA	ethylenediaminetetraacetic acid
EMF	electromotive force
ETH 500	tetradodecylammonium tetrakis(4-chlorophenyl)borate
F	Faraday constant (96 485 C mol^{-1})
Fc	ferrocenyl group
H-PDMS	Si–H-terminated poly(dimethylsiloxane)
i	electrical current [A]
I	primary ion
i_{lim}	diffusion-limited current related to maximal diffusion flux within a certain diffusion layer [A]
ISE	ion-selective electrode
ISFET	ion-selective field effect transistor
ITIES	interface of two immiscible electrolyte solutions
J	interfering ion or any kind of ion
J_J	total flux of ion J [mol cm^{-2} s^{-1}]
$K_{I,J}^{pot}$	potentiometric selectivity coefficient
k_I	distribution coefficient of free primary ions between aqueous phase and membrane
KTFPB	potassium tetrakis-[3,5-bis-(trifluoromethyl)phenyl]borate
L	ligand, ionophore
LC	liquid contact
LDL	lower detection limit [mol L^{-1}]
MMA-DMA	methyl methacrylate-decyl methacrylate copolymer
n_I	stoichiometric number of the primary ion-ionophore complex

NaTFPB	sodium tetrakis-[3,5-bis-(trifluoromethyl)phenyl]borate
o-NPOE	2-nitrophenyl octyl ether
NTA	nitrilotriacetic acid
org	organic (membrane) phase
PANI	polyaniline
PEDOT	poly(3,4-ethylenedioxythiophene)
PMHS	poly(methylhydrosiloxane)
POT	poly(3-octylthiophene)
PPy	polypyrrole
PPy_FeCN	polypyrrole doped with potassium hexacyanoferrate(II)/(III)
PPy_KCl	polypyrrole doped with potassium chloride
PVC	poly(vinyl chloride)
PVF	poly(vinylferrocene)
R	universal gas constant (8.314 J K^{-1} mol^{-1})
ref	reference bridge electrolyte solution
R_M	inner membrane resistance [Ω]
S	ionic sites
s	sample solution
SAM	self-assembled monolayer
SC	solid contact
s_I	sensitivity (slope) of linear response function of an ISE responding to ion I [mV decade^{-1}]
T	absolute temperature [K]
THF	tetrahydrofuran
u_J	absolute mobility of ion J [cm^2 mol s^{-1} J^{-1}]
z_I, z_J	charge number of ion I, J

β_{I,n_I}	stability constant of $1:n_I$ primary ion-ionophore complex
∂	aqueous Nernstian diffusion layer in the sample solution [μm]
∂^*	aqueous Nernstian diffusion layer in the internal solution [μm]
μ	chemical potential [J mol^{-1}]
$\tilde{\mu}$	electrochemical potential [J mol^{-1}]
Φ	electric potential [V]
$\Delta\Phi_M$	potential drop within the membrane [V]
$\Delta\Phi'$	Galvani potential difference arising at the membrane/sample solution phase boundary [V]
$\Delta\Phi''$	Galvani potential difference arising at the membrane/inner filling solution phase boundary [V]

10 References

(1)   Morf, W. E. *Chemische Sensoren,* in: Analytische Chemie III, Vorlesungsscript, ETH Zürich: Zürich, 1999.

(2)   Otto, M. *Analytische Chemie,* VCH: Weinheim, New York, Basel, Cambridge, Tokyo, 1995.

(3)   Bakker, E.; Bühlmann, P.; Pretsch, E. *Chem. Rev.* **1997**, *97,* 3083-3132, Carrier-based ion-selective electrodes and bulk optodes: 1. General characteristics.

(4)   Morf, W. E. *The Principles of Ion-Selective Electrodes and of Membrane Transport,* Elsevier: Amsterdam, Oxford, New York, 1981.

(5)   Bühlmann, P.; Pretsch, E.; Bakker, E. *Chem. Rev.* **1998**, *98,* 1593-1687, Carrier-based ion-selective electrodes and bulk optodes: 2. Ionophores for potentiometric and optical sensors.

(6)   Bakker, E.; Pretsch, E. *Anal. Chem.* **2002**, *74,* 420A-426A, The new wave of ion-selective electrodes.

(7)   Ceresa, A.; Bakker, E.; Hattendorf, B.; Günther, D.; Pretsch, E. *Anal. Chem.* **2001**, *73,* 343-351, Potentiometric polymeric membrane electrodes for measurement of environmental samples at trace levels: New requirements for selectivities and measuring protocols, and comparison with ICPMS.

(8)   Bühlmann, P.; Yajima, S.; Tohda, K.; Umezawa, K.; Nishizawa, S.; Umezawa, Y. *Electroanalysis* **1995**, *7,* 811-816, Studies on the phase boundaries and the significance of ionic sites of liquid membrane ion-selective electrodes.

(9)   Ammann, D.; Pretsch, E.; Simon, W.; Lindner, E.; Bezegh, A.; Pungor, E. *Anal. Chim. Acta* **1985**, *171,* 119-129, Lipophilic salts as membrane additives and their influence on the properties of macro- and microelectrodes based on neutral carriers.

(10)   Nägele, M.; Mi, Y.; Bakker, E.; Pretsch, E. *Anal. Chem.* **1998**, *70,* 1686-1691, Influence of lipophilic inert electrolyte on the selectivity of polymer membrane electrodes.

(11)   Henderson, P. *Z. Phys. Chem.* **1907**, *59,* 118-127, Zur Thermodynamic der Flüssigkeitsketten.

(12)   Debye, P.; Hückel, E. *Phys. Z.* **1923**, *24,* 185-206, Zur Theorie der Elektrolyte.

(13)   Pungor, E. *Pure Appl. Chem.* **1992**, *64,* 503-507, Working mechanism of ion-selective electrodes.

(14)   Bakker, E.; Nägele, M.; Schaller, U.; Pretsch, E. *Electroanalysis* **1995**, *7,* 817-822, Applicability of the phase boundary potential model to the mechanistic understanding of solvent polymeric membrane-based ion-selective electrodes.

(15)   Mikhelson, K. N.; Lewenstam, A.; Didina, S. E. *Electroanalysis* **1999**, *11,* 793-798, Contribution of the diffusion potential to the membrane potential and to the ion-selective electrode response.

(16)   Bakker, E. *J. Electrochem. Soc.* **1996**, *143*, L83-L85, Determination of improved selectivity coefficients of polymer membrane ion-selective electrodes by conditioning with a discriminated ion.

(17)   Bakker, E. *Anal. Chem.* **1997**, *69*, 1061-1069, Determination of unbiased selectivity coefficient of neutral carrier-based cation-selective electrodes.

(18)   Bakker, E.; Pretsch, E.; Bühlmann, P. *Anal. Chem.* **2000**, *72*, 1127-1133, Selectivity of potentiometric ion sensors.

(19)   Nägele, M.; Bakker, E.; Pretsch, E. *Anal. Chem.* **1999**, *71*, 1041-1048, General description of the simultaneous response of potentiometric ionophore-based sensors to ion of different charge.

(20)   Guilbault, G. G.; Durst, R. A.; Frant, M. S.; Freiser, H.; Hansen, E. H.; Light, T. S.; E. Pungor; Rechnitz, G.; Rice, N. M.; Rohm, T. J.; Simon, W.; Thomas, J. D. R. *Pure Appl. Chem.* **1976**, *48*, 127-132, Recommendations for nomenclature of ion-selective electrodes.

(21)   Sokalski, T.; Zwickl, T.; Bakker, E.; Pretsch, E. *Anal. Chem.* **1999**, *71*, 1204-1209, Lowering the detection limit of solvent polymeric ion-selective electrodes. 1. Modeling the influence of steady-state ion fluxes.

(22)   Tohda, K.; Umezawa, Y.; Yoshiyagawa, S.; Hashimoto, S.; Kawasaki, M. *Anal. Chem.* **1995**, *67*, 570-577, Cation permselectivity at the phase boundary of ionophore-incorporated solvent polymeric membrane as studied by optical second harmonic generation.

(23)   Yajima, S.; Tohda, K.; Bühlmann, P.; Umezawa, Y. *Anal. Chem.* **1997**, *69*, 1919-1924, Donnan exclusion failure of neutral ionophore-based ion-selective electrodes studied by optical second-harmonic generation.

(24)   Zwickl, T.; Sokalski, T.; Pretsch, E. *Electroanalysis* **1999**, *11*, 673-680, Steady-state model calculations predicting the influence of key parameters on the lower detection limit and ruggedness of solvent polymeric membrane ion-selective electrodes.

(25)   Morf, W. E.; Badertscher, M.; Zwickl, T.; de Rooij, N. F.; Pretsch, E. *J. Phys. Chem. B* **1999**, *103*, 11346-11356, Effects of ion transport on the potential response of ionophore based membrane electrodes: A theoretical approach.

(26)   Ceresa, A.; Radu, A.; Peper, S.; Bakker, E.; Pretsch, E. *Anal. Chem.* **2002**, *74*, 4027-4036, Rational design of potentiometric trace level ion sensors. A Ag^+-selective electrode with a 100 ppt detection limit.

(27)   Lerchi, M.; Bakker, E.; Rusterholz, B.; Simon, W. *Anal. Chem.* **1992**, *64*, 1534-1540, Lead-selective bulk optodes based on neutral ionophores with subnanomolar detection limits.

(28)   Sokalski, T.; Maj-Zurawska, M.; Hulanicki, A. *Mikrochim. Acta* **1991**, *I*, 285-291, Determination of true selectivity coefficients of neutral carrier calcium selective electrode.

(29)   Schefer, U.; Ammann, D.; Pretsch, E.; Oesch, U.; Simon, W. *Anal. Chem.* **1986**, *58*, 2282-2285, Neutral carrier based Ca^{2+}-selective electrode with detection limit in the sub-nanomolar range.

(30) Schneider, B.; Zwickl, T.; Federer, B.; E. Pretsch; Lindner, E. *Anal. Chem.* **1996**, *68*, 4342-4350, Spectro-potentiometry: A new method for *in situ* imaging of concentration profiles in ion-selective membranes with simultaneous recording of potential-time transients.

(31) Mathison, S.; Bakker, E. *Anal. Chem.* **1998**, *70*, 303-309, Effect of transmembrane electrolyte diffusion on the detection limit of carrier-based potentiometric ion sensors.

(32) Sokalski, T.; Ceresa, A.; Fibbioli, M.; Zwickl, R.; Bakker, E.; Pretsch, E. *Anal. Chem.* **1999**, *71*, 1210-1214, Lowering the detection limit of solvent polymeric ion-selective membrane electrodes. 2. Influence of composition of sample and internal electrolyte solution.

(33) Vigassy, T.; Morf, W. E.; Badertscher, M.; Ceresa, A.; de Rooij, N. F.; Pretsch, E. *Sens. and Actuators B* **2001**, *76*, 477-482, Making use of ion fluxes through potentiometric sensor membranes: ISEs with step responses at critical ion activities.

(34) Peper, S.; Ceresa, A.; Bakker, E.; Pretsch, E. *Anal. Chem.* **2001**, *73*, 3768-3775, Improved detection limits and sensitivities of potentiometric titrations.

(35) Qin, W.; Zwickl, T.; Pretsch, E. *Anal. Chem.* **2000**, *72*, 3236-3240, Improved detection limits and unbiased selectivity coefficients obtained by using ion-exchange resins in the inner reference solution of ion selective polymeric membrane electrodes.

(36) Sokalski, T.; Ceresa, A.; Zwickl, T.; Pretsch, E. *J. Am. Chem. Soc.* **1997**, *119*, 11347-11348, Large improvement of the lower detection limit of ion-selective polymer membrane electrode.

(37) Ceresa, A.; Sokalski, T.; Pretsch, E. *J. Electroanal. Chem.* **2001**, *501*, 70-76, Influence of key parameters on the lower detection limit and response function of solvent polymeric membrane ion-selective electrodes.

(38) Vigassy, T.; Gyurcsányi, R. E.; Pretsch, E. *Electroanalysis* **2003**, *15*, 375-382, Influence of incorporated lipophilic particles on ion fluxes through polymeric ion-selective membranes.

(39) Sudhölter, E. J. R.; van der Wal, P. D.; Skowronska-Ptasinska, M.; van den Berg, A.; Bergveld, P.; Reinhoudt, D. N. *Anal. Chim. Acta* **1990**, *230*, 59-65, Modification of ISFETs by covalent anchoring of poly(hydroxyethyl methacrylate) hydrogel - Introduction of a thermodynamically defined semiconductor-sensing membrane interface.

(40) Lindner, E.; Cosofret, V. V.; Ufer, S.; Buck, R. P.; Kusy, R. P.; Ash, R. B.; Nagle, H. T. *J. Chem. Soc.-Faraday Trans.* **1993**, *89*, 361-367, Flexible (Kapton-based) microsensor arrays of high-stability for cardiovascular applications.

(41) Lindner, E.; Cosofret, V. V.; Ufer, S.; Johnson, T. A.; Ash, R. B.; Nagle, H. T.; Neuman, M. R.; Buck, R. P. *Fresenius J. Anal. Chem.* **1993**, *346*, 584-588, In-vivo and in-vitro testing of microelectronically fabricated planar sensors designed for applications in cardiology.

(42)   Cattrall, R. W.; Freiser, H. *Anal. Chem.* **1971**, *43*, 1905-1906, Coated wire ion selective electrodes.

(43)   Hulanicki, A.; Trojanowicz, M. *Anal. Chim. Acta* **1976**, *87*, 411-417, Calcium-selective electrodes with PVC membranes and solid internal contacts.

(44)   Cattrall, R. W.; Drew, D. M.; Hamilton, I. C. *Anal. Chim. Acta* **1975**, *76*, 269-277, Some alkylphosphoric acid esters for use in coated-wire calcium-selective electrodes.

(45)   Cattrall, R. W.; Hamilton, I. C. *Ion-Selective Electrode Reviews* **1984**, *6*, 125-172, Coated-wire ion-selective electrodes.

(46)   Hauser, P. C.; Chiang, D. W. L.; Wright, G. A. *Anal. Chim. Acta* **1995**, *302*, 241-248, A potassium-ion selective electrode with valinomycin based poly(vinyl chloride) membrane and a poly(vinyl ferrocene) solid contact.

(47)   Cha, G. S.; Liu, D.; Meyerhoff, M. E.; Cantor, H. C.; Midgley, A. R.; Goldberg, H. D.; Brown, R. B. *Anal. Chem.* **1991**, *63*, 1666-1672, Electrochemical performance, biocompatibility and adhesion of new polymer matrices for solid-state ion sensors.

(48)   Liu, D.; Meruva, R. K.; Brown, R. B.; Meyerhoff, M. E. *Anal. Chim. Acta* **1996**, *321*, 173-183, Enhancing EMF stability of solid-state ion-selective sensors by incorporating lipophilic silver-ligand complexes within polymeric films.

(49)   Michalska, A.; Hulanicki, A.; Lewenstam, A. *Microchem J.* **1997**, *57*, 59-64, All-solid-state potentiometric sensors for potassium and sodium based on poly(pyrrole) solid contact.

(50)   Gyurcsányi, R. E.; Nybäck, A. S.; Tóth, K.; Nagy, G.; Ivaska, A. *Analyst* **1998**, *123*, 1339-1944, Novel polypyrrole based all-solid-state potassium-selective microelectrodes.

(51)   Zieli'nska, R.; Mulik, E.; Michalska, A.; Achmatowicz, A.; Maj-Zurawska, M. *Anal. Chim. Acta* **2002**, *451*, 243-249, All-solid-state planar miniature ion-selective chloride electrode.

(52)   Michalska, A.; Dumanska, J.; Maksymiuk, K. *Anal. Chem.* **2003**, *75*, 4964-4974, Lowering the detection limit of ion-selective plastic membrane electrodes with conducting polymer solid contact and conducting polymer potentiometric sensors.

(53)   Bobacka, J.; Lindfors, T.; McCarrick, M.; Ivaska, A.; Lewenstam, A. *Anal. Chem.* **1995**, *67*, 3819-3823, Single-piece all-solid-state ion-selective electrode.

(54)   Sjöberg, P.; J.Bobacka; Lewenstam, A.; Ivaska, A. *Electroanalysis* **1998**, *11*, 821-824, All-solid-state chloride-selective electrode based on poly(3-octylthiophene) and tridodecylmethylammonium chloride.

(55)   Bobacka, J.; Ivaska, A.; Lewenstam, A. *Anal. Chim. Acta* **1999**, *385*, 195-202, Plasticizer-free all-solid-state potassium-selective electrode based on poly(3-octylthiophene) and valinomycin.

(56) Bobacka, J. *Anal. Chem.* **1999**, *71*, 4932-4937, Potential stability of all-solid-state ion-selective electrodes using conducting polymers as ion-to-electron transducers.

(57) Song, F.; Ha, J.; Park, B.; Kwak, T. H.; Kim, I. T.; Nam, H.; Cha, G. S. *Talanta* **2002**, *57*, 263-270, All-solid-state carbonate-selective electrode based on a molecular tweezer-type neutral carrier with solvent-soluble conducting polymer solid contact.

(58) Lindfors, T.; Ivaska, A. *Anal. Chim. Acta* **2001**, *437*, 171-182, Calcium-selective electrode based on polyaniline functionalized with bis[4-(1,1,3,3-tetramethylbutyl)phenyl]phosphate.

(59) Fibbioli, M.; Morf, W. E.; Badertscher, M.; Rooij, N. F. d.; Pretsch, E. *Electroanalysis* **2000**, *12*, 1286-1292, Potential drifts of solid-contacted ion-selective electrodes due to zero-current ion fluxes through the sensor membrane.

(60) Fibbioli, M.; Bandyopadhyay, K.; Liu, S. G.; Echegoyen, L.; Enger, O.; Diederich, F.; Gingery, D.; Bühlmann, P.; Perrson, H.; Suter, U. W.; Pretsch, E. *Chem. Mater.* **2002**, *14*, 1721-1729, Redox-active self-assembled monolayers for solid-contacted polymeric membrane ion-selective electrodes.

(61) Fibbioli, M.; Bandyopadhyay, K.; Liu, S. G.; Echegoyen, L.; Enger, O.; Diederich, F.; Bühlmann, P.; Pretsch, E. *Chem. Commun.* **2000**, *5*, 339-340, Redox-active self-assembled monolayers as novel solid contacts for ion-selective electrodes.

(62) Lindner, E.; Buck, R. P. *Anal. Chem.* **2000**, *72*, 336A-345A, Microfabricated potentiometric electrodes and their in vivo applications.

(63) Lindner, E.; Cosofret, V. V.; Ufer, S.; Buck, R. P.; Kao, W. J.; Neuman, M. R.; Anderson, J. M. *J. Biomed. Mater. Res.* **1994**, *28*, 591-601, Ion-selective membranes with low plasticizer content: Electroanalytical characterization and biocompatibility studies.

(64) Kimura, K.; Matsuba, T.; Tsujimura, Y.; Yokoyama, M. *Anal. Chem.* **1992**, *64*, 2508-2511, Unsymmetrical calix[4]arene ionophore silicone-rubber composite membranes for high-performance sodium ion-sensitive field-effect transistors.

(65) Tsujimura, Y.; Sunagawa, T.; Yokoyama, A.; Kimura, K. *Analyst* **1996**, *121*, 1705-1709, Sodium ion-selective electrodes based on silicone-rubber membranes covalently incorporating neutral carriers.

(66) Oh, B. K.; Kim, C. Y.; Lee, H. J.; Rho, K. L.; Cha, G. S.; Nam, H. *Anal. Chem.* **1996**, *68*, 503-508, One-component room temperature vulcanizing-type silicone rubber based calcium-selective electrodes.

(67) Berrocal, M. J.; Badr, I. H. A.; Gao, D. O.; Bachas, L. G. *Anal. Chem.* **2001**, *73*, 5328-5333, Reducing the thrombogenicity of ion-selective electrode membranes through the use of a silicone-modified segmented polyurethane.

(68) Ambrose, T. M.; Meyerhoff, M. E. *Anal. Chim. Acta* **1999**, *378*, 119-126, Optical ion sensing with immobilized thin films of photocrosslinked decyl methacrylate.

(69)   Peper, S.; Tsagkatakis, I.; Bakker, E. *Anal. Chim. Acta* **2001**, *442*, 25-33, Cross-linked dodecyl acrylate microspheres: Novel matrices for plasticizer-free optical ion sensing.

(70)   Moody, G. J.; Slater, J. M.; Thomas, J. D. R. *Analyst* **1988**, *113*, 103-108, Membrane design and photocuring encapsulation of flatpack based ion-sensitive field-effect transistors.

(71)   Cardwell, T. J.; Cattrall, R. W.; Iles, P. J.; Hamilton, I. C. *Anal. Chim. Acta* **1988**, *204*, 329-332, Photo-cured polymers in ion-selective electrode membranes. 3. A potassium electrode for flow-injection analysis.

(72)   Heng, L. Y.; Hall, E. A. H. *Anal. Chim. Acta* **1996**, *324*, 47-56, Methacrylate-acrylate based polymers of low plasticiser content for potassium ion-selective membranes.

(73)   Heng, L. Y.; Hall, E. A. H. *Anal. Chem.* **2000**, *72*, 42-51, Producing "self-plasticizing" ion-selective membranes.

(74)   Heng, L. Y.; Hall, E. A. H. *Anal. Chim. Acta* **2000**, *403*, 77-89, Methacrylic-acrylic polymers in ion-selective membranes: Achieving the right polymer recipe.

(75)   Heng, L. Y.; Hall, E. A. H. *Electroanalysis* **2000**, *12*, 178-186, One-step synthesis of K^+-selective methacrylic-acrylic copolymers containing grafted ionophore and requiring no plasticizer.

(76)   Heng, L. Y.; Hall, E. A. H. *Electroanalysis* **2000**, *12*, 187-193, Taking the plasticizer out of methacrylic-acrylic membranes for K^+-selective electrodes.

(77)   Heng, L. Y.; Hall, E. A. H. *Anal. Chim. Acta* **2001**, *443*, 25-40, Assessing a photocured self-plasticised acrylic membrane recipe for Na^+ and K^+ ion selective electrodes.

(78)   Malinowska, E.; Gawart, L.; Parzuchowski, P.; Rokicki, G.; Brzózka, Z. *Anal. Chim. Acta* **2000**, *421*, 93-101, Novel approach of immobilization of calix[4]arene type ionophore in 'self-plasticized' polymeric membrane.

(79)   Qin, Y.; Peper, S.; Bakker, E. *Electroanalysis* **2002**, *14*, 1375-1381, Plasticizer-free polymer membrane ion-selective electrodes containing a methacrylic copolymer matrix.

(80)   Qin, Y.; Peper, S.; Radu, A.; Ceresa, A.; Bakker, E. *Anal. Chem.* **2003**, *75*, 3038-3045, Plasticizer-free polymer containing a covalently immobilized Ca^{2+}-selective ionophore for potentiometric and optical sensors.

(81)   Heng, L. Y.; Tóth, K.; Hall, E. A. H. *Talanta* **2004**, *63*, 73-87, Ion-transport and diffusion coefficients of non-plasticised methacrylic-acrylic ion-selective membranes.

(82)   Michalska, A. J.; Appaih-Kusi, C.; Heng, L. Y.; Walkiewicz, S.; Hall, E. A. H. *Anal. Chem.* **2004**, *76*, 2031-2039, An experimental study of membrane materials and inner contacting layers for ion-selective K^+ electrodes with a stable response and good dynamic range.

(83) Ulman, A. *An Introduction to Ultrathin Organic Films: From Langmuir-Blodgett to Self-Assembly*, Academic Press: Boston, San Diego, New York, London, Sidney, Tokio, Toronto, 1991.

(84) Wang, J. *Analytical Electrochemistry*, Wiley-VCH: New York, Chichester, Weinheim, Brisbane, Singapore, Toronto, 2000.

(85) Bard, A. J.; Faulkner, L. R. *Electrochemical Methods*, J. Wiley and Sons, Inc.: New York, Chichester, Weinheim, Brisbane, Singapore, Toronto, 2001.

(86) Gyurcsányi, R. E.; Rangisetty, N.; Clifton, S.; Pendley, B. D.; Lindner, E. *Talanta* **2004**, *63*, 89-99, Microfabricated ISEs: Critical comparison of inherently conducting polymer and hydrogel based inner contacts.

(87) Fibbioli, M.; Morf, W. E.; Badertscher, M.; Rooij, N. F. D.; Pretsch, E. *Electroanalysis* **2000**, *12*, 1286-1292, Potential drifts of solid-contacted ion-selective electrodes due to zero-current ion fluxes through the sensor membrane.

(88) Creager, S.; Hockett, L. A.; Rowe, G. K. *Langmuir* **1991**, *8*, 854-861, Consequences of microscopic surface roughness for molecular self-assembly.

(89) Hirayama, M. K. N.; Caseri, W. R.; Suter, U. W. *Appl. Surface Sci.* **1999**, *143*, 256-264, Strongly attached ultrathin polymer layers on metal surfaces obtained by activation of Si-H bonds.

(90) Albinati, A.; Caseri, W. R.; Pregosin, P. S. *Organometallics* **1987**, *6*, 788-793, Hydrosilylation with platinum complexes. Preparation, low-temperature NMR spectra, and X-ray crystal structure of the novel bis-olefin catalyst cis-$PtCl_2(PhCH=CH_2)_2$.

(91) Caseri, W.; Pregosin, P. S. *Organometallics* **1988**, *7*, 1373-1380, Hydrosilylation chemistry and catalysis with cis-$PtCl_2(PhCH=CH_2)_2$.

(92) Caseri, W.; Pregosin, P. S. *J. Organomet. Chem.* **1988**, *356*, 259-269, Mechanistic aspects of the platinum catalyzed hydrosilylation of $PhCH=CH_2$ with Et_3SiH.

(93) Hirayama, M. K. N.; Caseri, W. R.; Suter, U. W. *J. Colloid Interface Sci.* **1999**, *216*, 250-256, Ultrathin polymer films on gold surfaces through activation of Si-H bonds.

(94) Hirayama, M. K. N.; Soares, M. C.; Caseri, W. R.; Suter, U. W.; Goussev, O. *J. Adhesion* **2000**, *72*, 51-63, Activated poly(hydromethylsiloxane)s as novel adhesion promoters for metallic surfaces.

(95) Zhang, X.; Deckert, V.; Steiger, B.; M.K.N., H.; Suter, U. W.; Pretsch, E. *Talanta* **2004**, *63*, 159-165, Covalent binding of biorecognition groups to solids using poly(hydromethylsiloxane) as linkage.

(96) Wang, J. X.; Collinson, M. M. *J. Electroanal. Chem.* **1998**, *455*, 127-137, Electrochemical characterization of inorganic/organic hybrid films prepared from ferrocene modified silanes.

(97) Fibbioli, M. *Ph. D. Thesis*, No. 13789, ETH, Zürich, 2000.

(98) Cannes, C.; Kanoufi, F.; Bard, A. J. *J. Electroanal. Chem.* **2003**, *547*, 83-91, Cyclic voltammetry and scanning electrochemical microscopy of ferrocenemethanol at monolayer and bilayer-modified gold electrodes.

(99) Amatore, C.; Savéant, J. M.; Tessier, D. *J. Electroanal. Chem.* **1983**, *147*, 39-51, Charge-transfer at partially blocked surfaces - A model for the case of microscopic active and inactive sites.

(100) Chen, J.; Burrell, A. K.; Collis, G. E.; Officer, D. L.; Swiegers, G. F.; Too, C. O.; Wallace, G. G. *Electrochim. Acta* **2002**, *47*, 2715-2724, Preparation, characterisation and biosensor application of conducting polymers based on ferrocene substituted thiophene and terthiophene.

(101) Lewis, T. W.; Wallace, G. G.; Smyth, M. R. *Analyst* **1999**, *124*, 213-219, Electrofunctional polymers: their role in the development of new analytical systems.

(102) Zotti, G., Ed. *Conductive Polymers: Synthesis and Electrical Properties*, 2, John Wiley & Sons Ltd.: Chichester, 1997.

(103) Heeger, A. J. *Rev. Mod. Phys.* **2001**, *73*, 681-700, Nobel lecture: Semiconducting and metallic polymers: The fourth generation of polymeric materials.

(104) MacDiarmid, A. G. *Rev. Mod. Phys.* **2001**, *73*, 701-712, Nobel lecture: "Synthetic metals": A novel role for organic polymers.

(105) Shirakawa, H. *Rev. Mod. Phys.* **2001**, *73*, 713-718, Nobel lecture: The discovery of polyacetylene film - The dawning of an era of conducting polymers.

(106) Schopf, G.; Kossmehl, G., Eds. *Polythiophenes-Electrically Conductive Polymers*, 129, Springer-Verlag: Berlin, 1997.

(107) Kossmehl, G.; Niemitz, M. *Synth. Met.* **1991**, *41-43*, 1065-1071, Preparation and controlled wettability of poly(2,2'-bithienyl-5,5'-diyl) layers.

(108) Bobacka, J.; Ivaska, A.; Lewenstam, A. *Electroanalysis* **2003**, *15*, 366-374, Potentiometric ion sensors based on conducting polymers.

(109) Satoh, M.; Kaneto, K.; Yoshino, K. *Synth. Met.* **1986**, *14*, 289-296, Dependences of electrical and mechanical-properties of conducting polypyrrole films on conditions of electrochemical polymerization in an aqueous-medium.

(110) Maddison, D. S.; Unsworth, J. *Synth. Met.* **1989**, *30*, 47-55, Optimization of synthesis conditions of polypyrrole from aqueous-solutions.

(111) Dong, S.; Sun, Z.; Lu, Z. *Analyst* **1988**, *113*, 1525-1528, Chloride chemical sensor based on an organic conducting polypyrrole polymer.

(112) Dong, S.; Sun, Z.; Lu, Z. *J. Chem. Soc. Comm.* **1988**, 993-995, A new kind of chemical sensor based on a conducting polymer film.

(113) Michalska, A.; Walkiewicz, S.; Maksymiuk, K.; Hall, E. A. H. *Electroanalysis* **2002**, *14*, 1236-1244, Potentiometric responses of poly(pyrrole) films surface modified by Nafion.

(114) Michalska, A. J.; Hall, E. A. H. *Electroanalysis* **1999**, *11*, 756-762, Inducing a cationic response in poly(pyrrole) films.

(115) Hulanicki, A.; Michalska, A.; Lewenstam, A. *Talanta* **1994**, *41*, 323-325, Bifunctionality of chemical sensors based on the conducting polymer polypyrrole.

References

(116) Lewenstam, A.; Bobacka, J.; Ivaska, A. *J. Electroanal. Chem.* **1994**, *368*, 23-31, Mechanism of ionic and redox sensitivity of p-type conducting polymers. 1. Theory.

(117) Bobacka, J.; Gao, Z. Q.; Ivaska, A.; Lewenstam, A. *J. Electroanal. Chem.* **1994**, *368*, 33-41, Mechanism of ionic and redox sensitivity of p-type conducting polymers. 2. Experimental-study of polypyrrole.

(118) Pei, Q.; Qian, R. *Synth. Met.* **1991**, *45*, 35-48, Protonation and deprotonation of polypyrrole chain in aqueous solutions.

(119) Pei, Q. B.; Qian, R. Y. *Electrochim. Acta* **1992**, *37*, 1075-1081, Electrode-potentials of electronically conducting polymer polypyrrole.

(120) Michalska, A.; Maksymiuk, K.; Hulanicki, A. *J. Electroanal. Chem.* **1995**, *392*, 63-68, On the nature of the potentiometric response of polypyrrole in acidic solutions.

(121) Michalska, A.; Maksymiuk, K. *Electrochim. Acta* **1999**, *44*, 2125-2129, The specific influence of hydrogen ions on poly(pyrrole) potentiometry.

(122) Maksymiuk, K.; Bobacka, J.; Ivaska, A.; Lewenstam, A. *Anal. Lett.* **2000**, *33*, 1339-1360, Coupled redox and pH potentiometric responses of electrodes coated with polypyrrole.

(123) Michalska, A.; Maksymiuk, K. *Microchim. Acta* **2003**, *143*, 163-175, Counter-ion influence on polypyrrole potentiometric pH sensitivity.

(124) Lindfors, T.; Ivaska, A. *J. Electroanal. Chem.* **2002**, *531*, 43-52, pH sensitivity of polyaniline and its substituted derivatives.

(125) Zhang, X. J.; Ogorevc, B.; Wang, J. *Anal. Chim. Acta* **2002**, *452*, 1-10, Solid-state pH nanoelectrode based on polyaniline thin film electrodeposited onto ion-beam etched carbon fiber.

(126) Lindino, C. A.; Bulhoes, L. O. S. *Anal. Chim. Acta* **1996**, *334*, 317-322, The potentiometric response of chemically modified electrodes.

(127) Osaka, T.; Komaba, S.; Amano, A. *J. Electrochem. Soc.* **1998**, *145*, 406-408, Highly sensitive microbiosensor for creatinine based on the combination of inactive polypyrrole with polyion complexes.

(128) Karyakin, A. A.; Vuki, M.; Lukachova, L. V.; Karyakina, E. E.; Orlov, A. V.; Karpachova, G. P.; Wang, J. *Analytical Chemistry* **1999**, *71*, 2534-2540, Processible polyaniline as an advanced potentiometric pH transducer. Application to biosensors.

(129) Pandey, P. C.; Singh, G. *Talanta* **2001**, *55*, 773-782, Tetraphenylborate doped polyaniline based novel pH sensor and solid-state urea biosensor.

(130) Migdalski, J.; Blaz, T.; Lewenstam, A. *Anal. Chim. Acta* **1996**, *322*, 141-149, Conducting polymer-based ion-selective electrodes.

(131) Sjöberg, P.; Bobacka, J.; Lewenstam, A.; Ivaska, A. *Electroanalysis* **1999**, *11*, 821-824, All-solid-state chloride-selective electrode based on poly(3-octylthiophene) and tridodecylmethylammonium chloride.

(132) Sjöberg-Eerola, P.; Bobacka, J.; Sokalski, T.; Mieczkowski, J.; Ivaska, A.; Lewenstam, A. *Electroanalysis* **2004**, *16*, 379-385, All-solid-state chloride

sensors with poly(3-octylthiopene) matrix and trihexadecylmethylammonium chlorides as an ion exchanger salt.

(133) Lindfors, T.; Sjöberg, P.; Bobacka, J.; Lewenstam, A.; Ivaska, A. *Anal. Chim. Acta* **1999**, *385*, 163-173, Characterization of a single-piece all-solid-state lithium-selective electrode based on soluble conducting polyaniline.

(134) Lindfors, T.; Ervela, S.; Ivaska, A. *J. Electroanal. Chem.* **2003**, *560*, 69-78, Polyaniline as pH-sensitive component in plasticized PVC membranes.

(135) Cadogan, A.; Gao, Z. Q.; Lewenstam, A.; Ivaska, A.; Diamond, D. *Analytical Chemistry* **1992**, *64*, 2496-2501, All-solid-state sodium-selective electrode based on a calixarene ionophore in a poly(vinyl chloride) membrane with a polypyrrole solid contact.

(136) Michalska, A.; Hulanicki, A.; Lewenstam, A. *Analyst* **1994**, *119*, 2417-2420, All-solid-state hydrogen ion-selective electrode based on a conducting poly(pyrrole) solid contact.

(137) Hulanicki, A.; Michalska, A. *Electroanalysis* **1995**, *7*, 692-693, All-solid-state chloride-selective electrode with poly(pyrrole) solid contact.

(138) Momma, T.; Komaba, S.; Yamamoto, M.; Osaka, T.; Yamauchi, S. *Sens. Actuator B-Chem.* **1995**, *25*, 724-728, All-solid-state potassium-selective electrode using double-layer film of polypyrrole/polyanion composite and plasticized poly(vinyl chloride) containing Valinomycin.

(139) Momma, T.; Yamamoto, M.; Komaba, S.; Osaka, T. *J. Electroanal. Chem.* **1996**, *407*, 91-96, Analysis of the long-term potential stability of an all-solid-state potassium-selective eectrode with electroactive polypyrrole film.

(140) Kovács, B.; Csóka, B.; Nagy, G.; Ivaska, A. *Anal. Chim. Acta* **2001**, *437*, 67-76, All-solid-state surfactant sensing electrode using conductive polymer as internal electric contact.

(141) Pandey, P. C.; Singh, G.; Srivastava, P. K. *Electroanalysis* **2002**, *14*, 427-432, Electrochemical synthesis of tetraphenylborate doped polypyrrole and its applications in designing a novel zinc and potassium ion sensor.

(142) Duma'nska, J.; Maksymiuk, K. *Electroanalysis* **2001**, *13*, 567-573, Studies on spontaneous charging/discharging processes of polypyrrole in aqueous electrolyte solutions.

(143) Kriván, E.; Visy, C.; Kankare, J. *J. Phys. Chem. B* **2003**, *107*, 1302-1308, Deprotonation and dihydration of pristine PPy/DS films during open-circuit relaxation: An ignored factor in detemining the properties of conducting polymers.

(144) Han, W. S.; Park, M. Y.; Chung, K. C.; Cho, D. H.; Hong, T. K. *Electroanalysis* **2001**, *13*, 955-959, All solid state hydrogen ion-selective electrode based on a tribenzylamine neutral carrier in a poly(vinyl chloride) membrane with a poly(aniline) solid contact.

(145) Grekovich, A. L.; Markuzina, N. N.; Mikhelson, K. N.; Bochenska, M.; Lewenstam, A. *Electroanalysis* **2002**, *14*, 551-555, Conventional and solid-

contact lithium-selective electrodes based on tris (N,N-dicyclohexylamide) neutral ionophore.

(146) Bobacka, J.; Lahtinen, T.; Nordman, J.; Häggström, S.; Rissanen, K.; Lewenstam, A.; Ivaska, A. *Electroanalysis* **2001**, *13*, 723-726, All-solid-state Ag⁺-ISE based on [2.2.2] p,p,p-cyclophane.

(147) Vázquez, M.; Danielsson, P.; Bobacka, J.; Lewenstam, A.; Ivaska, A. *Sens. Actuator B-Chem.* **2004**, *97*, 182-189, Solution-cast films of poly(3,4-ethylenedioxythiophene) as ion-to-electron transducers in all-solid-state ion-selective electrodes.

(148) Vázquez, M.; Bobacka, J.; Ivaska, A.; Lewenstam, A. *Talanta* **2004**, *62*, 57-63, Small-volume radial flow cell for all-solid-state ion-selective electrodes.

(149) Bobacka, J.; McCarrick, M.; Lewenstam, A.; Ivaska, A. *Analyst* **1994**, *119*, 1985-1991, All solid-state poly(vinyl chloride) membrane ion-selective electrodes with poly(3-octylthiophene) solid internal contact.

(150) Bobacka, J.; Alaviuhkola, T.; Hietapelto, V.; Koskinen, H.; Lewenstam, A.; Lämsä, M.; Pursiainen, J.; Ivaska, A. *Talanta* **2002**, *58*, 341-349, Solid-contact ion-selective electrodes for aromatic cations based on π-coordinating soft carriers.

(151) Vázquez, M.; Bobacka, J.; Ivaska, A.; Lewenstam, A. *Sens. Actuators, B* **2002**, *82*, 7-13, Influence of oxygen and carbon dioxide on the electrochemical stability of poly(3,4-ethylenedioxythiophene) used as ion-to-electron transducer in all-solid-state ion-selective electrodes.

(152) Michalska, A.; Konopka, A.; Maj-Zurawska, M. *Anal. Chem.* **2003**, *75*, 141-144, All-solid-state calcium solvent polymeric membrane electrode for low-level concentration measurements.

(153) Michalska, A.; Duma´nska, J.; Maksymiuk, K. *Anal. Chem.* **2003**, *75*, 4964-4974, Lowering the detection limit of ion-selective plastic membrane electrodes with conducting polymer solid contact and conducting polymer potentiometric sensors.

(154) Lindner, E.; Gyurcsányi, R. E.; Buck, R. P. *Electroanalysis* **1999**, *11*, 695-702, Tailored transport through ion-selective membranes for improved detection limits and selectivity coefficients.

(155) Pergel, K.; Gyurcsányi, R. E.; Tóth, K.; Lindner, E. *Anal. Chem.* **2001**, *73*, 4249-4253, Picomolar detection limits with current-polarized Pb²⁺ ion-selective membranes.

(156) Ceresa, A.; Pretsch, E. *Anal. Chim. Acta* **1999**, *395*, 41-52, Determination of formal complex formation constants of various Pb²⁺ ionophores in the sensor membrane phase.

(157) Horváth, V.; Horvai, G. *Anal. Chim. Acta* **1993**, *273*, 145-152, Cyclic voltammetric experiments with plasticized PVC membranes.

(158) Morf, W. E.; Wuhrmann, P.; Simon, W. *Anal. Chem.* **1976**, *48*, 1031-1039, Transport properties of neutral carrier ion-selective membranes.

(159) Thoma, A. P.; Viviani-Nauer, A.; Arvanitis, S.; Morf, W. E.; Simon, W. *Anal. Chem.* **1977**, *49*, 1567-1572, Mechanism of neutral carrier mediated ion-transport through ion-selective bulk membranes.

(160) Horváth, V.; Horvai, G.; Pungor, E. *Mikrochim. Acta* **1990**, *1*, 217-224, Amperometric measurements with ion-selective electrode membranes in a flow system.

(161) Horvai, G.; Pungor, E. *Anal. Chim. Acta* **1991**, *243*, 55-59, Amperometric determination of hydrogen and hydroxyl ion concentrations in unbuffered solutions in the pH range 5-9.

(162) Pergel, K.; Gyurcsányi, R. E.; Tóth, K.; Lindner, E. *Anal. Chem.* **2001**, *73*, 4249-4253, Picomolar detection limits with current-polarized Pb^{2+} ion-selective membranes.

(163) Morf, W. E.; Badertscher, M.; Zwickl, T.; de Rooij, N. F.; Pretsch, E. *J. Electroanal. Chem.* **2002**, *526*, 19-28, Effects of controlled current on the response behavior of polymeric membrane ion-selective electrodes.

(164) Jadhav, S.; Bakker, E. *Anal. Chem.* **1999**, *71*, 3657-3664, Voltammetric and amperometric transduction for solvent polymeric membrane ion sensors.

(165) Jadhav, S.; Meir, A. J.; Bakker, E. *Electroanalysis* **2000**, *12*, 1251-1257, Normal pulse voltammetry as improved quantitative detection mode for amperometric solvent polymeric membrane ion sensors.

(166) Jadhav, S.; Bakker, E. *Anal. Chem.* **2001**, *73*, 80-90, Selectivity behavior and multianalyte detection capability of voltammetric ionophore-based plasticised polymeric membrane sensors.

(167) Long, R.; Bakker, E. *Electroanalysis* **2003**, *15*, 1261-1269, Spectral imaging and electrochemical study on the response mechanism of ionophore-based polymeric membrane amperometric pH sensors.

(168) Shvarev, A.; Bakker, E. *Anal. Chem.* **2003**, *75*, 4541-4550, Pulsed galvanostatic control of ionophore-based polymeric ion sensors.

(169) Shvarev, A.; Bakker, E. *J. Am. Chem. Soc.* **2003**, *125*, 11192-11193, Reversible electrochemical detection of nonelectroactive polyions.

(170) Shvarev, A.; Bakker, E. *Talanta* **2004**, *63*, 195-200, Distinguishing free and total calcium with a single pulsed galvanostatic ion-selective electrode.

(171) Samec, Z.; Marecek, V.; Koryta, J.; Khalil, M. W. *J. Electroanal. Chem.* **1977**, *83*, 393-397, Investigation of ion transfer across the interface between two immiscible electrolyte-solutions by cyclic voltammetry.

(172) Koryta, J. *Electrochim. Acta* **1979**, *24*, 293-300, Electrochemical polarization phenomena at the interface of two immiscible electrolyte-solutions.

(173) Koryta, J. *Electrochim. Acta* **1984**, *29*, 445-452, Electrochemical polarization phenomena at the interface of two immiscible electrolyte-solutions-II. Progress since 1978.

(174) Koryta, J. *Electrochim. Acta* **1988**, *33*, 189-197, Electrochemical polarization phenomena at the interface of two immiscible electrolyte-solutions-III. Progress since 1983.

(175) Senda, M.; Kakiuchi, T.; Osakai, T. *Electrochim. Acta* **1991**, *36*, 253-262, Electrochemistry at the interface between two immiscible electrolyte-solutions.

(176) Shirai, O.; Kihara, S.; Yoshida, Y.; Matsui, M. *J. Electroanal. Chem.* **1995**, *389*, 61-70, Ion transfer through a liquid membrane or a bilayer-lipid membrane in the presence of sufficient electrolytes.

(177) Samec, Z.; Samcová, E.; Girault, H. H. *Talanta* **2004**, *63*, 21-32, Ion amperometry at the interface between two immiscible electrolyte solutions in view of realizing the amperometric ion-selective electrode.

(178) Sawada, S.; Torii, H.; Osakai, T.; Kimoto, T. *Anal. Chem.* **1998**, *70*, 4286-4290, Pulse amperometric detection of lithium in artificial serum using a flow injection system with a liquid/liquid-type ion-selective electrode.

(179) Cammann, K.; Ahlers, B.; Henn, D.; Dumschat, C.; Shulga, A. A. *Sens. Actuator B-Chem.* **1996**, *35*, 26-31, New sensing principles for ion detection.

(180) Lee, H. J.; Girault, H. H. *Anal. Chem.* **1998**, *70*, 4280-4285, Amperometric ion detector for ion chromatography.

(181) Lee, H. J.; Pereira, C. M.; Silva, A. F.; Girault, H. H. *Anal. Chem.* **2000**, *72*, 5562-5566, Pulse amperometric detection of salt concentrations by flow injection analysis using ionodes.

(182) Lee, H. J.; Beattie, P. D.; Seddon, B. J.; Osborne, M. D.; Girault, H. H. *J. Electroanal. Chem.* **1997**, *440*, 73-82, Amperometric ion sensors based on laser-patterned composite polymer membranes.

(183) Morf, W. E.; Badertscher, M.; Zwickl, T.; de Rooij, N. F.; Pretsch, E. *J. Phys. Chem. B* **1999**, *103*, 11346-11356, Effects of ion transport on the potential response of ionophore-based membrane electrodes: A theoretical approach.

(184) Kakiuchi, T. *Electrochim. Acta* **1998**, *44*, 171-179, A theory of voltammetry of ion transfer across a liquid membrane in the absence of supporting electrolytes using the Nernst-Planck equation and electroneutrality assumption.

(185) Zwickl, T. A. *Ph. D. Thesis*, No. 15485, ETH, Zürich, 2004.

(186) Morf, W. E.; Zwickl, T.; Pretsch, E.; de Rooij, N. F. *Chimia* **2003**, *57*, 639-642, Current response of ionophore-based ion-selective electrode membranes at controlled potential.

(187) Oesch, U.; Simon, W. *Anal. Chem.* **1980**, *52*, 692-700, Life time of neutral carrier based ion-selective liquid-membrane electrodes.

(188) Iglehart, M. L.; Buck, R. P.; Horvai, G.; Pungor, E. *Anal. Chem.* **1988**, *60*, 1018-1022, Plasticized poly(vinyl chloride) properties and characteristics of valinomycin electrodes - Current time responses to voltage steps.

(189) Pendley, B. D.; Gyurcsányi, R. E.; Buck, R. P.; Lindner, E. *Anal. Chem.* **2001**, *73*, 4599-4606, A chronoamperometric method to estimate changes in the membrane composition of ion-selective membranes.

(190) Schneider, B.; Zwickl, T.; Federer, B.; Pretsch, E.; Lindner, E. *Anal. Chem.* **1996**, *68*, 4342-4350, Spectropotentiometry: A new method for in situ

imaging of concentration profiles in ion-selective membranes with simultaneous recording of potential-time transients.

(191) Püntener, M.; Fibbioli, M.; Bakker, E.; Pretsch, E. *Electroanalysis* **2002**, *14*, 1329-1338, Response and diffusion behavior of mobile and covalently immobilized H^+-ionophores in polymeric membrane ion-selective electrodes.

(192) Long, R.; Bakker, E. *Anal. Chim. Acta* **2004**, *511*, 91-95, Optical determination of ionophore diffusion coefficients in plasticized poly(vinyl chloride) sensing films.

(193) Marcus, Y. *Ion Properties*, M. Dekker Inc.: New York, Basel, Hongkong, 1997.

(194) Samec, Z.; Langmaier, J.; Trojánek, A.; Samcová, E.; Málek, J. *Anal. Sci.* **1998**, *14*, 35-41, Transfer of protonated anesthetics across the water o-nitrophenyl octyl ether interface: Effect of the ion structure on the transfer kinetics and pharmacological activity.

(195) Sarada, T.; Sawyer, L. C.; Ostler, M. I. *J. Membr. Sci.* **1983**, *15*, 97-113, Three dimensional structure of celgard$^{(R)}$ microporous membranes.

Curriculum Vitae

1976	Born on February 24 in Basel, Switzerland
1983-1992	Primary and secondary school in Muttenz (BL)
1992-1995	Comprehensive secondary school at Gymnasium Muttenz, scientific department
1996	Practical work in a research laboratory at Ciba, textile dyes, Basel (3 months)
1996-2001	Chemistry studies at the Swiss Federal Institute of Technology Zurich (ETHZ), diploma thesis in the group of Prof. Dr. Ernö Pretsch
2001-2004	Ph.D. studies in the group of Prof. Dr. Ernö Pretsch on potentiometric sensors
2002-2004	Laboratory teaching assistant for polarography in Analytical Chemistry at ETHZ

Languages: German, English, French, Italian

Zurich, October 2004   Jolanda Sutter